Microscale gas flow:

A comparison of Grad's 13 moment equations and other continuum approaches

by

Toby Thatcher
B.Eng., University of Victoria (2002)

A Thesis Submitted in Partial Fulfillment of the
Requirements for the Degree of

Master of Applied Science

in the Department of Mechanical Engineering

Supervisor: Dr. H. Struchtrup

Abstract

Advances in manufacturing techniques over the last decade have made it possible to make electrical devices with dimensions as small as 90 nanometers [1]. Using similar techniques, devices that perform moving mechanical tasks less than 100 μm are being manufactured in quantity [2][3], e.g., pumps, turbines, valves and nozzles. These devices are incorporated into microelectromechanical systems (MEMS) that can be potentially used in devices such as medical and chemical sensors, and fuel cells. The gas and fluid flows in devices of this size exhibit behavior that can not be described by the classical Navier-Stokes and Fourier equations of continuum mechanics. This happens when flows become rarefied such that the mean free path (distance between two subsequent particle collisions) is not negligible compared to the characteristic length scale. The rarefaction of a fluid flow is also seen in the upper atmosphere for larger length scales, e.g., for re-entry for space craft and some supersonic jet aircraft.

Currently, when one looks to model fluid flow and heat transfer in a rarefied flow there are two predominantly accepted choices. Either one uses jump and slip boundary conditions with the Navier-Stokes and Fourier (NSF) equations, or a statistical particle model such as direct simulation Monte-Carlo (DSMC) [4] and the Boltzmann equation. DSMC is computationally intensive for complex flows and the NSF solutions are only valid for low degrees of rarefaction.

As an alternative to these methods we have used Grad's 13 moment expansion of the Boltzmann equation [5]. For its implementation, a set of boundary conditions and three numerical methods for the solution have been devised. The model is applied to the solution of 2-D micro Couette flow with heat transfer. Results are compared to those obtained from the Navier-Stokes-Fourier equations, reduced Burnett equations, Regularized 13 moment equations and DSMC simulations.

Supervisor: Dr. H. Struchtrup, (Department of Mechanical Engineering)

Table of Contents

List of Figures and Tables

List of Figures

List of Tables

Nomenclature

Common modifiers

A_0	reference property
A_w/A^w	wall value
$A_{<ij>} = \frac{1}{2}(A_{ij} + A_{ji}) - A_{kk}\delta_{ij}$	trace free symmetric part
$\hat{A}$	dimensionless property
$\bar{A}$	non-linear perturbation of A
$\tilde{A}$	constant value of A in perturbation theory

Grid modifiers

A_A	west wall property
A_B	east wall property
A_E	east grid point property
A_e	$\frac{1}{2}$ point east grid property
A_i	space grid point i value
A^n	time grid point n value
A_L	previous iteration value
A_P	central grid property
A_W	west grid property
A_w	$\frac{1}{2}$ point west grid property
A^{wall}	nearest wall value
A^*	predictor step value

Standard nomenclature

α	Cercignani velocity boundary adjustment [1]
β	Cercignani temperature boundary adjustment [1]
$C_i = c_i - v_i$	peculiar velocity $\left[\frac{\mathrm{m}}{\mathrm{s}}\right]$
c_i	particle velocity $\left[\frac{\mathrm{m}}{\mathrm{s}}\right]$

$\overline{c}$	mean velocity between particles $\left[\frac{\mathrm{m}}{\mathrm{s}}\right]$
CFL	Courant-Friedrichs-Lewy number [1]
δ	damping coefficient [1]
$\delta_{ij} = \begin{cases} 1 & \text{if } i = j \\ 0 & \text{otherwise} \end{cases}$	Dirac delta function [1]
ε	specific energy $\left[\frac{\mathrm{J}}{\mathrm{kg}}\right]$
ε	damping rate [1]
ε^n	order of Kn operator [1]
F	generalized fluxes
f	phase density $\left[\frac{\mathrm{s}^3}{\mathrm{m}^6}\right]$
f_M	Maxwellian phase density $\left[\frac{\mathrm{s}^3}{\mathrm{m}^6}\right]$
f_G	phase density at the wall $\left[\frac{\mathrm{s}^3}{\mathrm{m}^6}\right]$
f_w	wall thermalized Maxwellian phase density $\left[\frac{\mathrm{s}^3}{\mathrm{m}^6}\right]$
$\overline{g}$	mean particle velocity $\left[\frac{\mathrm{m}}{\mathrm{s}}\right]$
γ	Cercignani normal pressure boundary adjustment [1]
Kn	Knudsen number [1]
k	Boltzmann's constant $\left[1.3804\frac{\mathrm{J}}{\mathrm{K}}\right]$
L	characteristic length [m]
l	mean free path [m]
N	greatest time grid point [1]
n	number density $\left[\frac{1}{\mathrm{m}^3}\right]$
n_i	unit normal to the wall [1]
M	Mach number [1]
M	total mass of system [kg]
m	mass of particle [kg]
m	greatest time grid point [1]
θ	accommodation coefficient [1]
P_A	generalized productions
p	pressure [Pa]

$p_\alpha = p + p_{<22>}$	pressure constant [Pa]
p_{ij}	pressure tensor [Pa]
q_i	heat flux [W]
$R = \frac{k}{m}$	ideal gas constant $\left[\frac{\text{kJ}}{\text{kg K}}\right]$
ρ	density $\left[\frac{\text{kg}}{\text{m}^3}\right]$
$S(f)$	collision term $\left[\frac{\text{s}^2}{\text{m}^6}\right]$
s	gas type exponent [1]
σ	molecular diameter [m]
σ_{ij}	trace free part of the pressure tensor [Pa]
T	temperature [K]
t	time [s]
Δt	time step between iterations [s]
τ	mean free time [s]
u	specific internal energy $\left[\frac{\text{J}}{\text{kg}}\right]$
u_A	generalized quantities
μ	viscosity $\left[\frac{\text{kg}}{\text{m s}}\right]$
V_i	slip velocity $\left[\frac{\text{m}}{\text{s}}\right]$
v_i	barycentric velocity $\left[\frac{\text{m}}{\text{s}}\right]$
Δv	velocity difference between plates $\left[\frac{\text{m}}{\text{s}}\right]$
x_i	position in space [m]
Δx	space step on the numerical grid [m]
φ_A	moment A
ψ_A	expansion coefficients of φ_A
$m_{<ijk>}$, R_{ij}, Δ	deviations of higher moments

Chapter 1

Introduction

Advances in manufacturing techniques over the last decade have made it possible to make electrical devices with dimensions small as 90 nanometers [1]. Using similar techniques, devices that perform moving mechanical tasks smaller than 100 μm are now being manufactured in quantity [2][3]. Some of these devices are pumps, turbines, valves and nozzles. These devices are incorporated into microelectromechanical systems (MEMS), like fuel cells and medical devices.

The gas and fluid flow in devices of this size exhibits behavior that is beyond that of Navier-Stokes' and Fourier's descriptions of continuum mechanics. Flow can become rarefied such that the mean free path (the distance between two subsequent particle collisions) is not negligible compared to the characteristic length scale. This rarefaction of a fluid flow is also seen in the upper atmosphere for the larger length scales seen in re-entry for space craft and some supersonic jet aircraft.

Currently, when one looks to model fluid flow and heat transfer in a flow influenced by rarefaction, there are two predominantly accepted choices: Either using extended boundary conditions with the Navier-Stokes and Fourier (NSF) equations, or a statistical particle model such as direct simulation Monte-Carlo (DSMC) and the Boltzmann equation. DSMC is computationally intensive for complex flows and the NSF solutions are only valid for low degrees of rarefaction. There are several alternative approaches to modeling rarefied gas flow, predominantly based on simplifications of the Boltzmann equation. The most important of these are the Chapman-Enskog series expansion (NSF, Burnett equations

and super-Burnett equations)[6][7][8][9] and the method of moments in various adaptations [5][10][11][12][13][14].

This project is intended to compare an assortment of continuum equations for microscale flow. The goal being to validate and benchmark the Grad 13 moment equations [10] with bounded flow. This will be done by solving simple flow problems with Grad's 13 moment equations and NSF equations. Solutions will be found using computational fluid dynamics (CFD) and the finite volume method. This comparison will be done for plane Couette flow with heat transfer. The solutions will also be compared with DSMC calculations. The goal is a thorough comparison of micro flow equations including a range of usefulness of the three sets of equations with respect to Knudsen number, and temperature and velocity gradients.

The solution of Grad's 13 moment equations for Couette flow has not been done before, due to the lack of a complete set of jump and slip boundary conditions for the equations. The solution presented in this thesis uses a new set of boundary conditions and are the first full solution for the problem.

For larger Knudsen numbers and sharper velocity gradients, the results from the Grad 13 equations differ from exact solutions of the Boltzmann equation. A regularization of Grad's 13 moment equations [11][13][14] promises to give better results. These equations are also tested and the results indicate that they are superior to the Grad 13 moment equations.

Chapter 2

Background theory

2.1 Rarefied gas flow

Microscale or rarefied gas flow regimes are normally defined with respect to the mean free path or mean free time of particle. The mean free time or collision time is the mean time between individual particle collisions. The mean free path is the average distance traveled between collisions. For a perfect gas modeled as hard spheres the mean free time τ is

$$\tau = \frac{1}{\pi\sigma^2\bar{g}n}, \tag{2.1}$$

where σ, $\bar{g}$ and n are the molecular diameter, mean relative velocity between particles and number density, respectively. The number density is the simply the number of particles per unit volume. The mean free path l is

$$l = \tau\bar{c} = \frac{1}{\sqrt{2}\pi\sigma^2 n} = \frac{kT}{\sqrt{2}\pi\sigma^2 p}, \tag{2.2}$$

where k, T, p and $\bar{c}$ are the Boltzmann constant, temperature, pressure and mean particle velocity respectively [4]. The mean relative velocity is related to the mean particle velocity as

$$\bar{g} = \sqrt{2}\bar{c}. \tag{2.3}$$

The precise value of the mean free path and mean free time for a perfect gas can be related to the viscosity as

$$\tau = \mu\frac{m}{kT\rho} = \frac{\mu}{p}, \tag{2.4}$$

$$l = \frac{\mu\sqrt{2\frac{k}{m}T}}{p} \tag{2.5}$$

where m is the particle mass and ρ is the gas density. The viscosity μ is related to temperature as

$$\mu = \mu_0 \left(\frac{T}{T_0}\right)^s. \tag{2.6}$$

μ_0, the reference viscosity, and s, the gas type exponent, are related to the type of gas. T_0 is the reference temperature. For Maxwell molecules[1] $s = 1$ and for hard spheres $s = \frac{1}{2}$; see reference [4] for details and values for μ and s.

The dimensionless parameter that relates the characteristic length to the mean free path is the Knudsen number Kn.

$$Kn = \frac{l}{L} = \frac{\mu_0\sqrt{\frac{k}{m}T_0}}{p_0 L}, \tag{2.7}$$

where L is a characteristic length of the process and p_0, T_0 are typical values of pressure and temperature in the process. A gas is generally considered to be rarefied if $Kn > 0.001$ [2].

Microscale and rarefied gas flows are divided into four main categories based on the values of the Knudsen number. There are some slight discrepancies in literature as to exactly what separates these flow regimes, but most, e.g. [2][3] depict the regimes as below:

- Continuum flow

$$Kn < 0.001,$$

- Slip flow

$$0.001 \leq Kn < 0.1,$$

- Transitional flow

$$0.1 \leq Kn < 10,$$

[1]Maxwell molecules are a special simplification of molecules such that the intermolecular force varies with the inverse of the 5th power of distance between two particles. This simplifies many calculations in kinetic theory[6][8].

- Free molecular flow

$$Kn > 10.$$

Typically, in the continuum regime the flow and temperature field is modeled with conventional continuum mechanics, with the laws of Navier-Stokes and Fourier (NSF) [3][15] with no slip or jump boundary conditions at the walls. This no slip and jump condition means that temperature and velocity of the gas at the wall appear to be the temperature and velocity of the wall.

The slip flow regime is well approximated by using the NSF equations with velocity slip and temperature jump boundary conditions [2][3][8][16], which read,

$$v_i - v_w = \frac{2-\theta}{\theta} l \left(\frac{\partial v_i}{\partial x_j} \right) n_j + \frac{3}{4\sqrt{\pi}} l \sqrt{\frac{2kT}{m}} \frac{1}{T} \left(\frac{\partial T}{\partial x_i} + \frac{\partial T}{\partial x_j} n_i n_j \right), \tag{2.8}$$

$$T - T_w = \frac{2-\theta}{\theta} \frac{15}{8} l \left(\frac{\partial T}{\partial x_j} \right) n_j - \frac{1}{3\sqrt{\pi}} l \sqrt{\frac{2m}{kT}} T \left(\frac{\partial v_i}{\partial x_i} \right). \tag{2.9}$$

Here, θ is the accommodation coefficient which reflects the proportion of energy and tangential momentum exchanged between gas particles and wall particles. Jump and slip are proportional to the mean free path l or the Knudsen number Kn when a dimensionless formulation is used. This implies that jump and slip vanish for small Knudsen numbers, that is in the continuum regime.

In the transition regime the best accepted method of modeling the flow field is the direct simulation Monte-Carlo (DSMC) method [17]. This method, however, is very computationally intensive and as such must be limited to relatively simple flows [18].

Attempts are currently being made to model transition flows using various continuum techniques. This is most successfully being done using kinetic theory and the Boltzmann equation to derive with higher-order[2] continuum models. There are two predominant approaches, either the Burnett equations, obtained via the Chapmann-Enskog expansion of the Boltzmann equation [6][7][8], or the method of moments [6][10][19].

[2]Higher order than Navier Stokes and Fourier.

The Chapmann-Enskog expansion involves expanding the phase density in a power series of the Knudsen number. In this way one can derive the equations of Euler at zeroth order, the Navier-Stokes and Fourier equations at first order and the Burnett equations at second order. Until recently, the Burnett equations have not been used in numerical simulations due to instabilities for high frequency processes and missing boundary conditions. Lockerby & Reese [7], however, have claimed to avoid the extra boundary conditions, at steady state, through a corrected implementation of approximate boundary conditions in the numerical method. Higher order expansions, equations such as super-Burnett [9], have proven to be excessively complex and difficult to work with and as such have only been used to make corrections to the lower order equations [7].

The moment method involves replacing the Boltzmann equation by a set of first order partial differential equations for moments of the distribution function. Closure of the equations is obtained by approximating the phase density with an expansion in Hermite polynomials about the equilibrium distribution. This closure is referred to as Grad's closure [5]. The moment method with Grad closure has shown some promising results [10][12][19]. The moment method with 13 moments will be discussed further in subsequent sections.

More recent work [11] has led to a method of combining the Chapman-Enskog and Grad's closure method to produce a new system of 13 moment equations. These are known as the regularized 13 moment (R13) equations and will be discussed in Chapter 5.

2.2 Grads 13 moment theory

2.2.1 Basic qualities

Grad's moment method is based on kinetic theory and the Boltzmann equation. Kinetic theory accounts statistically for the particle movement and interaction through the phase density function. $f(x_i, t, c_i)$ is the phase density function, where $f d\boldsymbol{x} d\boldsymbol{c}$ is the number of particles in phase space element, $d\boldsymbol{x}d\boldsymbol{c}$, at a given position, time, and particle velocity. The

equation that governs the phase density is the Boltzmann equation [6],

$$\frac{\partial f}{\partial t} + c_k \frac{\partial f}{\partial x_k} = S(f), \tag{2.10}$$

where $S(f)$ is the collision term which accounts for particle interaction and is given by

$$S(f) = \int_{-\infty}^{\infty} \int_{\varepsilon=0}^{2\pi} \int_{\theta=0}^{\frac{\pi}{2}} \left(f' f_1' - f f_1\right) \sigma g \sin\theta \, d\theta d\varepsilon d\boldsymbol{c}_1. \tag{2.11}$$

Here, $f' = f(\boldsymbol{x}, t, \boldsymbol{c}')$ and the prime indicates the second particle. $\boldsymbol{c}$, $\boldsymbol{c}'$ are particle velocities before collision and $\boldsymbol{c}_1$, $\boldsymbol{c}_1'$ are particle velocities after the collision.

From the phase density one can calculate it's moments. Some of these moments are the mass density ρ, the momentum density ρv_i, pressure tensor p_{ij}, heat flux q_i and the energy density $\rho\varepsilon$, defined by

$$\begin{aligned}
\rho &= m \int f d\boldsymbol{c}, \\
\rho v_i &= m \int c_i f d\boldsymbol{c}, \\
p_{ij} &= m \int C_i C_j f d\boldsymbol{c}, \\
q_i &= \frac{m}{2} \int C^2 C_i f d\boldsymbol{c}, \\
\rho\varepsilon &= \frac{3}{2}\rho\frac{k}{m}T + \frac{\rho}{2}v^2 = \frac{m}{2}\int c^2 f d\boldsymbol{c},
\end{aligned} \tag{2.12}$$

where $C_i = c_i - v_i$ is the peculiar velocity and v_i is the center of mass velocity of the gas. The pressure tensor p_{ij} is symmetric and will be split into it's trace $p = \frac{1}{3}p_{kk}$, the pressure, and its trace-free-symmetric part $p_{<ij>}$ denoted also by σ_{ij}, given by

$$p_{<ij>} = \sigma_{ij} = p_{ij} - p\delta_{ij}.$$

2.2.2 Standard form

In Grad's moment method [5][6][10][11][19] it is assumed that the state of the gas is satisfactorily described by a set of moments of the phase density,

$$u_A = \int \psi_A(c_k) f dc. \tag{2.13}$$

For Grad's 13 moment method, ψ_A is chosen as $\psi_A = m\left\{1, c_i, \frac{1}{2}C^2, C_{<i}C_{j>}, \frac{1}{2}C^2 C_i\right\}$, where $A_{<ij>}$ indicates the trace free parts of the tensor A_{ij}. This corresponds to the moments ρ, ρv_i, $\frac{3}{2}\rho\frac{k}{m}T$, $p_{<ij>}$, q_i. Higher order expansions corresponding to more moments are possible [6][10][19][20], but will not be discussed here. The moment equations are obtained by multiplying the Boltzmann equation (2.10) with ψ_A and integrating over the velocity space. The resulting sets of equations are

$$\frac{\partial \rho}{\partial t} + \frac{\partial \rho v_k}{\partial x_k} = 0, \tag{2.14}$$

$$\frac{\partial \rho v_i}{\partial t} + \frac{\partial \left(\rho v_i v_k + p_{ik}\right)}{\partial x_k} = 0, \tag{2.15}$$

$$\frac{\partial \rho u}{\partial t} + \frac{\partial \left(\rho u v_k + q_k\right)}{\partial x_k} + p_{ik}\frac{\partial v_i}{\partial x_k} = 0, \tag{2.16}$$

$$\frac{\partial \sigma_{ij}}{\partial t} + \frac{4}{5}\frac{\partial q_{<i}}{\partial x_{j>}} + \frac{\partial \sigma_{ij} v_k}{\partial x_k} + \frac{\partial \varphi_{<ijk>}}{\partial x_k} + 2\sigma_{k<i}\frac{\partial v_{j>}}{\partial x_k} + 2p\frac{\partial v_{<i}}{\partial x_{j>}} = -\frac{\sigma_{ij}}{\tau}, \tag{2.17}$$

$$\begin{aligned} &\frac{\partial q_i}{\partial t} + \frac{\partial q_i v_k}{\partial x_k} + \frac{1}{2}\frac{\partial \varphi_{rr<ik>}}{\partial x_k} + \frac{1}{6}\frac{\partial \varphi_{rrss}}{\partial x_i} + \frac{7}{5}q_k\frac{\partial v_i}{\partial x_k} + \frac{2}{5}q_i\frac{\partial v_k}{\partial x_k} \\ &\quad -\frac{5}{2}\frac{k}{m}\sigma_{ik}\frac{\partial T}{\partial x_k} + \frac{2}{5}q_i\frac{\partial v_i}{\partial x_k} - \frac{\sigma_{ij}}{\rho}\frac{\partial \sigma_{jk}}{\partial x_k} - \frac{\sigma_{ik}}{\rho}\frac{\partial p}{\partial x_k} \\ &\quad -\frac{5}{2}\frac{k}{m}T\frac{\partial \sigma_{ik}}{\partial x_k} - \frac{5}{2}p\frac{k}{m}\frac{\partial T}{\partial x_k} + \varphi_{<ijk>}\frac{\partial v_j}{\partial x_k} = -\frac{2}{3}\frac{q_i}{\tau}. \end{aligned} \tag{2.18}$$

The collision time τ is given by Eqn. (2.4). Equations (2.14)-(2.16) are the conservation laws for mass, momentum and energy. Equation (2.17) is a general balance for the trace free stress tensor σ_{ij} and Eqn. (2.18) is a general balance for the heat flux q_i.

The set of equations is not closed, since it contains the additional moments $\varphi_{<ijk>}$, $\varphi_{rr<ik>}$, and φ_{rrss}. In order to close the equations, these must be related to the 13 moments ρ, ρv_i, $\frac{3}{2}\rho\frac{k}{m}T$, $p_{<ij>}$, q_i; this is done by means of Grad's distribution function [5]. This yields

$$\varphi_{<ijk>} = 0, \tag{2.19}$$

$$\varphi_{rr<ik>} = 7\frac{p}{\rho}p_{<ij>}, \tag{2.20}$$

$$\varphi_{rrss} = 15\frac{p^2}{\rho}. \tag{2.21}$$

The resulting moment equations are the balance laws Eqn.s (2.14)-(2.16) and the following two equations:

$$\frac{\partial p_{<ij>}}{\partial t} + \frac{4}{5}\frac{\partial q_{<i}}{\partial x_{j>}} + \frac{\partial p_{<ij>}v_k}{\partial x_k} + 2p_{<k<i>}\frac{\partial v_{j>}}{\partial x_k} + 2p\frac{\partial v_{<i}}{\partial x_{j>}} = -\frac{p_{<ij>}}{\tau}, \tag{2.22}$$

$$\begin{aligned}\frac{\partial q_i}{\partial t} + v_k\frac{\partial q_i}{\partial x_k} + \frac{7}{5}q_k\frac{\partial v_i}{\partial x_k} + \frac{7}{5}q_i\frac{\partial v_k}{\partial x_k} + \frac{2}{5}q_i\frac{\partial v_i}{\partial x_k} + \frac{7}{2}\frac{k}{m}p_{<ik>}\frac{\partial T}{\partial x_k} + \\ -\frac{p_{<ij>}}{\rho}\frac{\partial p_{<jk>}}{\partial x_k} - \frac{p_{<ik>}}{\rho}\frac{\partial p}{\partial x_k} + \frac{k}{m}T\frac{\partial p_{<ik>}}{\partial x_k} + \frac{5}{2}p\frac{k}{m}\frac{\partial T}{\partial x_k} = -\frac{2}{3}\frac{q_i}{\tau}.\end{aligned} \tag{2.23}$$

The previously shown Grad's closure is done by expanding the phase density around the local Maxwellian as

$$f = f_M\sum_{A=0}^{N}\Lambda_A\left(u_B\right)\psi_A, \tag{2.24}$$

here, the local Maxwellian is denoted as

$$f_M = \frac{\rho}{m}\left(\frac{m}{2\pi\, kT}\right)^{\frac{3}{2}}e^{-\frac{m}{2kt}C^2}. \tag{2.25}$$

The coefficients Λ_A of the expansion follow from the inversion of Eqn. (2.13) [5][21]. Expanded to the 13 moment case, Grad's phase density becomes

$$f = f_M\left[1 + \frac{\sigma_{ij}}{p}\frac{m}{2kT}C_iC_j + \frac{2}{5}\frac{\rho}{p^2}q_iC_i\left(\frac{m}{2kT}C^2 - \frac{5}{2}\right)\right]. \tag{2.26}$$

2.2.3 Conservative form

Choosing moments of the particle velocity c_i rather than the peculiar velocity C_i and following the same procedure yields the Grad 13 equations in conservative form. The moments now become,

$$\begin{aligned}
\rho v_k &= \int m c_k f d\mathbf{c}, \\
p_{ik} + \rho v_i v_k &= \int m c_i c_k f d\mathbf{c}, \\
\frac{3}{2}p + \rho v^2 = \rho\varepsilon &= \int \frac{m}{2} c^2 f d\mathbf{c}, \\
q_k + p_{ik}v_i + \frac{3}{2}pv_k + \frac{\rho}{2}v^2 v_k &= \int \frac{m}{2} c^2 c_k f d\mathbf{c}, \\
\sigma_{<ij>} + \rho v_{<i} v_{j>} &= \int m c_{<i} c_{j>} f d\mathbf{c}, \\
\rho_{<ij>k} + 2v_{<i}p_{j>k} + p_{<ij>}v_k + \rho v_{<i}v_{j>}v_k &= \int m c_{<i} c_{j>} c_k f d\mathbf{c}, \\
q_i + p_{ni}v_n + \frac{3}{2}pv_i + \frac{1}{2}\rho v^2 v_i &= \int \frac{m}{2} c^2 c_i f d\mathbf{c}, \\
\frac{1}{2}\rho_{nnik} + v_n\rho_{nik} + \frac{1}{2}v^2 p_{ik} + v_i q_k + v_n v_i p_{nk} & \\
+ v_k q_i + v_n v_k p_{ni} + \frac{3}{2}v_i v_k p + \frac{1}{2}\rho v^2 v_i v_k &= \int \frac{m}{2} c^2 c_i c_k f d\mathbf{c}.
\end{aligned} \tag{2.27}$$

Using the previously used closure, Eqn. (2.26), gives the moment equations in conservative from [22]

$$\frac{\partial \rho}{\partial t} + \frac{\partial (\rho v_k)}{\partial x_k} = 0, \tag{2.28}$$

$$\frac{\partial \rho v_i}{\partial t} + \frac{\partial (p_{ik} + \rho v_i v_k)}{\partial x_k} = 0, \tag{2.29}$$

$$\frac{\partial \left(\frac{3}{2}p + \frac{\rho}{2}v^2\right)}{\partial t} + \frac{\partial}{\partial x_k}\left(q_k + p_{ik}v_i + \frac{3}{2}pv_k + \frac{\rho}{2}v^2 v_k\right) = 0, \tag{2.30}$$

$$\frac{\partial (p_{<ij>} + \rho v_{<i} v)}{\partial t} \tag{2.31}$$

$$+\frac{\partial}{\partial x_k}\left(\frac{2}{5}\left(q_{<i}\delta_{j>k} + q_{<j}\delta_{i>k}\right) + 2v_{<i}p_{j>k} + p_{<ij>}v_k + \rho v_{<i}v_{j>}v_k\right) = -\frac{p_{<ij>}}{\tau}, \tag{2.32}$$

$$\begin{aligned}
&\frac{\partial}{\partial t}\left(q_i + p_{ni}v_n + \frac{3}{2}pv_i + \frac{1}{2}\rho v^2 v_i\right) \\
&+\frac{\partial}{\partial x_k}\left(\frac{7}{2}RTp_{<ik>} + \frac{5}{2}\frac{p^2}{\rho}\delta_{ik} + \frac{2}{5}q_n v_n \delta_{ik} + \frac{7}{5}q_i v_k + \frac{7}{5}q_k v_i + \frac{1}{2}v^2 p_{ik}\right. \\
&\left.+v_n v_i p_{nk} + v_n v_k p_{ni} + \frac{3}{2}v_i v_k p + \frac{1}{2}\rho v^2 v_i v_k\right) = -\frac{1}{\tau}\left(v_n p_{<ir>} + \frac{2}{3}q_i\right).
\end{aligned} \tag{2.33}$$

The equations above in conservative form are, of course, fully equivalent to Eqn.s (2.14), (2.15), (2.16), (2.22) and (2.23) and can be obtained by suitable linear combinations of these. Some numerical methods are designed for equations of this form while others are better suited to the other form, hence we present both forms.

Boundary conditions must be found for both forms of the Grad 13 equations. This presents some difficulty for a rarefied gas, as temperature jump and slip must be accounted for. Struchtrup & Weiss [20] suggest a method for this, which is discussed further in subsequent sections.

2.3 Direct simulation Monte Carlo

The Direct simulation Monte Carlo or DSMC method is often used as a generally accepted model for rarefied gas flow [2][3][4][7][16][23]. In fact the DSMC method is considered as a method for solving the Boltzmann equation [4]. Its shortcomings are that it is computationally intensive for smaller Knudsen number flows, such as in the slip flow regime and that it is not applicable to unsteady flows. We will use DSMC simulations in lieu of experimental results where many properties just cannot be measured.

The DSMC method considers sample molecules to describe the gas, where a number of sample molecules is considerably smaller than the actual number of particles in the flow. The sample particles undergo periods of free flight and collisions, where the velocities after the collisions are computed from statistical rules. Calculation of interactions and motion of particles are approximated over small time steps relative to the mean free time so that collisions and movement can be uncoupled. More information on the Monte Carlo method can be found in Ref. [4].

DSMC calculations in this thesis were carried out by other members of our research group[3]. This was done to facilitate this work and other work carried out by our group.

2.4 Plane Couette flow

Plane Couette flow is a standard benchmark problem for rarefied gas flows. Many different investigations have looked at Couette flow [2][3][7][12][16][19][23].

Plane Couette flow is the flow between two infinite parallel plates generated solely by relative motion of the plates, shown in Fig. 2-1 below. The flow is simple, and thus the equations are relatively easy to solve. Interesting rarefaction phenomena are present, however, such as temperature jump, velocity slip and heat flow parallel to the plates which is not driven by a temperature gradient and non-uniform pressure

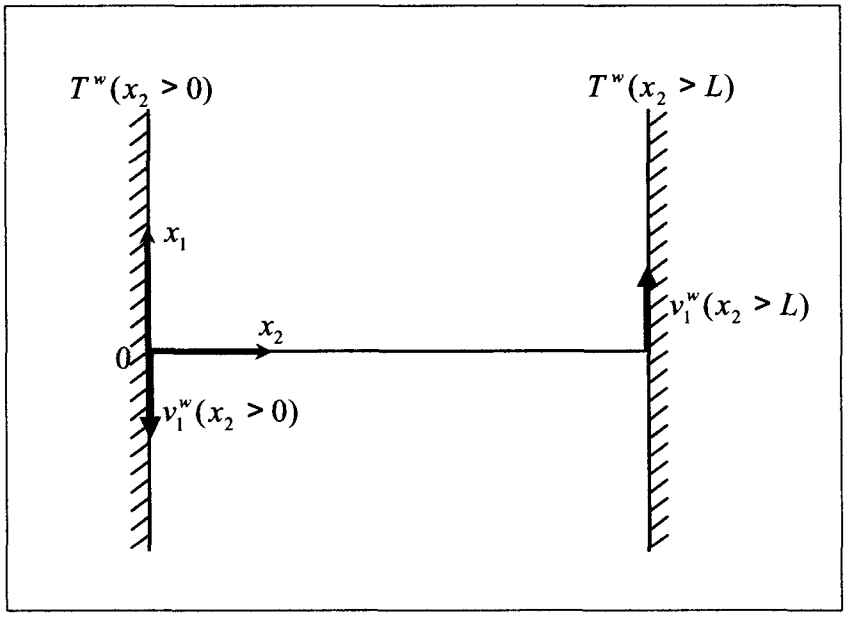

Figure 2-1: Plane Couette flow.

The characteristic length that determines the Knudsen number is the distance separating

[3]I would like to thank Adam Schuetze for this work.

the plates, denoted as L in Fig. 2-1 above. The key assumptions that we make are:

- The flow is laminar and no other external forces are acting on the fluid.
- Only two dimensions are considered.
- Temperature and velocities of the plates are prescribed.
- All quantities depend only on the space coordinate, x_2.

Although the temperature, pressure and velocity fields are uniform in the x_1 direction, the various fluxes are not necessarily only in the x_2 direction [2][3][7][16].

It is prudent to represent the equations in dimensionless form. The dimensionless variables are introduced as $\hat{T} = \frac{T}{T_0}$, $\hat{v} = \frac{v}{v_0}$ where $v_0 = \sqrt{\frac{k}{m}T_0}$, $\hat{x}_2 = \frac{x_2}{L}$, $\hat{p} = \frac{p}{p_0}$ where $p_0 = \rho_0 \frac{k}{m} T_0$, $\hat{\rho} = \frac{\rho}{\rho_0}$ where $\rho_0 = \frac{p_0}{\frac{k}{m}T_0}$, $\hat{q} = \frac{q}{q_0}$ where $q_0 = \rho_0 \left(\frac{k}{m}T_0\right)^{\frac{3}{2}}$ and $\hat{\mu} = \frac{\mu}{\mu 0}$ where $\mu_0 = Kn\frac{p_0 L}{\sqrt{\frac{k}{m}T_0}}$. The reference properties T_0, v_0 and ρ_0 have been chosen as

$$T_0 = \frac{1}{2}\left[T^w\left(x_2 = 0\right) + T^w\left(x_2 = L\right)\right],$$
$$v_0 = v_1^w\left(x_2 = 0\right),$$
$$\rho_0 = \frac{1}{L}\int \rho dx.$$

Recalling Eqn.s (2.4) and (2.6), we can find $\tau = \frac{\hat{\mu}}{\hat{p}} Kn \frac{L}{\sqrt{\frac{k}{m}T_0}}$ where $\hat{\mu} = \hat{T}^s$. In steady state, the velocity perpendicular to the plates, v_2, vanishes. In the impending sections we shall be interested in computing the steady state and thus can set $v_2 = 0$.

The numerical methods used will be time dependent, so that the assumption $v_2 = 0$ can be violated. A simple method which allows to use $v_2 = 0$ throughout a time dependent computation relies on readjusting the mass during the computation. This must be done as follows: The 2^{nd} component of the momentum balance (with $v_2 = 0$) assumes the form

$$\frac{\partial\left(\hat{p} + \hat{p}_{<22>}\right)}{\partial \hat{x}_2} = 0 \implies \hat{p} + \hat{p}_{<22>} = \hat{p}_\alpha = const. \tag{2.34}$$

$\hat{p}_a$ is a constant of integration. The integral of density with respect to $\hat{x}_2$ is given by the

initial state, so that

$$\hat{M} = \int_0^1 \hat{\rho} d\hat{x}_2 = \int_0^1 \frac{\hat{p}}{\hat{T}} d\hat{x}_2 = \int_0^1 \frac{\hat{p}_\alpha - \hat{p}_{<22>}}{\hat{T}} d\hat{x}_2 = const. \tag{2.35}$$

With this, the computation of $\hat{v}_2$ is replaced by properly adjusting the constant of integration $\hat{p}_\alpha$.

The normal stress $\hat{p}_{<11>}$ is uncoupled from the equation set and is hence neglected. The resulting set of non-dimensional Grad 13 equations for Couette flow in standard form and with $\hat{v}_2 = 0$, are:

The momentum balance equations are

$$\frac{\partial \hat{\rho}\hat{v}_1}{\partial \hat{t}} + \frac{\partial \hat{p}_{<12>}}{\partial \hat{x}_2} = 0, \tag{2.36}$$

The energy balance equation is,

$$\frac{\partial \hat{\rho}\hat{u}}{\partial \hat{t}} + \frac{\partial \hat{q}_2}{\partial \hat{x}_2} + \hat{p}_{<12>}\frac{\partial \hat{v}_1}{\partial \hat{x}_2} = 0. \tag{2.37}$$

The pressure tensor equations are

$$\frac{\partial \hat{p}_{<12>}}{\partial \hat{t}} + \frac{2}{5}\frac{\partial \hat{q}_1}{\partial \hat{x}_2} + \hat{p}_\alpha \frac{\partial \hat{v}_1}{\partial \hat{x}_2} = -\frac{1}{Kn}\frac{\hat{p}}{\hat{\mu}}\hat{p}_{<12>}, \tag{2.38}$$

$$\frac{\partial \hat{p}_{<22>}}{\partial \hat{t}} + \frac{6}{5}\frac{\partial \hat{q}_2}{\partial \hat{x}_2} = -\frac{1}{Kn}\frac{\hat{p}}{\hat{\mu}}\hat{p}_{<22>}. \tag{2.39}$$

The heat flux equations are

$$\frac{\partial \hat{q}_1}{\partial \hat{t}} + \frac{7}{5}\hat{q}_2\frac{\partial \hat{v}_1}{\partial \hat{x}_2} + \frac{7}{2}\hat{p}_{<12>}\frac{\partial \hat{T}}{\partial \hat{x}_2} = -\frac{1}{Kn}\frac{\hat{p}}{\hat{\mu}}\hat{q}_1, \tag{2.40}$$

$$\frac{\partial \hat{q}_2}{\partial \hat{t}} + \frac{2}{5}\hat{q}_1\frac{\partial \hat{v}_1}{\partial \hat{x}_2} + \frac{5}{2}\left(\hat{p}_\alpha + \frac{2}{5}\hat{p}_{<22>}\right)\frac{\partial \hat{T}}{\partial \hat{x}_2} - \hat{T}\frac{\partial \hat{p}}{\partial \hat{x}_2} = -\frac{1}{Kn}\frac{\hat{p}}{\hat{\mu}}\frac{2}{3}\hat{q}_2. \tag{2.41}$$

In conservative form the equations for $\hat{\sigma}_{<11>}$ and $\hat{v}_2$ are not uncoupled and thus cannot be neglected as in the divergent form of the equations. The conservative form of the Grad 13 equations for Couette flow are given below.

The mass balance equation is

$$\frac{\partial \hat{\rho}}{\partial \hat{t}} + \frac{\partial \left(\hat{\rho}\hat{v}_2\right)}{\partial \hat{x}_2} = 0. \tag{2.42}$$

The momentum balance equations are

$$\frac{\partial \hat{\rho}\hat{v}_1}{\partial \hat{t}} + \frac{\partial \left(\hat{\sigma}_{12} + \hat{\rho}\hat{v}_1\hat{v}_2\right)}{\partial \hat{x}_2} = 0, \tag{2.43}$$

$$\frac{\partial \hat{\rho}\hat{v}_2}{\partial \hat{t}} + \frac{\partial \left(\hat{\sigma}_{22} + \hat{p} + \hat{\rho}\hat{v}_2^2\right)}{\partial \hat{x}_2} = 0. \tag{2.44}$$

The energy balance equation is

$$\frac{\partial \left(\frac{3}{2}\hat{p} + \frac{\hat{\rho}}{2}\left(\hat{v}_1^2 + \hat{v}_2^2\right)\right)}{\partial \hat{t}} + \frac{\partial \left(\frac{5}{2}\hat{p}\hat{v}_2 + \hat{q}_2 + \hat{\sigma}_{12}\hat{v}_1 + \hat{\sigma}_{22}\hat{v}_2 + \frac{\hat{\rho}}{2}\left(\hat{v}_1^2 + \hat{v}_2^2\right)\hat{v}_2\right)}{\partial \hat{x}_2} = 0. \tag{2.45}$$

The pressure tensor equations are

$$\frac{\partial \left(\hat{\sigma}_{12} + \hat{\rho}\hat{v}_1\hat{v}_2\right)}{\partial \hat{t}} + \frac{\partial \left(\frac{2}{5}\hat{q}_1 + \hat{v}_1\left(\hat{\sigma}_{22} + \hat{p}\right) + 2\hat{v}_2\hat{\sigma}_{12} + \hat{\rho}\hat{v}_1\hat{v}_2\hat{v}_2\right)}{\partial \hat{x}_2} = -\frac{\hat{p}}{\hat{\mu}}\frac{\hat{\sigma}_{12}}{Kn}, \tag{2.46}$$

$$\frac{\partial \left(\hat{\sigma}_{11} + \hat{\rho}\hat{v}_1^2 - \frac{1}{3}\hat{\rho}\left(\hat{v}_1^2 + \hat{v}_2^2\right)\right)}{\partial t} + \frac{\partial \left(-\frac{4}{15}\hat{q}_2 + \frac{4}{3}\hat{v}_1\hat{\sigma}_{12} - \frac{2}{3}\hat{v}_2\left(\hat{\sigma}_{22} + \hat{p}\right) + \hat{\sigma}_{11}\hat{v}_2 + \hat{\rho}\left(\frac{2}{3}\hat{v}_1^2\hat{v}_2 - \frac{1}{3}\hat{v}_2^2\hat{v}_2\right)\right)}{\partial \hat{x}_2} = -\frac{\hat{p}}{\hat{\mu}}\frac{\hat{\sigma}_{11}}{Kn}, \tag{2.47}$$

$$\frac{\partial \left(\hat{\sigma}_{22} + \rho\hat{v}_2^2 - \frac{1}{3}\hat{\rho}\left(\hat{v}_1^2 + \hat{v}_2^2\right)\right)}{\partial \hat{t}} + \frac{\partial \left(\frac{8}{15}\hat{q}_2 + \hat{v}_2\left(\frac{7}{3}\hat{\sigma}_{22} + \frac{4}{3}\hat{p}\right) - \frac{2}{3}\hat{v}_1\hat{\sigma}_{12} + \hat{\rho}\left(\frac{2}{3}\hat{v}_2^2\hat{v}_2 - \frac{1}{3}\hat{v}_1^2\hat{v}_2\right)\right)}{\partial \hat{x}_2} = -\frac{\hat{p}}{\hat{\mu}}\frac{\hat{\sigma}_{22}}{Kn}. \tag{2.48}$$

The last two equations can be simplified by adding $\frac{2}{3}\times$ energy balance. This is useful as it uncouples the gradients of $\hat{\sigma}_{11}$ and $\hat{\sigma}_{22}$ in the $\hat{\sigma}_{11}$ and $\hat{\sigma}_{22}$ equations. The resulting $\hat{\sigma}_{11}$ and

$\hat{\sigma}_{22}$ equations are

$$\frac{\partial\left(\hat{p}+\hat{\sigma}_{11}+\hat{\rho}\hat{v}_1^2\right)}{\partial\hat{t}}+\frac{\partial\left(\frac{2}{5}\hat{q}_2+2\hat{v}_1\hat{\sigma}_{12}+\hat{v}_2\left(\hat{\sigma}_{11}+\hat{p}\right)+\hat{\rho}\hat{v}_1^2\hat{v}_2\right)}{\partial\hat{x}_2}=-\frac{\hat{p}}{\hat{\mu}}\frac{\hat{\sigma}_{11}}{Kn}, \tag{2.49}$$

$$\frac{\partial\left(\hat{p}+\hat{\sigma}_{22}+\rho\hat{v}_2^2\right)}{\partial\hat{t}}+\frac{\partial\left(\frac{6}{5}\hat{q}_2+3\hat{v}_2\left(\hat{\sigma}_{22}+\hat{p}\right)+\hat{\rho}\hat{v}_2^2\hat{v}_2\right)}{\partial\hat{x}_2}=-\frac{\hat{p}}{\hat{\mu}}\frac{\hat{\sigma}_{22}}{Kn}. \tag{2.50}$$

The heat flux equations are

$$\begin{aligned}&\frac{\partial\left(\hat{q}_1+\hat{\sigma}_{11}\hat{v}_1+\hat{\sigma}_{12}\hat{v}_2+\frac{5}{2}\hat{p}\hat{v}_1+\frac{1}{2}\hat{\rho}\left(\hat{v}_1^2+\hat{v}_2^2\right)\hat{v}_1\right)}{\partial\hat{t}}\\&+\frac{\partial}{\partial\hat{x}_2}\left(\frac{7}{2}\frac{\hat{p}}{\hat{\rho}}\hat{\sigma}_{12}+\frac{7}{5}\hat{q}_1\hat{v}_2+\frac{7}{5}\hat{q}_2\hat{v}_1+\frac{1}{2}\hat{v}^2\hat{\sigma}_{12}+\hat{v}_1^2\hat{\sigma}_{12}+\hat{v}_2\hat{v}_1\hat{\sigma}_{22}+\hat{v}_2^2\hat{\sigma}_{12}\right.\\&\left.+\hat{v}_1\hat{v}_2\hat{\sigma}_{11}+\frac{7}{2}\hat{v}_1\hat{v}_2\hat{p}+\frac{1}{2}\hat{\rho}\hat{v}^2\hat{v}_1\hat{v}_2\right)=-\frac{\hat{p}}{\hat{\mu}}\frac{1}{Kn}\left(\hat{v}_1\hat{\sigma}_{11}+\hat{v}_2\hat{\sigma}_{12}+\frac{2}{3}\hat{q}_1\right),\end{aligned} \tag{2.51}$$

$$\begin{aligned}&\frac{\partial\left(\hat{q}_2+\hat{\sigma}_{22}\hat{v}_2+\hat{\sigma}_{12}\hat{v}_1+\frac{5}{2}\hat{p}\hat{v}_2+\frac{1}{2}\hat{\rho}\left(\hat{v}_1^2+\hat{v}_2^2\right)\hat{v}_2\right)}{\partial\hat{t}}\\&+\frac{\partial}{\partial\hat{x}_2}\left(\frac{7}{2}\frac{\hat{p}}{\hat{\rho}}\hat{\sigma}_{22}+\frac{5}{2}\frac{\hat{p}^2}{\hat{\rho}}+\frac{16}{5}\hat{v}_2\hat{q}_2+\frac{2}{5}\hat{q}_1\hat{v}_1+\frac{1}{2}\hat{v}^2\left(\hat{p}+\hat{\sigma}_{22}\right)+2\hat{v}_1\hat{v}_2\hat{\sigma}_{12}\right.\\&\left.+2\hat{v}_2^2\hat{\sigma}_{22}+\frac{7}{2}\hat{v}_2^2\hat{p}+\frac{1}{2}\hat{\rho}\hat{v}^2\hat{v}_2^2\right)=-\frac{\hat{p}}{\hat{\mu}}\frac{1}{Kn}\left(\hat{v}_1\hat{\sigma}_{12}+\hat{v}_2\hat{\sigma}_{22}+\frac{2}{3}\hat{q}_2\right).\end{aligned} \tag{2.52}$$

2.5 Boundary conditions

Providing boundary conditions presents a problem for moment theories as many of the moments require boundary conditions, and only few boundary values are controlled in experiments. Some of these are subject to jump and slip in rarefied flows. We look at the basic properties of the phase density and the forces and fluxes at the boundary, to compute boundary conditions.

2.5.1 Maxwell Boundary Conditions

The most commonly used boundary conditions for the Boltzmann Eqn. (2.10) follow from Maxwell's boundary conditions for the phase density [21]. These are based on the assump-

tion that particles interact with the wall in only two ways: A particle that collides with the wall is either specularly reflected or undergoes an entirely diffuse interaction (thermalization). In specular reflection the particle keeps all its momentum except that the component normal to the wall is reversed, in particular no energy is exchanged between the wall and the particle, only normal momentum. The diffuse interacting particles are thermalized at the wall and leave the wall with a velocity characterized by the Maxwell distribution at the wall temperature and velocity. The fraction of particles that are thermalized is represented by the accommodation coefficient θ. Combining these two effects gives way to the boundary condition for the phase density

$$\hat{f} = \begin{cases} \theta f_w + (1-\theta) f_G\left(-n_k C_k^w\right), & n_k C_k^w \geq 0 \\ f_N & n_k C_k^w \leq 0 \end{cases}. \tag{2.53}$$

n_k is the normal of the wall, pointing into the gas, f_G denotes the distribution directly at the wall, and $f_G\left(-n_k C_k^w\right)$ is the corresponding distribution of elastically reflected particles. Here f_w is the Maxwellian of thermalized particles at wall conditions,

$$f_w = f_m(\rho_w, T_w, v_i^w) = \frac{\rho_w}{m}\left(\frac{m}{2\pi k T_w}\right)^{\frac{3}{2}} e^{-\frac{m}{2kT_w}\left(c_k - v_k^w\right)^2}. \tag{2.54}$$

The density of thermalized particles ρ_w follows from the condition that no particles are accumulated at the wall, i.e., mass flow to the wall is equal to mass flow away from the wall. This can be formulated as,

$$m\int_{n_k C_k^w \geq 0} \hat{f} C_k^w n_k d\boldsymbol{c} = -m\int_{n_k C_k^w \leq 0} \hat{f} C_k^w n_k d\boldsymbol{c}. \tag{2.55}$$

2.5.2 Flux Boundary Conditions

Consider a moment represented as a quantity u_A, its flux F_{Ak} and its production P_A, given by:

$$u_A = m \int \psi_A f d\boldsymbol{c}, \tag{2.56}$$

$$F_{Ak} = m \int \psi_A c_k f d\boldsymbol{c}, \tag{2.57}$$

$$P_A = m \int \psi_A S d\boldsymbol{c}. \tag{2.58}$$

Introducing these terms into the Boltzmann equation (2.10) and integrating gives a basic conservation equation,

$$\frac{\partial u_A}{\partial t} + \frac{\partial F_{Ak}}{\partial x_k} = P_A. \tag{2.59}$$

Equation (2.59) is then integrated over the boundary element dV shown in Figure 2-2.

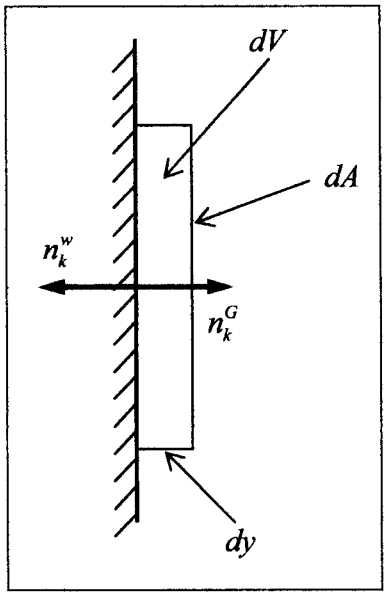

Figure 2-2: Boundary Layer

The resulting balance is

$$\int_{dV} \frac{\partial u_A}{\partial t} dV + \oint_{\partial V} F_{Ak} n_k dA = \int_{dV} P_A dV. \tag{2.60}$$

Now we can let the boundary element thickness go to zero, $dy \to 0$, which yields

$$\oint_{\partial V} F_{Ak} n_k dA = 0, \tag{2.61}$$

since the volume integrals vanish. Neglecting the top and bottom of the control volume as $dy \to 0$, leaves just two surfaces over which F_{Ak} can be balanced,

$$\int F^w_{Ak} n^w_k dA - \int F^G_{Ak} n^G_k dA = 0, \tag{2.62}$$

for all A. The superscript G indicates the fluxes in the gas side of the boundary layer. It then follows by introducing Eqn. (2.57) and the Maxwell boundary conditions Eqn. (2.53),

$$m \int \psi_A c_k n_k \left(f_G - \hat{f} \right) d\boldsymbol{c} = 0, \tag{2.63}$$

where f_G is the phase density due to the gas properties and $\hat{f}$ is Maxwell's boundary phase density of equation (2.53). Dividing up into phase density of particles going right (away from the wall) and those going left (towards the wall),

$$\begin{aligned} & m \int_{c_k n_k \geq 0} c_k n_k \left(f_G - \hat{f} \right) d\boldsymbol{c} + m \int_{c_k n_k \leq 0} c_k n_k \left(f_G - \hat{f} \right) d\boldsymbol{c} = 0, \quad f_G \; for \; C^w_k n_k < 0 \\ \Longrightarrow \; & m \int_{c_k n_k \geq 0} c_k n_k \left(f_G - \theta f_w - (1-\theta) f_G \left(-n_k C^W_k \right) \right) d\boldsymbol{c} = 0, \end{aligned} \tag{2.64}$$

where $f_G \cong f_{13}$, as given in Eqn. (2.26).

Noting that,

$$C_k^w = c_k - v_k^w,$$
$$V_k = v_k - v_k^w,$$
$$\Rightarrow C_k = c_k - v_k = C_k^w + v_k^w - v_k = C_k^w - V_k,$$

and for a solid surface,

$$V_k n_k = 0,$$
$$\Rightarrow C_k n_k = C_k^w n_k.$$

Now Eqn. (2.63) can be used to find boundary conditions for the various moments.

1. Mass: $\psi_A = 1$,

$$m \int\limits_{c_k n_k \geq 0} 1 C_k^w n_k \left(f_G - \hat{f} \right) d\boldsymbol{c} = 0 \tag{2.65}$$

where $\hat{f}$ is the Maxwell condition at the wall as in Eqn. (2.53) and f_G is the phase density of the gas represented by Grad's phase density Eqn. (2.26) for Grad 13 equations.

Now converting to spherical coordinates, where $n_k = \{\cos\theta \sin\phi,\ \sin\theta \sin\phi,\ \cos\phi\}$, and integrating over the half space, yields

$$\Rightarrow \int_0^\infty C^3 \int_{-\pi}^{\pi} \int_0^{\frac{\pi}{2}} \left\{ f_{13}\left(n_k C_k\right) + (1-\theta) f_{13}\left(-n_k C_k\right) \right\} \sin 2\theta \, d\theta d\phi dc$$
$$- \theta \int_0^\infty C^3 f_w \int_{-\pi}^{\pi} \int_0^{\frac{\pi}{2}} \sin 2\theta \, d\theta d\phi dc = 0, \tag{2.66}$$

$$\Rightarrow \int_0^\infty C^3 \int_{-\pi}^{\pi} \int_0^{\frac{\pi}{2}} \left\{ f_{13}\left(n_k C_k\right) + (1-\theta) f_{13}\left(-n_k C_k\right) \right\} \sin 2\theta \, d\theta d\phi dc - \pi\theta \int_0^\infty C^3 f_w dc = 0, \tag{2.67}$$

$$\begin{aligned}
&\Rightarrow \pi \int_0^\infty C^3 (2-\theta) f_M dc \\
&+ \frac{p_{<ij>}}{p} \frac{m}{2kT} \int_0^\infty C^3 \int_{-\pi}^{\pi} \int_0^{\frac{\pi}{2}} C_i C_j (2-\theta) f_M \sin 2\theta \, d\theta d\phi dc + \ldots \\
&- \theta\pi \int_0^\infty C^3 f_w dc = 0.
\end{aligned} \tag{2.68}$$

The terms indicated by ... can be shown to cancel to zero. This integration is then preformed by considering the integration over the half space angles. It follows that

$$\frac{1}{2\pi} \int_{-\pi}^{\pi} \int_0^{\frac{\pi}{2}} C_i C_j \sin 2\theta d\theta d\phi = C^2 \left(a\delta_{ij} + b n_i n_j \right). \tag{2.69}$$

Now multiplying both the integral and the integrand by δ_{ij},

$$\begin{aligned}
\frac{1}{2\pi} \int_{-\pi}^{\pi} \int_0^{\frac{\pi}{2}} C^2 \sin 2\theta d\theta d\phi &= C^2 (3a + b), \\
\Rightarrow 3a + b &= \frac{1}{2}.
\end{aligned} \tag{2.70}$$

Now multiplying both integral and integrand by $n_i n_j$,

$$\begin{aligned}
\frac{1}{2\pi} \int_{-\pi}^{\pi} \int_0^{\frac{\pi}{2}} (C_i n_i)^2 \sin 2\theta d\theta d\phi &= C^2 (a + b), \\
\Rightarrow a + b &= \frac{1}{4}.
\end{aligned} \tag{2.71}$$

This becomes two equations for the two unknowns resulting in $a = \frac{1}{8}$ and $b = \frac{1}{8}$. It then follows that the remaining half space integral is,

$$\begin{aligned}
&\pi \int_0^\infty C^3 (2-\theta) f_M dc \\
&+ 2\pi \frac{p_{<ij>}}{p} \frac{m}{2kT} \int_0^\infty C^5 (2-\theta) f_M \left(\frac{1}{8}\delta_{ij} + \frac{1}{8} n_i n_j \right) dc \\
&- \theta\pi \int_0^\infty C^3 \hat{f} dc = 0.
\end{aligned} \tag{2.72}$$

This is then integrated over the velocity,

$$\begin{aligned}
&(2-\theta)\,\frac{\rho}{m}\left(\frac{1}{\pi}\right)^{\frac{3}{2}}\left(\frac{m}{2kT}\right)^{-\frac{1}{2}} \\
&+(2-\theta)\,\frac{1}{2}\frac{p_{<ij>}}{p}\frac{m}{2kT}\frac{\rho}{m}\left(\frac{1}{\pi}\right)^{\frac{3}{2}}\left(\frac{m}{2kT}\right)^{-\frac{3}{2}} n_i n_j \\
&-\theta\frac{\rho_w}{m}\left(\frac{1}{\pi}\right)^{\frac{3}{2}}\left(\frac{m}{2kT_w}\right)^{-\frac{1}{2}} = 0.
\end{aligned} \tag{2.73}$$

Now considering that $p = \rho\frac{kT}{m}$ and defining $p_{<nn>} = p_{<ij>} n_i n_j$, gives

$$\rho_w\sqrt{\frac{kT_w}{m}} = \frac{2-\theta}{\theta}\sqrt{\frac{m}{kT}}\left(p + \frac{1}{2}p_{<nn>}\right). \tag{2.74}$$

This determines the mass density at the wall ρ_w for its elimination from the momentum and energy fluxes.

2. Momentum: $\psi_A = C_i^w = C_i + V_i$.

   Following a similar procedure of integration as above and incorporating Eqn. (2.74) results in the two momentum balance equations:

   An equation for the slip velocity follows from the tangential momentum,

$$V_i = \frac{-\frac{2-\theta}{\theta}\sqrt{\frac{\pi}{2}\frac{k}{m}T}\left(p_{<in>} - n_i p_{<nn>}\right) - \frac{1}{5}\left(q_i - n_i n_j q_j\right)}{p + \frac{1}{2}p_{<nn>}}. \tag{2.75}$$

   The momentum normal to the wall gives a boundary condition for $p_{<nn>}$,

$$\sqrt{\frac{T_w}{T}}\left(p + \frac{1}{2}p_{<nn>}\right) - \left(p + p_{<nn>}\right) = \frac{2-\theta}{\theta}\sqrt{\frac{2}{\pi}\frac{m}{kT}}\frac{2}{5}q_n. \tag{2.76}$$

3. Energy: $\psi_A = C^2$.

   Following the same procedure of integration as for the previous two balances, gives a condition for the temperature jump,

$$\frac{T_w}{T} - 1 = \frac{\frac{2-\theta}{\theta}\sqrt{\frac{\pi}{2}\frac{m}{kT}}\frac{1}{2}q_n + \frac{1}{4}p_{<nn>}}{p + \frac{1}{2}p_{<nn>}} - \frac{1}{4}\frac{m}{kT}V^2 \tag{2.77}$$

   This equation relates temperature jump to q_n, $p_{<nn>}$ and V_k.

Struchtrup and Weiss [20] follow a similar method that uses the balance of force and continuity of energy flux to arrive at the same results. The second condition for momentum, Eqn. 2.76, however, is new. This set of boundary conditions gives seven boundary equations to compliment the Grad 13 moment equations will turn out to be sufficient for Couette flow.

These methods for finding boundary conditions have been used previously by Chapman and Cowling [8] for jump and slip boundary conditions similar to Eqn.s (2.75 and 2.77).

2.5.3 Adjusting the boundary conditions for the Knudsen layer

It is known that the previous argument for Maxwell boundary conditions neglects the effects of the Knudsen boundary layers [6]. The Knudsen or kinetic boundary layer is a boundary layer that occurs in addition to temperature jump and velocity slip between the wall and bulk flow. It has been successfully modeled to different extents with various approximations of the Boltzmann equation, but not with the Grad 13 moment method or most other continuum solutions [24].

Cercignani [6] and others calculate adjustments to the boundary conditions through the direct solution of simplified models of the Boltzmann equation. The effect of these adjustments can be seen in Fig. 2-3 below.

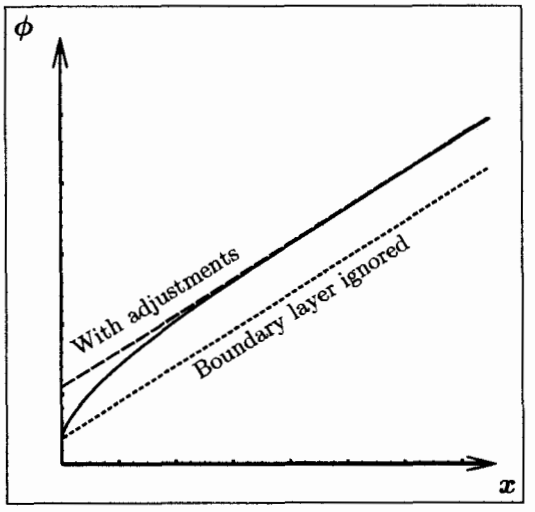

Figure 2-3: Boundary layer adjustments, following [6].

Figure 2-3 shows the actual result (solid line) and the two solutions that don't show the Knudsen layer (dashed), for a generic quantity, ϕ. As Fig.2-3 shows, the Knudsen layer gives an additional contribution to the jump, which should be accommodated.

We introduce the factors α, β and γ to account for these adjustments and they appear in the boundary conditions which are now simplified for Couette flow and in dimensionless form. This Knudsen layer adjustments appear in bold in the following equations,

$$\hat{V}_1 = \frac{-\frac{2-\theta}{\theta}\boldsymbol{\alpha}\sqrt{\frac{\pi}{2}\hat{T}}\hat{p}_{<12>}n_2 - \frac{1}{5}\hat{q}_1}{\hat{p} + \frac{1}{2}\hat{p}_{<22>}}, \tag{2.78}$$

$$\hat{p}_{<22>} = -2\frac{\frac{2-\theta}{\theta}\boldsymbol{\gamma}\frac{2}{5}\sqrt{\frac{\pi}{2}}\hat{q}_2 n_2 + \left(\sqrt{\hat{T}} - \sqrt{\hat{T}_w}\right)p_\alpha}{\sqrt{\hat{T}_w}}, \tag{2.79}$$

$$\frac{\hat{T}_w}{\hat{T}} - 1 = \frac{\frac{2-\theta}{\theta}\boldsymbol{\beta}\sqrt{\frac{\pi}{2}\hat{T}}\frac{1}{2}\hat{q}_2 n_2 + \frac{1}{4}\hat{p}_{<22>}}{\hat{p} + \frac{1}{2}\hat{p}_{<22>}} - \frac{1}{4}\hat{V}^2. \tag{2.80}$$

In Cercignani's book [6] values for α and β are found as $\alpha = 1.1466$ and $\beta = 1.1682$. Cercignani can not find the value of γ as he does not consider the normal force $p_{<nn>}$ boundary condition. The following paragraph will present a method for finding a value for γ.

In Sec. 2.6 it will be seen from the Chapman-Enskog expansion that the contribution of $p_{<22>}$ and q_1 are of second order and greater in the Knudsen number, while $p_{<22>}$, q_1 for Couette flow are of first order. This knowledge of the lowest order contribution can now be used to get an idea of the order of the boundary conditions.

We let ε^n preceding a moment, indicate the n^{th} order of magnitude of that moment. Incorporating this into the boundary condition Eqn.s (2.78)-(2.80) and expanding to the lowest order yields for slip velocity

$$\hat{V}_1 = \frac{-\frac{2-\theta}{\theta}\alpha\sqrt{\frac{\pi}{2}\hat{T}}\varepsilon\hat{p}_{<12>}n_2 - \frac{1}{5}\varepsilon^2\hat{q}_1}{\hat{p}_\alpha - \frac{1}{2}\varepsilon^2\hat{p}_{<22>}} \simeq -\varepsilon\frac{2-\theta}{\theta}\alpha\sqrt{\frac{\pi}{2}}\frac{\hat{p}_{<12>}}{p_\alpha}n_2. \tag{2.81}$$

This shows that the velocity slip $\hat{V}_1$ is of first order in its lowest order contribution. This can now be used to determine the lowest order contribution of the temperature jump condition,

$$\begin{aligned}\frac{\hat{T}_w}{\hat{T}} - 1 &= \frac{\frac{2-\theta}{\theta}\beta\sqrt{\frac{\pi}{2}\hat{T}}\frac{1}{2}\varepsilon\hat{q}_2 n_2 + \frac{1}{4}\varepsilon^2\hat{p}_{<22>}}{\hat{p}_\alpha - \frac{1}{2}\varepsilon^2\hat{p}_{<22>}} - \frac{1}{4}\left(\varepsilon\hat{V}\right)^2 \simeq \varepsilon\frac{2-\theta}{\theta}\beta\sqrt{\frac{\pi}{2}}\frac{1}{2}\frac{\hat{q}_2 n_2}{p_\alpha} \\ &\Longrightarrow \quad \hat{T} - \hat{T}_w \simeq -\varepsilon\frac{2-\theta}{\theta}\beta\sqrt{\frac{\pi}{2}}\frac{1}{2}\frac{\hat{q}_2}{p_\alpha}\hat{T}.\end{aligned} \tag{2.82}$$

This shows the temperature jump is also first order in its lowest order contribution. We now use this in our equation for $p_{<22>}$, Eqn. (2.79), to get

$$\hat{p}_{<22>} = -2\frac{\frac{2-\theta}{\theta}\gamma\frac{2}{5}\sqrt{\frac{\pi}{2}}\varepsilon\hat{q}_2 n_2 + \left(\sqrt{\hat{T}} - \sqrt{\varepsilon\frac{2-\theta}{\theta}\beta\sqrt{\frac{\pi}{2}}\frac{1}{2}\frac{\hat{q}_2 n_2}{p_\alpha}\hat{T} + \hat{T}}\right)p_\alpha}{\sqrt{\varepsilon\frac{2-\theta}{\theta}\beta\sqrt{\frac{\pi}{2}}\frac{1}{2}\frac{\hat{q}_2 n_2}{p_\alpha}\hat{T} + \hat{T}}}. \tag{2.83}$$

This does not yet give a clear idea of order so we take a Taylor series expansion in ε about zero to find,

$$\hat{p}_{<22>} = -\varepsilon\frac{2-\theta}{\theta}\sqrt{\frac{\pi}{2}}\hat{q}_2 n_2\frac{1}{\sqrt{\hat{T}}}\left(\frac{\pi}{4}\beta - \frac{4}{5}\gamma\right), \tag{2.84}$$

as the leading term of the expansion. Now considering that $p_{<22>}$ in the bulk is of second order, (Sec. 2.6), we assume that it must also be so at the boundary. To satisfy this requirement, the first order contribution in Eqn. (2.84) must vanish. Therefore,

$$\gamma = \frac{5\pi}{16}\beta.$$

With the value from Cercignani above for $\beta = 1.1682$, it follows that $\gamma = 1.1469$.

2.6 Chapman-Enskog expansion of the Grad 13 equations

By applying the perturbation method of Chapman and Enskog [6][8][21][24] to the Grad 13 equations, one finds the Navier-Stokes and Fourier equations. This expansion will be demonstrated here only for the equations reduced for Couette flow in divergent form, Eqn.s (2.36)-(2.41) applied to steady state. Expansion of the full Grad 13 equations is left out for brevity, see [11] for this full expansion.

The Chapman-Enskog expansion is based on a power series expansion of non-equilibrium variables with respect to the Knudsen number. For example the variable $p_{<22>}$ becomes,

$$p_{<22>} = p^{(0)}_{<22>} + Kn\, p^{(1)}_{<22>} + Kn^2\, p^{(2)}_{<22>} + \dots , \tag{2.85}$$

$p_{<12>}$, q_1, and q_2 are expanded similarly. The hat indicating dimensionless variables is now dropped and all subsequent terms will be considered dimensionless unless indicated otherwise. The equilibrium quantities ρ, v_i and T are not expanded.

The $p_{<12>}$, $p_{<22>}$, q_1, and q_2 balances of Eqn.s (2.38)-(2.41) can all be written similar to the $p_{<12>}$ balance below,

$$p_{<12>}\frac{p_\alpha - p_{<22>}}{Kn} = -\mu\left(\frac{2}{5}\frac{\partial q_1}{\partial x_2} + p_\alpha\frac{\partial v}{\partial x_2}\right), \tag{2.86}$$

such that the right hand side (RHS) of the balances are linear in $p_{<12>}$, $p_{<22>}$, q_1, and q_2,

respectively. Now expanding in Kn to 2^{nd} order, Eqn.2.86 becomes

$$\begin{aligned}
&-\frac{1}{Kn}\left(p^{(0)}_{<12>}\left[p^{(0)}_{<22>}-p_\alpha\right]\right)\\
&-1\left(p^{(0)}_{<12>}\,p^{(1)}_{<22>}+p^{(1)}_{<12>}\left[p^{(0)}_{<22>}-p_\alpha\right]\right)\\
&-Kn\left(p^{(0)}_{<12>}\,p^{(2)}_{<22>}+p^{(1)}_{<12>}\,p^{(1)}_{<22>}+p^{(2)}_{<12>}\left[p^{(0)}_{<22>}-p_\alpha\right]\right)\\
&-Kn^2\left(p^{(0)}_{<12>}\,p^{(3)}_{<22>}+p^{(1)}_{<12>}\,p^{(2)}_{<22>}+p^{(2)}_{<12>}\,p^{(1)}_{<22>}+p^{(3)}_{<12>}\left[p^{(0)}_{<22>}-p_\alpha\right]\right)+\ldots\\
&=-\mu\left(\frac{2}{5}\frac{\partial q^{(0)}_1}{\partial x_2}+\frac{2}{5}Kn\frac{\partial q^{(1)}_1}{\partial x_2}+\frac{2}{5}Kn^2\frac{\partial q^{(2)}_1}{\partial x_2}+\ldots+p_\alpha\frac{\partial v}{\partial x_2}\right)
\end{aligned}\tag{2.87}$$

The other equations yield similar results due to their similar form. Separating into orders of Kn, by equating the coefficients of the powers of Kn, gives:

$\mathcal{O}\left(Kn^{-1}\right)$:

$$p^{(0)}_{<12>}=0,\;\; p^{(0)}_{<22>}=0,\;\; q^{(0)}_1=0,\;\; q^{(0)}_2=0,$$

$\mathcal{O}\left(Kn^{0}\right)$:

$$p^{(1)}_{<12>}=-\mu\frac{\partial v}{\partial x_2},$$

$$p^{(1)}_{<22>}=0,$$

$$q^{(1)}_1=0,$$

$$q^{(1)}_2=-\frac{15}{4}\mu\frac{\partial T}{\partial x_2}.$$

Note that the $\mathcal{O}\left(Kn^{-1}\right)$ values have been used to eliminate terms.

$\mathcal{O}\left(Kn^{1}\right)$:

$$p^{(2)}_{<12>}=0,$$

$$p^{(2)}_{<22>}=-\frac{6}{5}\frac{\mu}{p_\alpha}\frac{\partial q^{(1)}_2}{\partial x_2}=\frac{9}{2}\frac{\mu}{p_\alpha}\frac{\partial}{\partial x_2}\left(\mu\frac{\partial T}{\partial x_2}\right),$$

$$q^{(2)}_1=\frac{105}{8}\frac{\mu^2}{p_\alpha}\frac{\partial T}{\partial x_2}\frac{\partial v}{\partial x_2},$$

$$q^{(2)}_2=0.$$

Now, the $\mathcal{O}\left(Kn^{-1}\right)$ and $\mathcal{O}\left(Kn^{0}\right)$ values have been used to eliminate terms. Substituting back into the expanded terms as in Eqn. (2.85) to first order, yields the equations of

Navier-Stokes and Fourier (for the special case of Couette flow),

$$p_{<12>} = -Kn\ \mu\frac{\partial v}{\partial x_2}, \tag{2.88}$$

$$p_{<22>} = 0, \tag{2.89}$$

$$q_1 = 0, \tag{2.90}$$

$$q_2 = -Kn\frac{15}{4}\mu\frac{\partial T}{\partial x_2}. \tag{2.91}$$

With terms of order $\mathcal{O}\left(Kn^2\right)$ included one obtains,

$$p_{<12>} = -Kn\ \mu\frac{\partial v}{\partial x_2}, \tag{2.92}$$

$$p_{<22>} = Kn^2\frac{9}{2}\frac{\mu}{p_\alpha}\frac{\partial}{\partial x_2}\left(\mu\frac{\partial T}{\partial x_2}\right) = -Kn\frac{6}{5}\frac{\mu}{p_\alpha}\frac{\partial q_2}{\partial x_2}, \tag{2.93}$$

$$q_1 = Kn^2\frac{105}{8}\frac{\mu^2}{p_\alpha}\frac{\partial T}{\partial x_2}\frac{\partial v}{\partial x_2} = \frac{7}{2}\frac{\mu}{p_\alpha}p_{<12>}q_2, \tag{2.94}$$

$$q_2 = -Kn\frac{15}{4}\mu\frac{\partial T}{\partial x_2} \tag{2.95}$$

Applying the energy balance law Eqn. (2.37) for steady state in addition to Eqn. (2.92) and simplifying gives,

$$p_{<22>} = -\frac{6}{5}\frac{p_{<12>}^2}{p_\alpha}. \tag{2.96}$$

This second order result yields contributions to $p_{<22>}$ and q_1 that are present in the Burnett equations [7][8] and we therefore call Eqn.s (2.92)-(2.96) the reduced Burnett expansion. The full Burnett equations have some other contributions that are not captured by this expansion [7][8].

2.7 Linearization

2.7.1 Linear Navier-Stokes and Fourier

One good benchmark to compare with the Grad 13 equations are the standard equations of Navier-Stokes and Fourier (NSF). Simplified for Couette flow, the set of NSF equations is Eqn.s (2.36), (2.37), (2.88), and (2.91). If we consider constant viscosity and steady state, the system becomes analytically solvable and is

$$\frac{d^2 v_1}{dx_2^2} = 0, \tag{2.97}$$

$$\frac{15}{4}\frac{d^2 T}{dx_2^2} + \left(\frac{dv_1}{dx_2}\right)^2 = 0. \tag{2.98}$$

The linearized boundary conditions for slip velocity Eqn. (2.78) combined with Eqn. (2.88) read

$$v_1 - v_w = \frac{2-\theta}{\theta}\alpha\sqrt{\frac{\pi}{2}}Kn\frac{\mu_0}{p_0}\frac{dv_1}{dx_2}n_2. \tag{2.99}$$

With these BCs, the solution of Eqn. (2.97) for velocity becomes

$$v_1 = \frac{v_w^R - v_w^L}{2\,a+1}x_2 + \frac{a\left(v_w^R + v_w^L\right) - v_w^L}{2\,a+1}, \tag{2.100}$$

where

$$a = 2\frac{2-\theta}{\theta}\alpha\sqrt{\frac{\pi}{2}}Kn\frac{\mu_0}{p_0}. \tag{2.101}$$

v_w^R and v_w^L are the dimensionless right and left plate velocities, respectively. Using Eqn. (2.80) with Eqn. (2.91) and linearizing the temperature boundary conditions yields

$$T_w - T = -\frac{2-\theta}{\theta}\beta\sqrt{\frac{\pi}{2}}\frac{15}{8}Kn\frac{\mu_0}{p_0}T_0\frac{dT}{dx_2}n_2. \tag{2.102}$$

Applying this solution to Eqn. (2.98) and considering the previous solution for velocity, the solution for temperature is

$$T = \frac{2}{15}\left(\frac{v_w^R - v_w^L}{2\,a+1}\right)^2 x_2^2 + Bx_2 + C. \tag{2.103}$$

The constants B and C are determined in a straightforward manner from the boundary conditions. We consider the case where both walls have the same temperature T_0, which gives

$$T - T_0 = \frac{2}{15}\left(\frac{v_w^R - v_w^L}{2\,a+1}\right)^2 \left[x_2\,(1-x_2) + \frac{15}{16}\frac{a\beta}{\alpha}\right]. \tag{2.104}$$

2.7.2 Second order expansion

The next order in the Knudsen number expansion from Section 2.6 can easily be added to the above results of the linear NSF equations. This is simply done by inserting the results of the NSF solution into Eqn.s (2.94) and (2.96); this gives

$$q_1 = -\frac{7}{4}\frac{\mu_0^3}{p_0} Kn^2 \left(\frac{v_w^R - v_w^L}{2\,a+1}\right)^3 (2x_2 - 1), \tag{2.105}$$

and

$$p_{<22>} = -Kn^2 \frac{6}{5}\frac{\mu_0^2}{p_0}\left(\frac{v_w^R - v_w^L}{2\,a+1}\right)^2, \tag{2.106}$$

in the symmetric case where both walls have the same temperature. v, T, $p_{<12>}$ and q_2 have the same values as in the first order approach, which gives $q_1 = p_{<22>} = 0$.

2.7.3 Some linear results

Analytical results for the linearized solutions, of the NSF and reduced Burnett equations, Sec.s 2.7.1 and 2.7.2 have been calculated and plotted with the help of Mathematica®. Early stages of the transition regime ($Kn = 0.1$) gives a good representation of both the capabilities and the limitations of these linear results. It can be seen below, see Fig.s 2-4a to 2-4h, that some of the basic properties of the flow are represented, but significantly lack accuracy. Much of this loss of accuracy is due to the linearization. It will be seen later, in Ch. 4, that the non-linear solutions are by far more accurate and in the Grad 13 case show some of the Knudsen boundary layer properties.

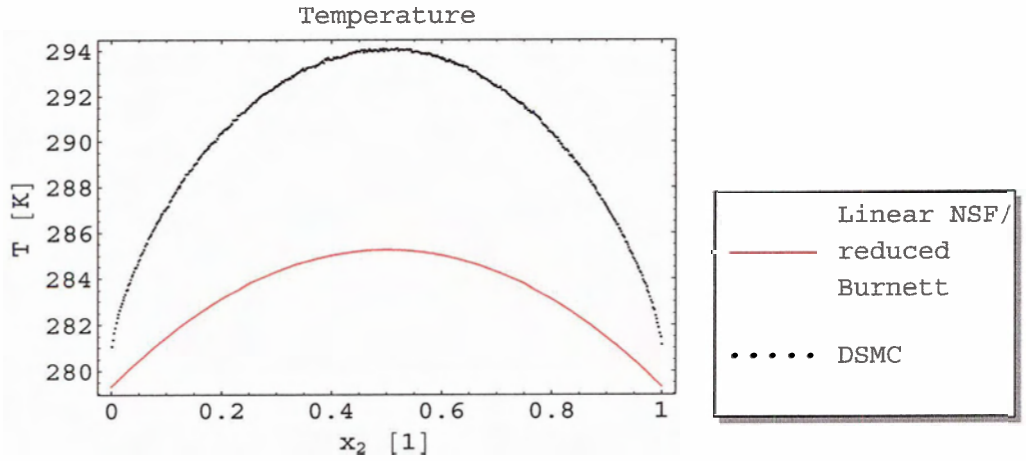

Figure 2-4a: Temperature at $Kn = 0.1$ and $\Delta v = 300\frac{\mathrm{m}}{\mathrm{s}}$

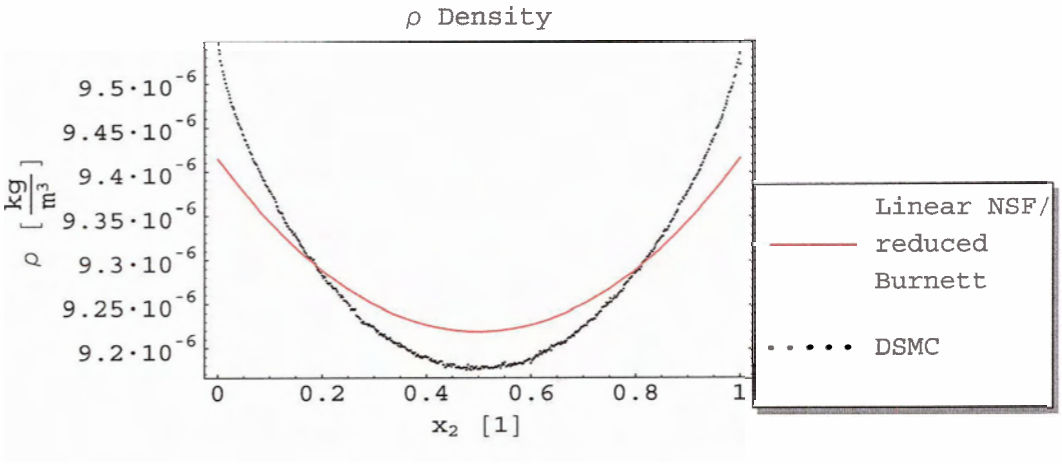

Figure 2-4b: Density at $Kn = 0.1$ and $\Delta v = 300\frac{\mathrm{m}}{\mathrm{s}}$

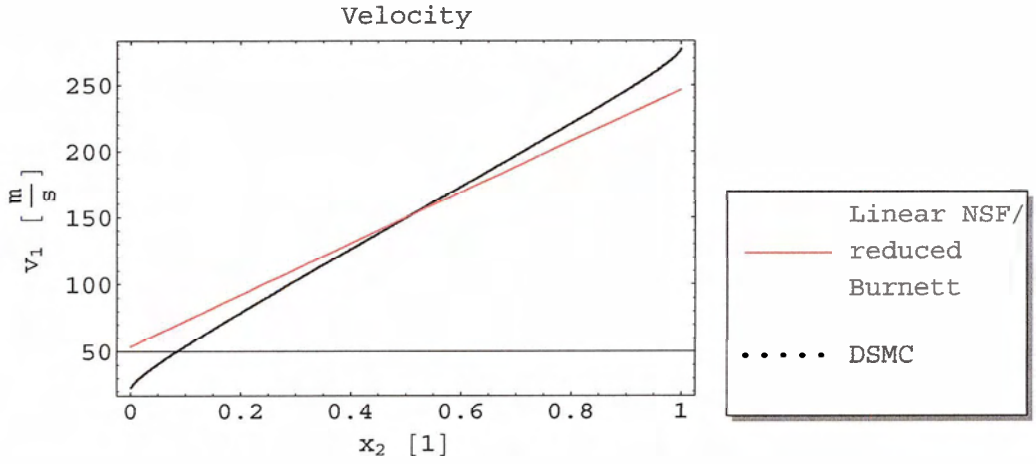

Figure 2-4c: Velocity v_1 at $Kn = 0.1$ and $\Delta v = 300\frac{\mathrm{m}}{\mathrm{s}}$

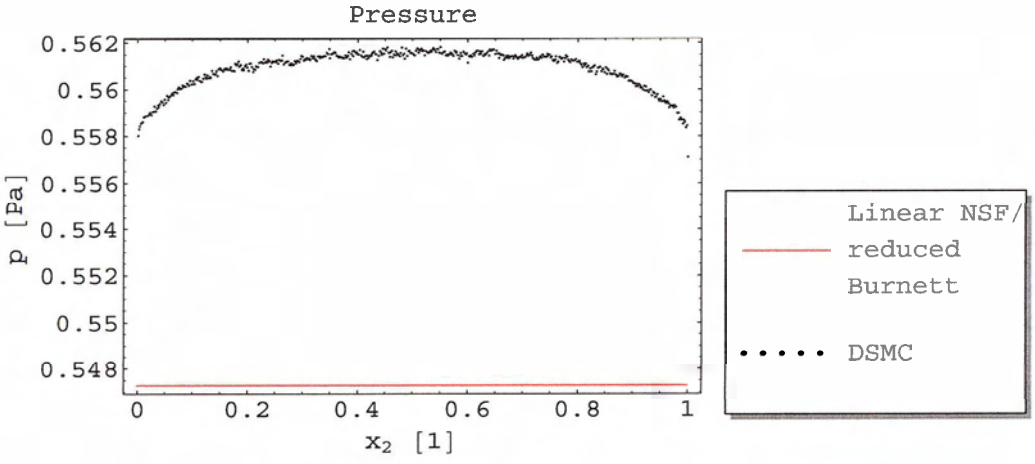

Figure 2-4d: Pressure at $Kn = 0.1$ and $\Delta v = 300\frac{\mathrm{m}}{\mathrm{s}}$

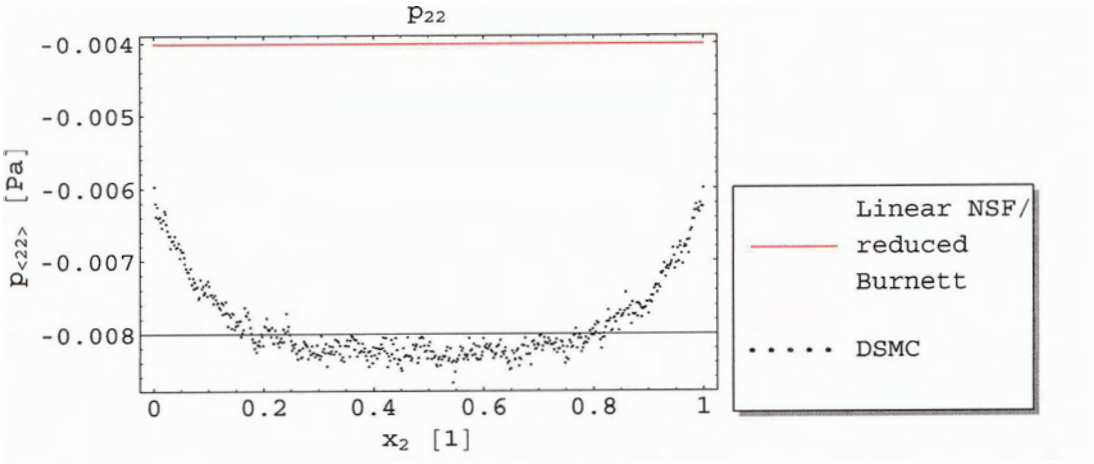

Figure 2-4e: $p_{<22>}$ at $Kn = 0.1$ and $\Delta v = 300\frac{\mathrm{m}}{\mathrm{s}}$

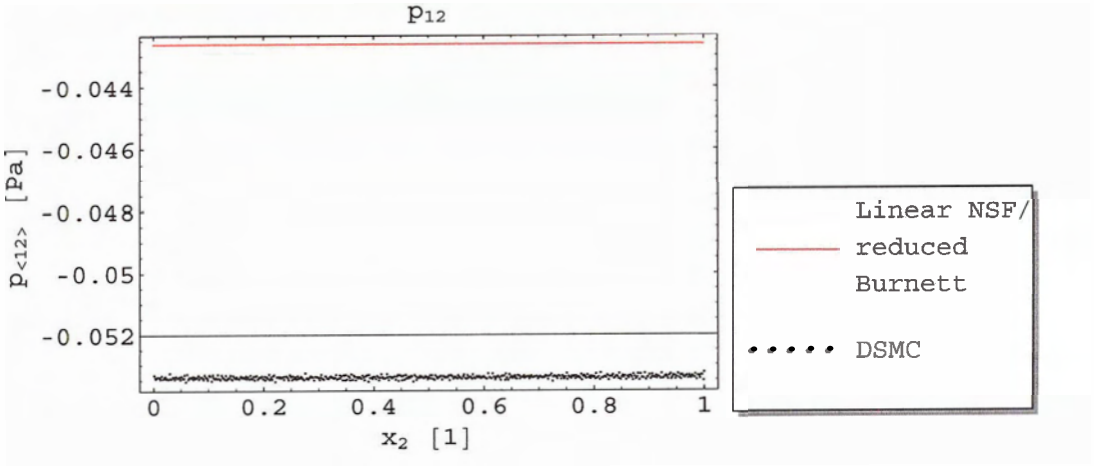

Figure 2-4f: $p_{<12>}$ at $Kn = 0.1$ and $\Delta v = 300\frac{\mathrm{m}}{\mathrm{s}}$

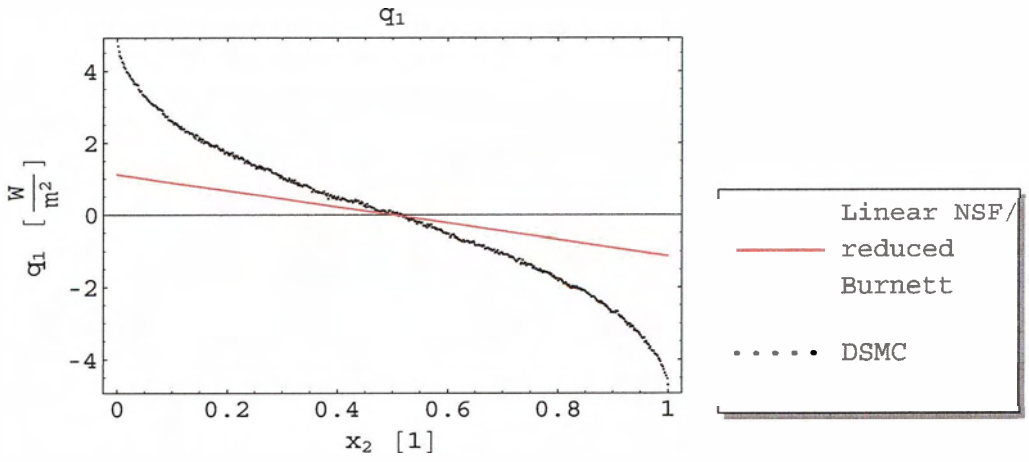

Figure 2-4g: q_1 at $Kn = 0.1$ and $\Delta v = 300\frac{\mathrm{m}}{\mathrm{s}}$

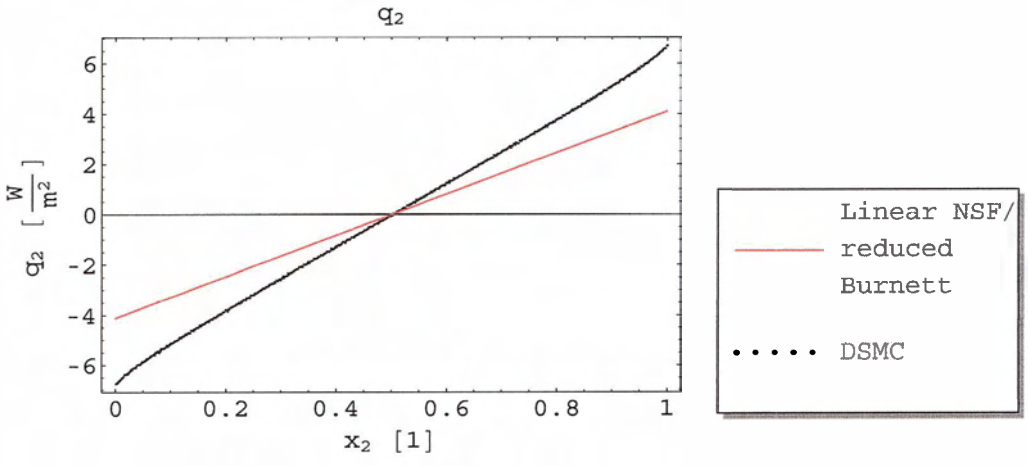

Figure 2-4h: q_2 at $Kn = 0.1$ and $\Delta v = 300\frac{\mathrm{m}}{\mathrm{s}}$

Chapter 3

Numerical Methods

The solution of the sets of Grad 13 equations is not feasible with analytical techniques, particularly the nonlinear forms. They instead have been approached with numerical techniques as is common in computational fluid dynamics (CFD). Several different numerical methods and approaches have been attempted to solve the Grad 13 equations for Couette flow, on a personal computer. Some approaches were programmed in C++, while others where done with the assistance of mathematical computing packages such as MATLAB® and Mathematica®. This section will outline these methods, but will only describe in detail those methods that were somewhat successful. First the unsuccessful methods will be mentioned, then the two methods that were successful will be described.

3.1 Finite volume method

Initially, the finite volume method common in CFD [25][26] was attempted. This method was somewhat difficult to formulate for the higher moment equations and its implementation did not converge to a stable solution. The inability of this approach to converge has been attributed to the hyperbolic nature of the equations at the boundaries. The inadequacy of the standard finite volume method for hyperbolic problems is well documented [26][27][28].

One of the current standards for dealing with hyperbolic problems within the confines of the finite volume method is the use of Riemann solvers common in methods such that of Roe and Godunov [29]. A Riemann approach has not been tried, as we are interested in the steady state solution and have no need to resolve traveling shocks. For this reason

it was assumed that a Riemann solver would be excessively complex and computationally intensive for this problem.

The finite volume method was not abandoned completely. Later it will be used in conjunction with MacCormack's method to solve the equations.

3.2 Finite difference relaxation method

Another common approach to solving systems of nonlinear ordinary differential equations (ODEs) is by simple finite difference equations. In order to increase the speed of the convergence of these equations, they are either formulated implicitly as is common in the finite volume method, or use Newton's method [30][31], and this was done here. This method provided a very convenient approach to applying the jump, slip and $p_{<22>}$ boundary conditions and proved very efficient for solving the Navier Stokes equations for Couette flow. With some finesse it was sometimes possible to converge on solutions for Grad 13 Couette flow with this technique. The solutions for the higher moments, however, always contained oscillations at the grid points.

A commercial code that uses a procedure similar to the above relaxation method was also attempted. The `bvp4c` function of MATLAB® implements the three-stage Lobatto IIIa formula [32], which is a more sophisticated version of the relaxation method. The `bvp4c` function only provides limited control of the numerical method as it contains algorithms to optimize the solution. This made obtaining converged results difficult. In some cases where convergence was possible, the solution had similar oscillations to that of the relaxation method.

3.3 Finite element and other techniques

Other techniques for solution were briefly attempted using commercially available code for numerical modeling. One of these was the finite element package FEMLAB®. A standard

formulation of a ODE problem was tried, but convergence was not obtained. More could probably have been done with a finite element method, but as modeling of hyperbolic equations is not straightforward with this approach, it was not attempted.

Another technique attempted was by using the numerical ODE solver included with the Mathematica® software package. This implements a variant of the chasing or shooting method [30] for the solution of ODEs.

3.4 Method for solving the Navier-Stokes and Fourier equations

As reference and comparison case the Navier-Stokes and Fourier (NSF) equations will also be solved. In the linearized case (Sec. 2.7.1) these can be solved analytically. For the case with non-constant viscosity, it is easiest to use a numerical technique. The above two methods of finite element and finite difference relaxation methods were used successfully for NSF solutions. It was decided, however, to use the more common finite volume method for comparison of the results [25][26].

This finite volume method involves integrating Eqn.s (2.36) and (2.37) at steady state over a control volume encompassing a grid point and central differencing Eqn.s (2.88), and (2.91) at the edges of the control volume. The result of this is an independent linear system for velocity and a linear system for temperature, which are solved consecutively. In order to allow for the nonlinear effect of temperature on pressure and viscosity, the previously mentioned process is iterated with corrected pressure and viscosity until convergence criteria are met. Exact details of the implementation of this method are left out, as it is easy to reproduce following Ref.s [25][26] and is almost identical to the scheme presented in the MacCormack scheme for temperature and velocity, shown below in Sec. 3.6.

The reduced Burnett equations can be computed with this method by central differencing Eqn.s (2.94) and (2.96) with the results from the above NSF method.

3.5 MacCormack's method

One recommended finite difference scheme for nonlinear hyperbolic problems is the MacCormack scheme [27][28][33]. The MacCormack scheme is essentially a two step variant of the common Lax-Wendroff method [27]. Like the Lax-Wendroff scheme, the MacCormack method is based on a $\mathcal{O}\left((\Delta t)^2\right)$ truncated Taylor series.

We explain this method on a simple system of hyperbolic equations,

$$\frac{\partial \boldsymbol{u}}{\partial t} + \frac{\partial \boldsymbol{F}(\boldsymbol{u})}{\partial x} = 0. \tag{3.1}$$

The MacCormack method for such a system proceeds in several steps. The predictor step,

$$\frac{\boldsymbol{u}_i^* - \boldsymbol{u}_i^n}{\Delta t} = \frac{\boldsymbol{F}_{i+1}^n - \boldsymbol{F}_i^n}{\Delta x}, \tag{3.2}$$

predicts a temporary value $\boldsymbol{u}_i^*$ for $\boldsymbol{u}_i$ at the next time step. Notice that the subscript denotes position along a grid $i = 0, 1, 2, ...m$ in space and the superscript the positions on a grid $n = 0, 1, 2, ...N$ in time. The star $(*)$ represents a temporary value at the position $n + 1$ in time. The corrector step then differences in the opposite direction as,

$$\frac{\boldsymbol{u}_i^{n+1} - \boldsymbol{u}_i^{n+\frac{1}{2}}}{\frac{1}{2}\Delta t} = \frac{\boldsymbol{F}_i^* - \boldsymbol{F}_{i-1}^*}{\Delta x}, \tag{3.3}$$

where

$$\boldsymbol{u}_i^{n+\frac{1}{2}} = \frac{1}{2}\left(\boldsymbol{u}_i^* + \boldsymbol{u}_i^n\right). \tag{3.4}$$

Writing this in explicit form, the MacCormack method becomes:
The predictor step

$$\boldsymbol{u}_i^* = \boldsymbol{u}_i^n - \frac{\Delta t}{\Delta x}\left(\boldsymbol{F}_{i+1}^n - \boldsymbol{F}_i^n\right) \tag{3.5}$$

and the corrector step

$$\boldsymbol{u}_i^{n+1} = \frac{1}{2}\left[\left(\boldsymbol{u}_i^* + \boldsymbol{u}_i^n\right) - \frac{\Delta t}{\Delta x}\left(\boldsymbol{F}_i^* - \boldsymbol{F}_{i-1}^*\right)\right]. \tag{3.6}$$

The arrangement of forward to backward differencing in space between steps can be interchanged. For linear problems this method can be used implicitly to form two bidiagonal systems.

Our system of equations is more complicated as we have a nonlinear source term. Lorimer [33] suggests and justifies a simple method for a non-conservative system, which can be written as

$$\frac{\partial \boldsymbol{u}}{\partial t} + \boldsymbol{A}(\boldsymbol{u}) \frac{\partial \boldsymbol{u}}{\partial x} = \boldsymbol{B}(\boldsymbol{u}). \tag{3.7}$$

The corresponding MacCormack method is:
The predictor step

$$\boldsymbol{u}_i^* = \boldsymbol{u}_i^n - \frac{\Delta t}{\Delta x} \boldsymbol{A}(\boldsymbol{u}_i^n) \left(\boldsymbol{u}_{i+1}^n - \boldsymbol{u}_i^n\right) - \Delta t \, \boldsymbol{B}(\boldsymbol{u}_i^n) \tag{3.8}$$

and the corrector step

$$\boldsymbol{u}_i^{n+1} = \frac{1}{2}\left[(\boldsymbol{u}_i^* + \boldsymbol{u}_i^n) - \frac{\Delta t}{\Delta x} \boldsymbol{A}(\boldsymbol{u}_i^*) \left(\boldsymbol{u}_i^* - \boldsymbol{u}_{i-1}^*\right) - \Delta t \, \boldsymbol{B}(\boldsymbol{u}_i^*)\right]. \tag{3.9}$$

The stability of this scheme is determined by the Courant-Friedrichs-Lewy (CFL) number defined as

$$CFL = a\frac{\Delta t}{\Delta x}, \tag{3.10}$$

where a is the largest eigenvalue of $\boldsymbol{A}(\boldsymbol{u})$. The scheme is stable for $CFL \leq 1$ [33].

When applied directly to the non-conservative form of the Grad 13 equations for Couette flow, convergence was possible, but the solution was slow and oscillations consistent with dispersion error[1] were present. In order to speed up convergence, it was noticed that the momentum balance Eqn. (2.36) and the energy balance Eqn. (2.37) could be solved implicitly as in the finite volume method. To correct for the dispersion error, a damping term of fourth order could be added explicitly to the $p_{<22>}$ and q_2 equations as is suggested by their hyperbolic nature as per Section 2.7. The resulting method will be called the

[1] A numerical error often found in hyperbolic problems, where the solution oscillates near a discontinuity such as a shock or in our case in the boundary conditions.

modified MacCormack's scheme (MMS).

3.6 Modified MacCormack's scheme

The modified MacCormack's scheme begins as a standard finite volume formulation around the divergent or non-conservative Eqn.s (2.36)-(2.41) with boundary conditions Eqn.s (2.78), (2.79) and (2.80), repeated now for convenience (hats indicating dimensionless form have been dropped):

$$\frac{\partial \rho v_1}{\partial t} + \frac{\partial p_{<12>}}{\partial x_2} = 0, \tag{3.11}$$

$$\frac{\partial p}{\partial x_2} + \frac{\partial p_{<22>}}{\partial x_2} = 0, \tag{3.12}$$

$$p + p_{<22>} = p_\alpha, \tag{3.13}$$

$$\int \rho dx_2 = \int \frac{p_\alpha - p_{<22>}}{T} dx_2 = Const, \tag{3.14}$$

$$\frac{\partial \rho u}{\partial t} + \frac{\partial q_2}{\partial x_2} + p_{<12>} \frac{\partial v_1}{\partial x_2} = 0, \tag{3.15}$$

$$\frac{\partial p_{<12>}}{\partial t} + \frac{2}{5} \frac{\partial q_1}{\partial x_2} + p_\alpha \frac{\partial v_1}{\partial x_2} = -\frac{1}{Kn} \frac{p}{\mu} p_{<12>}, \tag{3.16}$$

$$\frac{\partial p_{<22>}}{\partial t} + \frac{6}{5} \frac{\partial q_2}{\partial x_2} = -\frac{1}{Kn} \frac{p}{\mu} p_{<22>}, \tag{3.17}$$

$$\frac{\partial q_1}{\partial t} + \frac{7}{5} q_2 \frac{\partial v_1}{\partial x_2} + \frac{7}{2} p_{<12>} \frac{\partial T}{\partial x_2} = -\frac{1}{Kn} \frac{p}{\mu} q_1, \tag{3.18}$$

and

$$\frac{\partial q_2}{\partial t} + \frac{2}{5} q_1 \frac{\partial v_1}{\partial x_2} + \frac{5}{2} \left(p_\alpha + \frac{2}{5} p_{<22>} \right) \frac{\partial T}{\partial x_2} - T \frac{\partial p}{\partial x_2} = -\frac{1}{Kn} \frac{p}{\mu} q_2, \tag{3.19}$$

with the boundary conditions ($n_2 = 1$ at the left wall, $n_2 = -1$ at the right wall)

$$V_1 = \frac{-\frac{2-\theta}{\theta} \alpha \sqrt{\frac{\pi}{2} T} p_{<12>} n_2 - \frac{1}{5} q_1}{p + \frac{1}{2} p_{<22>}}, \tag{3.20}$$

$$p_{<22>} = -2\frac{\frac{2-\theta}{\theta}\gamma\frac{2}{5}\sqrt{\frac{\pi}{2}}q_2 n_2 + \left(\sqrt{T} - \sqrt{T_w}\right)p_\alpha}{\sqrt{\hat{T}_w}}, \tag{3.21}$$

$$\frac{T_w}{T} - 1 = \frac{\frac{2-\theta}{\theta}\beta\sqrt{\frac{\pi}{2}T}\frac{1}{2}q_2 n_2 + \frac{1}{4}p_{<22>}}{p + \frac{1}{2}p_{<22>}} - \frac{1}{4}V^2. \tag{3.22}$$

Figure 3-1 shows the control volumes (CVs) in dashed lines relative to the space grid that will be used. The shaded CVs are the boundaries and the central white CV stands for the interior points. Note that the common compass point notation of CFD has been used. Position i takes on P, the center of the compass, E the east side of i would be $i-1$, W would be $i+1$, e is $i-\frac{1}{2}$, and so on.

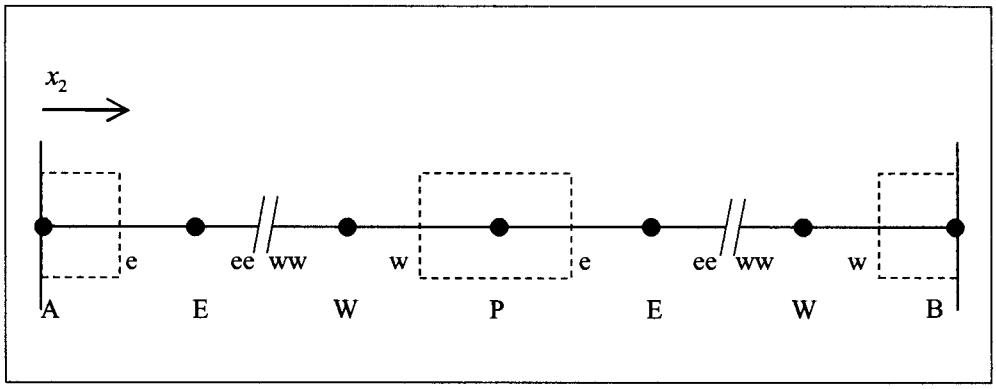

Figure 3-1: Discretization control volumes

The momentum and energy equations will be dealt with in steady state form and a solution for the temperature and velocity will be calculated implicitly for each time step. Explicit calculation of the other moments will then be used. This implicit/explicit method is designed to increase convergence in time. At the end of this section there is a process flow diagram Figure 3-2 that details the order of execution and how the overall solution is formed.

3.6.1 Momentum 1 (Velocity Distribution)

West BC

Integrating Eqn. (3.11) at steady state over the left CV in Fig. 3-1, from A to e, where A is the boundary point one step away from E, gives

$$\int_A^e \frac{\partial p_{<12>}}{\partial x_2} dV = (p_{<12>})_e - (p_{<12>})_A = 0. \tag{3.23}$$

Central differencing $(p_{<12>})_e$ from Eqn. (3.16) at steady state gives

$$(p_{<12>})_e = -Kn\frac{\mu_e}{p_e}\left(\frac{2}{5}\left(\frac{(q_1)_E - (q_1)_A}{\Delta x}\right)_L + p_\alpha\left(\frac{v_E - v_A}{\Delta x}\right)\right), \tag{3.24}$$

where

$$\mu_e = \mu\left((T_e)_L\right) = \left((T_e)_L\right)^s. \tag{3.25}$$

The subscript L denotes evaluation using values from the explicit calculations which will be shown later. Now noting $n_2 = 1$, $(p_{<12>})_A$ follows from the boundary condition Eqn. (3.20)

$$(p_{<12>})_A = -\frac{(v_A - v^{wall})\left(p_\alpha - \frac{1}{2}(p_{<22>})_A\right) + \frac{1}{5}(q_1)_A}{\frac{2-\theta}{\theta}\alpha\sqrt{\frac{\pi}{2}T_A}}. \tag{3.26}$$

Equation (3.23) with Eqn.s (3.24) and (3.26) is then discretized to form an expression relative to the interior velocities,

$$a_A v_A = a_E v_E + c_W v^{wall} + S_W, \tag{3.27}$$

where

$$a_E = Kn\frac{\mu_e}{p_e}\frac{p_\alpha}{\Delta x},$$
$$c_W = \frac{(p_\alpha - \frac{1}{2}(p_{<22>})_A}{\frac{2-\theta}{\theta}\alpha\sqrt{\frac{\pi}{2}T_A}},$$
$$a_A = a_E + c_W, \text{ and}$$
$$S_W = Kn\frac{\mu_e}{p_e}\frac{2}{5}\left(\frac{(q_1)_E - (q_1)_A}{\Delta x}\right)_L - \frac{\frac{1}{5}(q_1)_A}{\frac{2-\theta}{\theta}\alpha\sqrt{\frac{\pi}{2}T_A}}.$$

Central

Integrating Eqn. (3.11) at steady state over the middle CV in figure 3-1, from w to e gives

$$\int_w^e \frac{\partial p_{<12>}}{\partial x_2} dV = (p_{<12>})_e - (p_{<12>})_w = 0. \tag{3.28}$$

As before, substituting Eqn. (3.16) at steady state for $(p_{<12>})_e$ and $(p_{<12>})_w$ gives

$$(p_{<12>})_e = -Kn\frac{\mu_e}{p_e}\left(\frac{2}{5}\left(\frac{(q_1)_E - (q_1)_P}{\Delta x}\right)_L + p_\alpha\left(\frac{v_E - v_P}{\Delta x}\right)\right), \tag{3.29}$$

$$(p_{<12>})_w = -Kn\frac{\mu_w}{p_w}\left(\frac{2}{5}\left(\frac{(q_1)_P - (q_1)_W}{\Delta x}\right)_L + p_\alpha\left(\frac{v_P - v_W}{\Delta x}\right)\right), \tag{3.30}$$

where

$$\mu_w = \mu((T_w)_L) = ((T_w)_L)^s. \tag{3.31}$$

With this, Eqn. (3.28) is of the form

$$a_P v_P = a_W v_W + a_E v_E + S_L, \tag{3.32}$$

where

$$
\begin{aligned}
a_W &= Kn\frac{\mu_w}{p_w}\frac{p_\alpha}{\Delta x}, \\
a_E &= Kn\frac{\mu_e}{p_e}\frac{p_\alpha}{\Delta x}, \\
a_P &= a_W + a_E, \text{ and} \\
S_L &= -\frac{2}{5}\frac{\mu_w}{p_w}Kn\left(\frac{(q_1)_P - (q_1)_W}{\Delta x}\right)_L + \frac{2}{5}\frac{\mu_e}{p_e}Kn\left(\frac{(q_1)_E - (q_1)_P}{\Delta x}\right)_L.
\end{aligned}
$$

East BC

Just the opposite of the west BC with the boundary point being B and $n = -1$. The discretized equation becomes,

$$a_B v_B = a_W v_W + c_E v^{wall} + S_E, \tag{3.33}$$

where

$$
\begin{aligned}
a_W &= Kn\frac{\mu_w}{p_w}\frac{p_\alpha}{\Delta x}, \\
c_E &= \frac{(p_\alpha - \frac{1}{2}(p_{<22>})_A}{\frac{2-\theta}{\theta}\alpha\sqrt{\frac{\pi}{2}T_A}}, \\
a_B &= a_W + c_E, \\
S_E &= -Kn\frac{\mu_w}{p_w}\frac{2}{5}\left(\frac{(q_1)_B - (q_1)_W}{\Delta x}\right)_L - \frac{\frac{1}{5}(q_1)_B}{\frac{2-\theta}{\theta}\alpha\sqrt{\frac{\pi}{2}T_B}}.
\end{aligned}
$$

3.6.2 Momentum 2 (p_α) and mass conservation

Equation (3.12) leaves $p_\alpha = p + p_{<22>}$ to be determined. The total mass of the system is fixed in dimensionless quantities as

$$\int \rho dx = 1. \tag{3.34}$$

With the ideal gas law follows

$$\int \frac{p}{T} dx = \int \frac{p_\alpha - p_{<22>}}{T} dx = 1. \tag{3.35}$$

This leads to an iterative solution for p_α. If the entire domain of unknowns is calculated using a guess value of $\bar{p}_\alpha$, then the dimensionless mass M_0 of the system can be calculated as

$$M_0 = \sum_{i=0}^{m} \frac{p_i}{T_i} \Delta x = \sum_{i=0}^{m} \frac{\bar{p}_\alpha - (p_{<22>})_i}{T_i} \Delta x. \tag{3.36}$$

The new value of p_α is found by adjusting the pressure p_i by M_0 and forcing that adjustment onto the value of p_α as

$$p_\alpha = \frac{1}{m+1} \sum_{i=0}^{m} \left(\frac{p_i}{M_0} + (p_{<22>})_i \right), \tag{3.37}$$

where $i = 0$ is point A and $i = m$ is point B. $(p_{<22>})_i$ is used from its explicit calculation as in the MacCormack method, shown later. Values of p_i are then calculated from this corrected p_α and the values of $(p_{<22>})_i$.

3.6.3 Energy (Temperature distribution)

West BC

Integrating Eqn. (3.15) at steady state over the left CV in fig. 3-1, from A to e, where A is the boundary point one step away from E, gives

$$\int_A^e \left(\frac{\partial q_2}{\partial x_2} + p_{<12>} \frac{\partial v}{\partial x_2} \right) dV = (q_2)_e - (q_2)_A + \left[(p_{<12>})_A \left. \frac{\partial v}{\partial x_2} \right|_e \right] \frac{\Delta x}{2} = 0. \tag{3.38}$$

Discretizing $(q_2)_e$ from Eqn. (3.19),

$$(q_2)_e = -\frac{3}{2} Kn \frac{\mu_e}{p_e} \left[\left(\frac{2}{5} (q_1)_e \frac{v_E - v_A}{\Delta x} \right) + \frac{5}{2} \left(p_\alpha + \frac{2}{5} (p_{<22>})_e \right) \frac{T_E - T_A}{\Delta x} - \frac{T_A + T_E}{2} \frac{p_E - p_A}{\Delta x} \right]. \tag{3.39}$$

Notice that the source term is approximated by the value at the boundary, but there is no way of calculating $\left. \frac{\partial v}{\partial x_2} \right|_e$ so it is approximated by the finite difference value near the

boundary as

$$\left.\frac{\partial v}{\partial x_2}\right|_e = \frac{v_E - v_A}{\Delta x}. \tag{3.40}$$

$(p_{<12>})_A$ is as in Eqn. (3.26) and $(q_2)_A$ follows similarly from Eqn. (3.22) as

$$(q_2)_A = 2\frac{\left(T^{wall} - T_A + \frac{1}{4}V_A^2\right)\left(p_\alpha - \frac{1}{2}(p_{<22>})_A\right) + \frac{1}{4}(p_{<22>})_A T_A}{\frac{2-\theta}{\theta}\beta\sqrt{\frac{\pi}{2}(T_A)_L}}. \tag{3.41}$$

Again the previous equations with Eqn. (3.38) can be written as

$$b_A T_A = b_E T_E + d_E T^{wall} + S_W, \tag{3.42}$$

where

$$\begin{aligned}
b_A &= \frac{3}{2}\frac{Kn}{\Delta x}\frac{\mu_e}{p_e}\left[\frac{5}{2}p_\alpha + (p_{<22>})_A\right] + 2\frac{p_\alpha - \frac{1}{4}(p_{<22>})_A}{\frac{2-\theta}{\theta}\beta\sqrt{\frac{\pi}{2}(T_A)_L}},\\
b_E &= \frac{3}{2}\frac{Kn}{\Delta x}\frac{\mu_e}{p_e}\left[\frac{5}{2}p_\alpha + (p_{<22>})_E\right],\\
d_E &= 2\frac{(p_\alpha - \frac{1}{2}(p_{<22>})_A}{\frac{2-\theta}{\theta}\beta\sqrt{\frac{\pi}{2}(T_A)_L}}, \text{ and}\\
S_W &= \frac{3}{2}\frac{Kn}{\Delta x}\frac{\mu_e}{p_e}\left[\frac{2}{5}(q_1)_e(v_E - v_A)\right] + \frac{1}{4}V_A^2 d_E - \frac{v_E - v_A}{2}\left[(p_{<12>})_A\right]
\end{aligned}$$

Similar to the first momentum equation, remaining moment values are used from their explicit results which will be presented below.

Central

Now Eqn. (3.15) at steady state can be integrated over the CV w to e:

$$\int_w^e \left(\frac{\partial q_2}{\partial x_2} + p_{<12>}\frac{\partial v}{\partial x_2}\right) dV = (q_2)_e - (q_2)_w + \left[(p_{<12>})_e \left.\frac{\partial v}{\partial x_2}\right|_e + (p_{<12>})_w \left.\frac{\partial v}{\partial x_2}\right|_w\right]_L \frac{\Delta x}{2} = 0. \tag{3.43}$$

$(p_{<12>})_e$ and $(p_{<12>})_w$ are defined as previously in Eqn.s (3.29) and (3.30). Equation (3.19) at steady state is discretized to find values of $(q_2)_e$ and $(q_2)_w$ as,

$$(q_2)_e = -\frac{3}{2}Kn\frac{\mu_e}{p_e}\left[\left(\frac{2}{5}(q_1)_e\frac{v_E - v_P}{\Delta x}\right) + \frac{5}{2}\left(p_\alpha + \frac{2}{5}(p_{<22>})_e\right)\frac{T_E - T_P}{\Delta x} - \frac{T_P + T_E}{2}\frac{p_E - p_P}{\Delta x}\right], \tag{3.44}$$

$$(q_2)_w = -\frac{3}{2}Kn\frac{\mu_w}{p_w}\left[\left(\frac{2}{5}(q_1)_w\frac{v_P - v_W}{\Delta x}\right) + \frac{5}{2}\left(p_\alpha + \frac{2}{5}(p_{<22>})_w\right)\frac{T_P - T_W}{\Delta x} - \frac{T_P + T_W}{2}\frac{p_P - p_W}{\Delta x}\right]. \tag{3.45}$$

Thus, Eqn. (3.43) assumes the form

$$b_P T_P = b_W T_W + b_E T_E + S_T, \tag{3.46}$$

where

$$\begin{aligned}
b_W &= \frac{3}{2}\frac{Kn}{\Delta x}\frac{\mu_w}{p_w}\left[\frac{5}{2}p_\alpha + (p_{<22>})_W\right], \\
b_E &= \frac{3}{2}\frac{Kn}{\Delta x}\frac{\mu_e}{p_e}\left[\frac{5}{2}p_\alpha + (p_{<22>})_E\right], \\
b_P &= \frac{3}{2}\frac{Kn}{\Delta x}\left(\frac{\mu_w}{p_w} + \frac{\mu_e}{p_e}\right)\left(\frac{5}{2}p_\alpha + (p_{<22>})_P\right), \\
S_T &= \left[\frac{3}{5}\frac{Kn}{\Delta x}\frac{\mu_e}{p_e}((q_1)_e)_L - \frac{((p_{<12>})_e)_L}{2}\right](v_E - v_P) \\
&\quad - \left[\frac{3}{5}\frac{Kn}{\Delta x}\frac{\mu_w}{p_w}((q_1)_w)_L + \frac{((p_{<12>})_w)_L}{2}\right](v_P - v_W).
\end{aligned}$$

Note that $(p_{<12>})_w$ and $(p_{<12>})_e$ was discretized earlier. Also it was used that $(p_P - p_W)_L = -((p_{<22>})_P - (p_{<22>})_W)_L$ and $(p_E - p_P)_L = -((p_{<22>})_E - (p_{<22>})_P)_L$

East BC

Just the opposite of the west BC with the boundary point being B and $n = -1$. The discretized equation becomes,

$$b_B T_B = b_W T_E + d_W T^{wall} + S_E, \tag{3.47}$$

where

$$b_B = \frac{3}{2}\frac{Kn}{\Delta x}\frac{\mu_w}{p_w}\left[\frac{5}{2}p_\alpha + (p_{<22>})_B\right] + 2\frac{p_\alpha - \frac{1}{4}(p_{<22>})_A}{\frac{2-\theta}{\theta}\beta\sqrt{\frac{\pi}{2}(T_A)_L}},$$

$$b_W = \frac{3}{2}\frac{Kn}{\Delta x}\frac{\mu_w}{p_w}\left[\frac{5}{2}p_\alpha + (p_{<22>})_W\right],$$

$$d_W = 2\frac{p_\alpha - \frac{1}{2}(p_{<22>})_B}{\frac{2-\theta}{\theta}\beta\sqrt{\frac{\pi}{2}(T_B)_L}}, \text{ and}$$

$$S_E = -\frac{3}{2}\frac{Kn}{\Delta x}\frac{\mu_w}{p_w}\left[\frac{2}{5}(q_1)_w(v_B - v_W)\right] + \frac{1}{4}V_B^2 d_W - \frac{v_B - v_W}{2}\left[(p_{<12>})_B\right].$$

Equations (3.27, 3.32, and 3.33) and (3.42, 3.46, and 3.47) form two linear systems of equations that can be solved for temperature and velocity over the entire domain. These results will then need to be corrected and iterated to resolve nonlinear contributions.

3.6.4 Higher moments ($p_{<12>}$, $p_{<22>}$, q_1 and q_2 distributions)

West BC

$p_{<12>}$ and q_2 at the left wall are simply given by Eqn.s (3.26) and (3.41). $p_{<22>}$ is similarly just Eqn. (3.21) with $n = 1$, as

$$(p_{<22>})_A = -2\frac{\frac{2-\theta}{\theta}\gamma\frac{2}{5}\sqrt{\frac{\pi}{2}}(q_2)_A + \left(\sqrt{T_A} - \sqrt{T^{wall}}\right)p_\alpha}{\sqrt{T^{wall}}}. \tag{3.48}$$

There is no boundary condition for q_1, but counting seven equations, seven unknowns with six boundary conditions and one mass conservation condition is a complete set, thus no

condition for q_1 is required. This means the moment equation for q_1 Eqn. (3.18) must be valid at the boundary. Thus

$$(q_1)_A = \frac{1}{1+\frac{2}{3}\frac{\Delta t}{Kn}\frac{\mu_A}{p_A}}\left\{((q_1)_A)_L - \left[\frac{7}{5}(q_2)_A\left(\frac{v_E - v_A}{\Delta x}\right) + \frac{7}{2}(p_{<12>})_A\left(\frac{T_E - T_A}{\Delta x}\right)\right]\right\}. \tag{3.49}$$

The subscript L indicates the value from the previous iteration. We have now included the time dependent portion of Eqn. (3.18) as it allows us to relax the solution. By controlling the time step Δt, we control the stability criteria.

Central

Here we apply the MacCormack scheme Eqn.s (3.8) and (3.9) to the moment Eqn.s (3.16), (3.17), (3.18) and (3.19) as follows:
Predictor step,

$$(p_{<12>})^*_P = ((p_{<12>})_P)_L - \frac{\Delta t}{\Delta x}\left[\frac{2}{5}((q_1)_E - (q_1)_P)_L + p_\alpha(v_E - v_P)\right] - \frac{\Delta t}{Kn}((p_{<12>})_P)_L, \tag{3.50}$$

$$(p_{<22>})^*_P = ((p_{<22>})_P)_L - \frac{\Delta t}{\Delta x}\frac{6}{5}((q_2)_E - (q_2)_P)_L - \frac{\Delta t}{Kn}((p_{<22>})_P)_L, \tag{3.51}$$

$$(q_1)^*_P = ((q_1)_P)_L - \frac{\Delta t}{\Delta x}\frac{3}{2}\left[\frac{7}{5}((q_2)_E)_L(v_E - v_P) + \frac{7}{2}((p_{<12>})_E)_L(T_E - T_P)\right] - \frac{\Delta t}{Kn}((q_1)_P)_L, \tag{3.52}$$

$$\begin{aligned}(q_2)^*_P = ((q_2)_P)_L - \frac{\Delta t}{\Delta x}\frac{3}{2}\Bigg[&\frac{2}{5}((q_1)_E)_L(v_E - v_P) + \frac{5}{2}\left(p_\alpha + \frac{2}{5}((p_{<22>})_E)_L\right)(T_E - T_P) \\ &+T_E\left(((p_{<22>})_E)_L - ((p_{<22>})_P)_L\right)\Bigg] - \frac{\Delta t}{Kn}((q_2)_P)_L.\end{aligned} \tag{3.53}$$

Corrector step,

$$\begin{aligned}(p_{<12>})_P = &\frac{1}{2}\left[((p_{<12>})_P)_L + (p_{<12>})^*_P\right] \\ &- \frac{\Delta t}{\Delta x}\left[\frac{2}{5}((q_1)^*_P - (q_1)^*_W) + p_\alpha(v_P - v_W)\right] - \frac{\Delta t}{Kn}(p_{<12>})^*_P,\end{aligned} \tag{3.54}$$

$$(p_{<22>})_P = \frac{1}{2}\left[((p_{<22>})_P)_L + (p_{<22>})^*_P\right] - \frac{\Delta t}{\Delta x}\frac{6}{5}\left((q_2)^*_P - (q_2)^*_W\right) - \frac{\Delta t}{Kn}(p_{<22>})^*_P, \quad (3.55)$$

$$\begin{aligned}(q_1)_P = &\frac{1}{2}\left[((q_1)_P)_L + (q_1)^*_P\right] \\ &- \frac{\Delta t}{\Delta x}\frac{3}{2}\left[\frac{7}{5}(q_2)^*_W(v_P - v_W) + \frac{7}{2}(p_{<12>})^*_W(T_P - T_W)\right] - \frac{\Delta t}{Kn}(q_1)^*_P,\end{aligned} \quad (3.56)$$

$$\begin{aligned}(q_2)^*_P = &\frac{1}{2}\left[((q_2)_P)_L + (q_2)^*_P\right] - \frac{\Delta t}{\Delta x}\frac{3}{2}\left[\frac{2}{5}(q_1)^*_W(v_P - v_W)\right. \\ &\left.+\frac{5}{2}\left(p_\alpha + \frac{2}{5}(p_{<22>})^*_W\right)(T_P - T_W) + T_W\left((p_{<22>})^*_P - (p_{<22>})^*_W\right)\right] - \frac{\Delta t}{Kn}(q_2)^*_P.\end{aligned} \quad (3.57)$$

In order to ensure symmetry of the scheme, differencing of the above equations is alternated with each time step such that in one time step the predictor will be forward differenced and the corrector backward differenced as above. In the next time step this will be reversed so that the predictor is backward differenced and the corrector is forward differenced.

East BC

As always the east BC is simply the opposite of the west.

3.6.5 Damping or averaging

In order to compensate for dispersion error originating near the boundaries traveling throughout the solution domain, damping or averaging is added. This procedure is suggested by Hoffmann and Chiang [27]. In order to minimize the effect of numerical viscosity on the final solution, damping terms of higher order in space than the primary discretizations are explicitly added to the solution. The damping term can be expressed as a derivative of the damped property f to an order n as

$$D = -\delta(\Delta x)^n \frac{\partial^n f}{\partial x^n}, \quad (3.58)$$

where δ is the damping coefficient. The differential is then discretized using a central differencing formula based on Taylor series expansion of the neighboring points relative to the grid point in question. This finite difference formula for fourth order damping is

$$(\Delta x)^4 \frac{\partial^4 f}{\partial x^4} = f_{i-2} - 4f_{i-1} + 6f_i - 4f_{i+1} + f_{i+2}. \tag{3.59}$$

Expressed as an explicit correction this is implemented as

$$f_i^{new} = f_i - \varepsilon \left(f_{i-2} - 4f_{i-1} + 6f_i - 4f_{i+1} + f_{i+2} \right). \tag{3.60}$$

If a damping rate of $\varepsilon = \frac{\delta}{\Delta t} = \frac{1}{12}$ is used it can be seen that this explicitly averaging the solution at fourth order, as

$$f_i^{new} = \frac{-f_{i-2} + 4f_{i-1} + 6f_i + 4f_{i+1} - f_{i+2}}{12}. \tag{3.61}$$

Either the damping rate ε can be changed or the time step size Δt of each iteration adjusted to control the rate of damping. We applied this fourth order averaging to the q_2 and $p_{<22>}$ values as they show the most hyperbolic contribution in the analytical analysis of sec. 2.7.

3.6.6 Numerical flow diagram

Figure 3-2 shows how the modified MacCormack method explained above is implemented. The flow diagram shows that the method runs with a tolerance checking routine to detect convergence. In order to understand the results it was often run for a specified time rather than to a specified tolerance check. This allowed to better isolate the effect of time stepping.

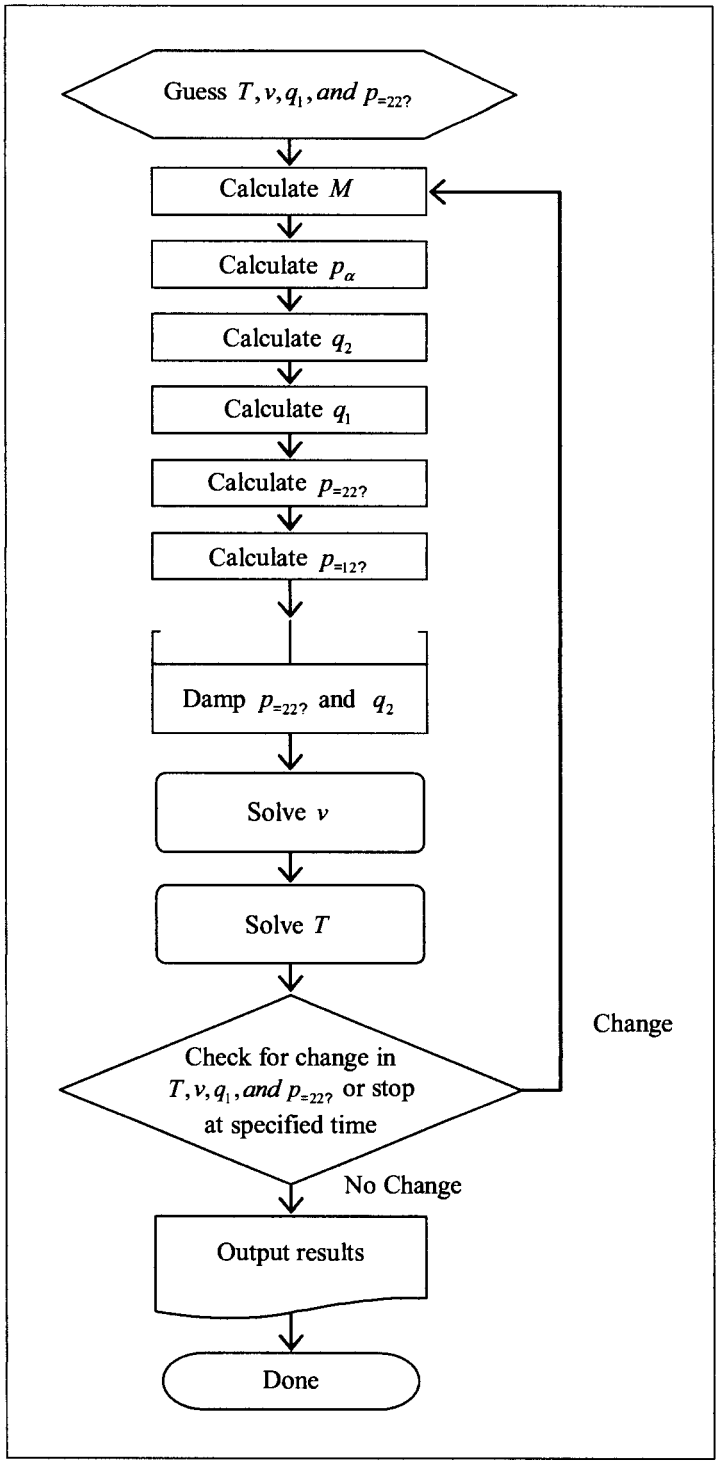

Figure 3-2: Modified MacCormack scheme process flow diagram.

The modified MacCormack scheme has some unknowns about the window of accuracy in

the time and space steps due to the combination of numerical viscosity and CFL condition.

3.7 Nessyahu-Tadmor method

More recently methods have been applied to hyperbolic conservation laws that compensate for numerical damping and do not require the Riemann problem to be solved. Such a scheme was developed by Nessyahu and Tadmor [34]. Liotta, Romano and Russo [35] made some improvements to the scheme and adapted it to balance laws with source terms in the form of the conservative Grad 13 equations.

The Grad 13 equations in conservative form, Eqn.s (2.42)-(2.52), constitute a system of equations of the form

$$\frac{\partial \boldsymbol{u}}{\partial t} + \frac{\partial \boldsymbol{f}(\boldsymbol{u})}{\partial x} = \boldsymbol{g}(\boldsymbol{u}). \tag{3.62}$$

The Nessyahu-Tadmor scheme is similar to the MacCormack's scheme except that now the spatial gradients in the predictor are determined by a min-mod reconstruction of the forward and backward differences. The scheme is also second order accurate in time and space. The explicit version of the scheme as outlined in [35] is as follows:
The predictor is

$$\boldsymbol{u}_i^* = \boldsymbol{u}_i^n + \frac{\Delta t}{2}\left(\boldsymbol{g}(\boldsymbol{u}_i^n) - \frac{1}{\Delta x}\boldsymbol{f}_i'\right), \tag{3.63}$$

where $\boldsymbol{f}_i'$ is given by a finite difference approximation of the spatial derivative. The idea here is to prevent numerical oscillations by choosing the lowest value between the forward and backward finite differences. The means to this end is the following min-mod reconstruction,

$$\boldsymbol{f}_i' = \mathrm{MM}\left(\boldsymbol{f}_{i+1} - \boldsymbol{f}_i,\ \boldsymbol{f}_i - \boldsymbol{f}_{i-1}\right), \tag{3.64}$$

where,

$$\mathrm{MM}(x,\ y) = \begin{cases} \mathrm{sgn}(x)\ \ \min\left(|x|, |y|\right) & \text{if } \mathrm{sgn}(x) = \mathrm{sgn}(y) \\ 0 & \text{otherwise.} \end{cases} \tag{3.65}$$

The explicit corrector, evaluated at the half space step, is

$$\begin{aligned}\boldsymbol{u}_{i+\frac{1}{2}}^{n+1} =& \frac{1}{2}\left(\boldsymbol{u}_i^n + \boldsymbol{u}_{i+1}^n\right) + \frac{1}{8}\left(\boldsymbol{u}_i'^n - \boldsymbol{u}_{i+1}'^n\right) - \frac{\Delta t}{\Delta x}\left(\boldsymbol{f}\left(\boldsymbol{u}_{i+1}^*\right) - \boldsymbol{f}\left(\boldsymbol{u}_i^*\right)\right) \\ &+ \frac{\Delta t}{2}\left(\boldsymbol{g}\left(\boldsymbol{u}_i^*\right) + \boldsymbol{g}\left(\boldsymbol{u}_{i+1}^*\right)\right). \end{aligned} \tag{3.66}$$

Liotta, Romano and Russo [35] also suggest a slight improvement in calculating the source term by using a higher accuracy quadrature in time. This has obvious benefits when applied to an implicit scheme, but may not be of benefit when applied explicitly. This implicit scheme using two point Radau quadrature, referred to in [35] as the uniformly implicit central scheme (UCS) is as follows:

The predictors are

$$\boldsymbol{u}_i^{n+\frac{1}{2}} = \boldsymbol{u}_i^n + \frac{\Delta t}{2}\left(\boldsymbol{g}\left(\boldsymbol{u}_i^{n+\frac{1}{2}}\right) - \frac{1}{\Delta x}\boldsymbol{f}_i'\right) \tag{3.67}$$

and

$$\boldsymbol{u}_i^{n+\frac{2}{3}} = \boldsymbol{u}_i^n + \frac{2\Delta t}{3}\left(\boldsymbol{g}\left(\boldsymbol{u}_i^{n+\frac{2}{3}}\right) - \frac{1}{\Delta x}\boldsymbol{f}_i'\right). \tag{3.68}$$

The implicit corrector is

$$\begin{aligned}\boldsymbol{u}_{i+\frac{1}{2}}^{n+1} =& \frac{1}{2}\left(\boldsymbol{u}_i^n + \boldsymbol{u}_{i+1}^n\right) + \frac{1}{8}\left(\boldsymbol{u}_i'^n - \boldsymbol{u}_{i+1}'^n\right) - \frac{\Delta t}{\Delta x}\left(\boldsymbol{f}\left(\boldsymbol{u}_{i+1}^{n+\frac{1}{2}}\right) - \boldsymbol{f}\left(\boldsymbol{u}_i^{n+\frac{1}{2}}\right)\right) \\ &+ \Delta t\left(\frac{3}{8}\boldsymbol{g}\left(\boldsymbol{u}_i^{n+\frac{1}{2}}\right) + \frac{3}{8}\boldsymbol{g}\left(\boldsymbol{u}_{i+1}^{n+\frac{2}{3}}\right) + \frac{1}{4}\boldsymbol{g}\left(\boldsymbol{u}_i^{n+1}\right)\right). \end{aligned} \tag{3.69}$$

There is some difficulty and very lengthy terms involved in describing the function $\boldsymbol{f}$ as a function of $\boldsymbol{u}$ for the conservative form equations of sec. 2.4. For this reason this it was implemented by knowing we can have central moments of the peculiar velocity as,

$$p_A = \{\rho,\ v_1,\ v_2,\ T,\ p_{11},\ p_{22},\ p_{12},\ q_1,\ q_2\}. \tag{3.70}$$

There are nine full moments of the microscopic velocity, U_k, that correspond to these, from Eqn.s (2.42)-(2.52) as,

$$U_1 = \rho$$

$$U_2 = \rho v_1$$

$$U_3 = \rho v_2$$

$$U_4 = \frac{3}{2}\rho T + \frac{\rho}{2}\left(v_1^2 + v_2^2\right)$$

$$U_5 = \sigma_{12} + \rho v_1 v_2$$

$$U_6 = \rho T + \sigma_{11} + \rho v_1^2$$

$$U_7 = \rho T + \sigma_{22} + \rho v_2^2$$

$$U_8 = q_1 + \sigma_{11} v_1 + \sigma_{12} v_2 + \frac{5}{2}\rho t v_1 + \frac{1}{2}\rho\left(v_1^2 + v_2^2\right) v_1$$

$$U_9 = q_2 + \sigma_{22} v_2 + \sigma_{12} v_1 + \frac{5}{2}\rho T v_2 + \frac{1}{2}\rho\left(v_1^2 + v_2^2\right) v_2$$

From these definitions, p_A and U_k can be interchanged. Considering the Grad 13 balance laws of conservative form, Eqn.s (2.42)-(2.52), expressed as being of the form

$$\frac{\partial U_k\left(p_A\right)}{\partial t} + \frac{\partial F_k\left(p_A\right)}{\partial x} = G_k\left(p_A\right). \tag{3.71}$$

The fluxes F_k and the productions G_k are functions of U_k, but are more simply implemented as functions of the central moments p_A, obtained as for U_k from Eqn.s (2.42)-(2.52), which correspondingly are functions of the full moments U_k. F_k and G_k as functions of p_A are

$$F_1 = \rho v_2,$$

$$F_2 = \sigma_{12} + \rho v_1 v_2,$$

$$F_3 = g s_{22} + p + \rho v_2^2,$$

$$F_4 = \frac{5}{2} p v_2 + q_2 + \sigma_{12} v_1 + \sigma_{22} v_2 + \frac{\rho}{2}\left(v_1^2 + v_2^2\right) v_2,$$

$$F_5 = \frac{2}{5} q_1 + v_1\left(\sigma_{22} + p\right) + 2 v_2 \sigma_{12} + \rho v_1 v_2 v_2,$$

$$F_6 = \frac{2}{5} q_2 + 2 v_1 \sigma_{12} + v_2\left(\sigma_{11} + p\right) + \rho v_1^2 v_2,$$

$$F_7 = \frac{6}{5}q_2 + 3v_2\left(\sigma_{22} + p\right) + \rho v_2^2 v_2,$$

$$F_8 = \frac{7}{2}\frac{p}{\rho}\sigma_{12} + \frac{7}{5}q_1 v_2 + \frac{7}{5}q_2 v_1 + \frac{1}{2}v^2\sigma_{12} + v_1^2\sigma_{12} + v_2 v_1\sigma_{22} + v_2^2\sigma_{12} + v_1 v_2\sigma_{11} + \frac{7}{2}v_1 v_2 p + \frac{1}{2}\sigma v^2 v_1 v_2,$$

$$F_9 = \frac{7}{2}\frac{p}{\rho}\sigma_{22} + \frac{5}{2}\frac{p^2}{\rho} + \frac{16}{5}v_2 q_2 + \frac{2}{5}q_1 v_1 + \frac{1}{2}v^2\left(p + \sigma_{22}\right) + 2v_1 v_2\sigma_{12} + 2v_2^2\sigma_{22} + \frac{7}{2}v_2^2 p + \frac{1}{2}\rho v^2 v_2^2,$$

$$G_1 = G_2 = G_3 = G_4 = 0,$$

$$G_5 = -\frac{p}{\mu}\frac{\sigma_{12}}{Kn},$$

$$G_6 = -\frac{p}{\mu}\frac{\sigma_{11}}{Kn},$$

$$G_7 = -\frac{p}{\mu}\frac{\sigma_{22}}{Kn},$$

$$G_8 = -\frac{p}{\mu}\frac{1}{Kn}\left(v_1\sigma_{11} + v_2\sigma_{12} + \frac{2}{3}q_1\right),$$

and

$$G_9 = -\frac{p}{\mu}\frac{1}{Kn}\left(v_1\sigma_{12} + v_2\sigma_{22} + \frac{2}{3}q_2\right).$$

Boundary conditions are implemented in a straightforward manner on the central moments just as in the higher moments of the modified MacCormack scheme. Moments that do not have BCs were assumed to follow their corresponding moment equations. For these, the only change that needed to be made was to ignore the min-mod reconstruction at the boundary and chose the finite difference immediately next to the boundary.

The implementation of the Nessyahu-Tadmor method is shown below in fig. 3-3. The implicit steps were evaluated by a simple iteration in each step.

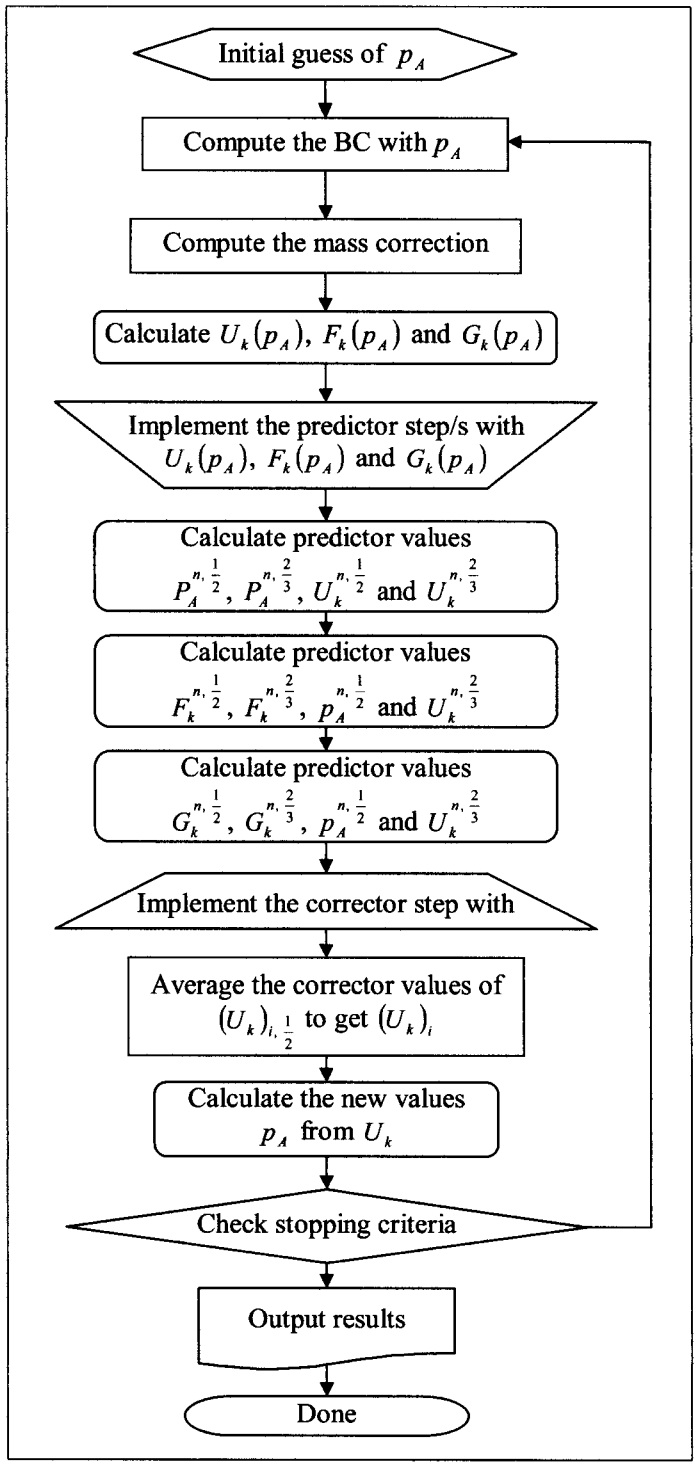

Figure 3-3: Nessyahu-Tadmor scheme process flow diagram.

Chapter 4

Results

All results presented in this section use an accommodation coefficient of $\theta = 1.0$ and represent Maxwell molecules ($s = 1.0$). Other values of s have been looked at but it is not felt that they would be instructive to the goals of this thesis.

Results also reflect steady state solutions. Steady state is considered to be reached when negligible change in the results appears from increased time.

4.1 Modified MacCormack's Scheme Results

The Modified MacCormack's scheme (MMS) gives good results for the slip flow regime($0.01 \leq Kn < 0.1$) and good information about the behavior of the Grad13 equations and the flow properties in the lower end of the transitional flow regime. The accuracy of the results depends on the amount of numerical damping applied. Some damping must be applied in order for the scheme to achieve stable results. Too much damping introduces excessive numerical energy dissipation and hence inaccurate results. Due to the strong non-linearity, an exact analytical range for the damping coefficient could not be determined. The amount of damping required was determined through trial and error by minimizing variation in the momentum and energy fluxes across the flow region.

4.1.1 Small Knudsen number and slip flow

At smaller Knudsen numbers in the slip flow regime ($0.01 \leq Kn < 0.1$) the Navier-Stokes and Fourier (NSF) equations require the addition of jump and slip boundary conditions and begin to become less than ideal equations for modeling gas flow. This regime is thus seen as a good testing ground for more extended models of rarefied gas flow such as the Grad 13 equations. At the lower end of this regime ($Kn = 0.01,\ 0.025$) the Grad 13 models should give the same results as the NSF equations. When the Knudsen number progresses higher ($Kn = 0.1$) the NSF equations become inaccurate in the boundary regions and a higher order model more accurately reflects the flow properties. The simple addition of the $\mathcal{O}\left(Kn^2\right)$ Chapman-Enskog expansion terms of Sec. (2.6) to the NSF equations, that are the reduced Burnett equations, provides some extended applicability. At $Kn = 0.1$ we see that the the NSF equations are no longer accurate and the Grad 13 equations are needed.

The following set of figures, Figs. 4-1a to 4-1h shows the case of Couette flow at $Kn = 0.01$ with a velocity difference of $\Delta v = 300\frac{\mathrm{m}}{\mathrm{s}}$ between the plates. This corresponds to a maximum Mach number of $M = \frac{\Delta v}{\sqrt{\frac{5}{3}\frac{k}{m}T_0}} = 0.97$. The Modified MacCormack's Scheme (MMS) of Sec. (3.6) are compared to the NSF and Direct Simulation Monty Carlo (DSMC) results.

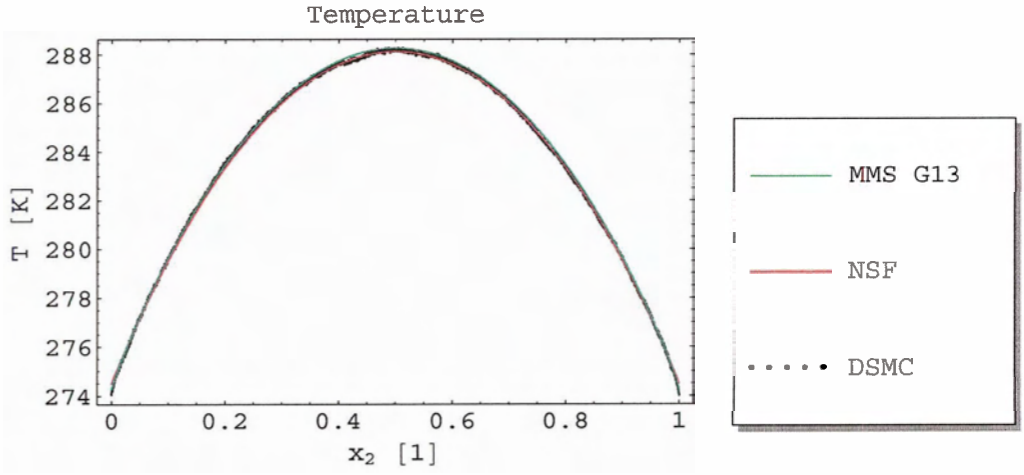

Figure 4-1a: Temperature at $Kn = 0.01$ and $\Delta v = 300\frac{\mathrm{m}}{\mathrm{s}}$

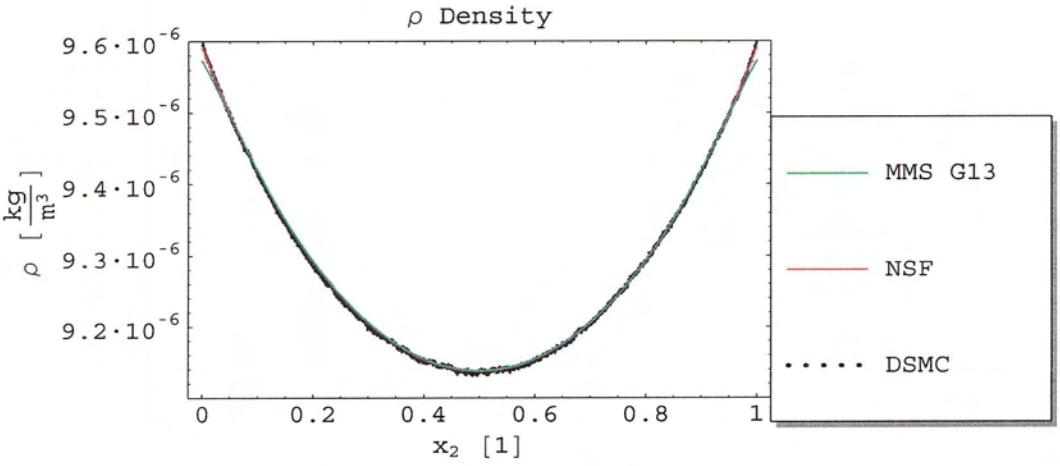

Figure 4-1b: Density at $Kn = 0.01$ and $\Delta v = 300\frac{\mathrm{m}}{\mathrm{s}}$

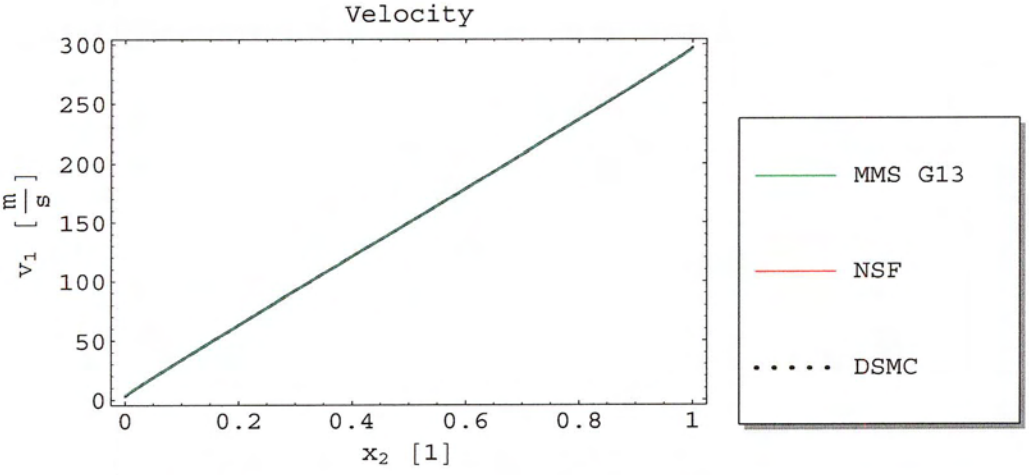

Figure 4-1c: Velocity v_1 at $Kn = 0.01$ and $\Delta v = 300\frac{\mathrm{m}}{\mathrm{s}}$

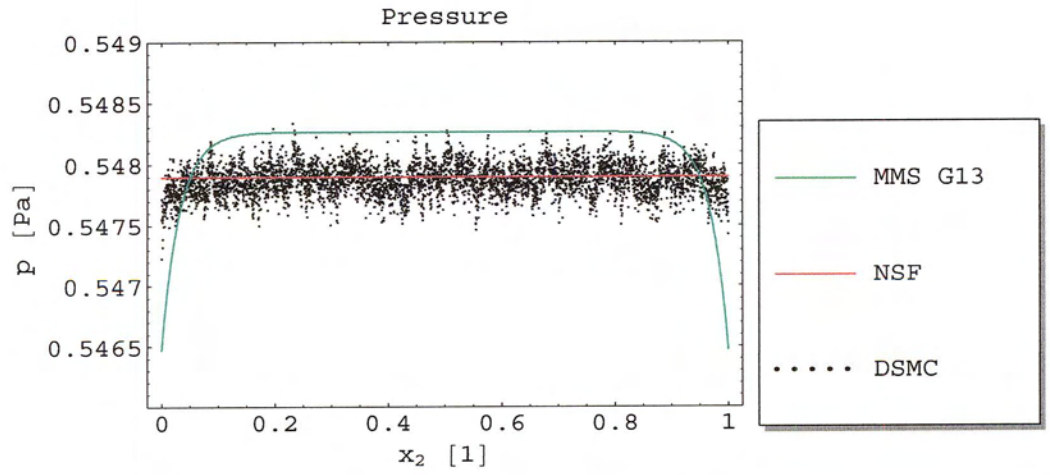

Figure 4-1d: Pressure at $Kn = 0.01$ and $\Delta v = 300\frac{\mathrm{m}}{\mathrm{s}}$

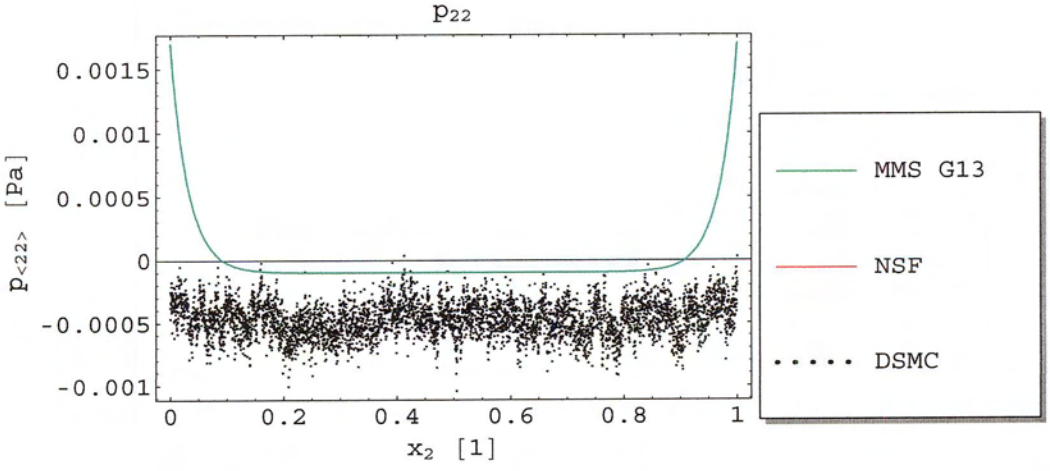

Figure 4-1e: $p_{<22>}$ at $Kn = 0.01$ and $\Delta v = 300\frac{\mathrm{m}}{\mathrm{s}}$

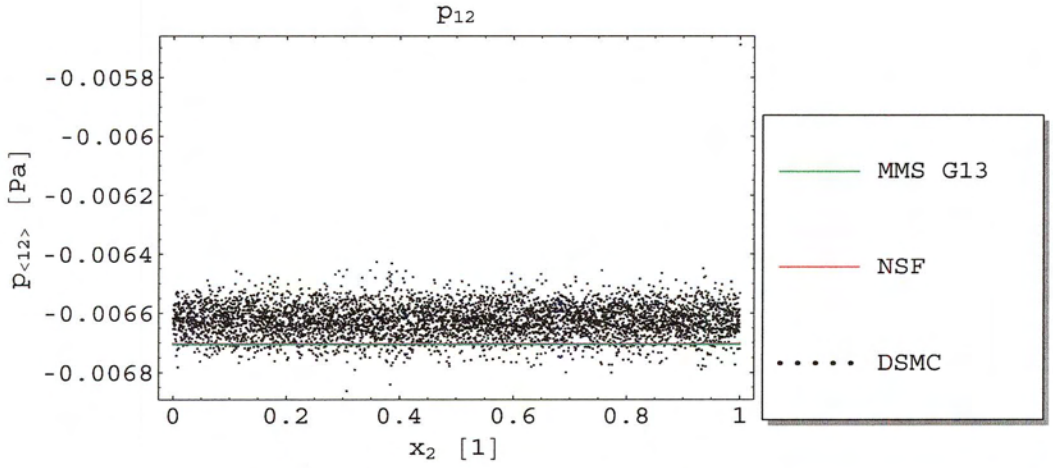

Figure 4-1f: $p_{<12>}$ at $Kn = 0.01$ and $\Delta v = 300\frac{\mathrm{m}}{\mathrm{s}}$

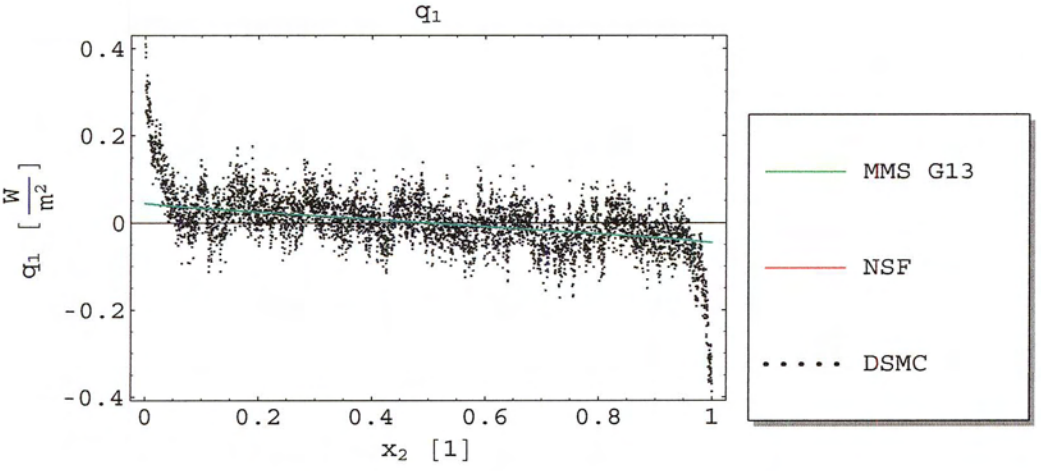

Figure 4-1g: q_1 at $Kn = 0.01$ and $\Delta v = 300\frac{\mathrm{m}}{\mathrm{s}}$

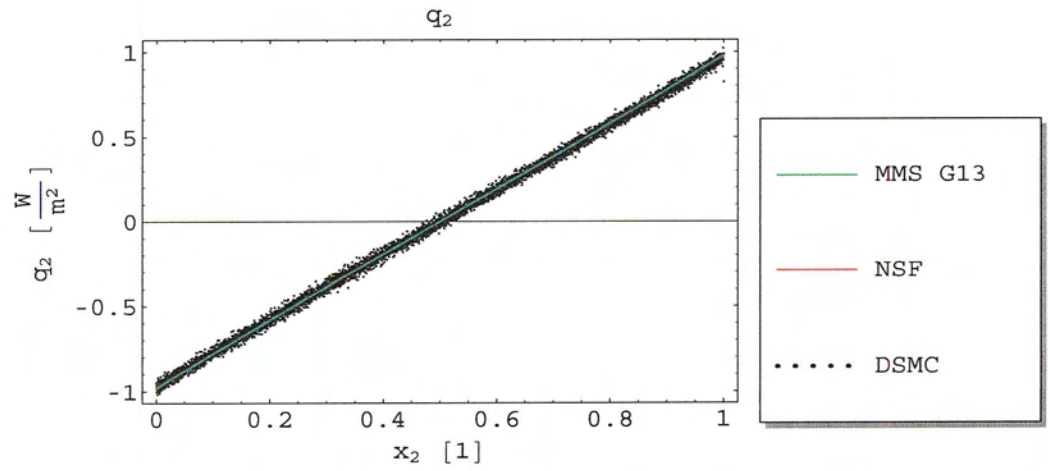

Figure 4-1h: q_2 at $Kn = 0.01$ and $\Delta v = 300\frac{\mathrm{m}}{\mathrm{s}}$

Close inspection of Fig. 4-1a to 4-1h shows that the Grad 13 results obtained with the MMS are such close a match to the NSF and DSMC results that Grad 13 and NSF cannot be distinguished. Navier, Stokes and Fourier results for $p_{<22>}$ (Fig. 4-1e) and q_1 (Fig. 4-1g) are of course unavailable or zero as this properties are not modeled in the NSF equations.

Of interest for this case is that the computation time on a current workstation[1] is on the order of seconds for the NSF, minutes for the MMS and weeks for the DSMC in this case.

Now we keep the Knudsen number at $Kn = 0.01$, but increase the velocity difference to $\Delta v = 600\frac{\mathrm{m}}{\mathrm{s}}$, $M = 1.95$. Figures 4-2a to 4-2h show that the NSF equations are still adequate. It can be seen, however, that $p_{<22>}$ and q_1, which are zero in the NSF theory, are beginning to become significant. The grad 13 equations capture the bulk values of $p_{<22>}$ and q_1 well. While small differences are observed at the boundaries, that are within the Knudsen layer.

[1]Single processor running at approximately 2 GHz with native 64 bit floating point arithmetic.

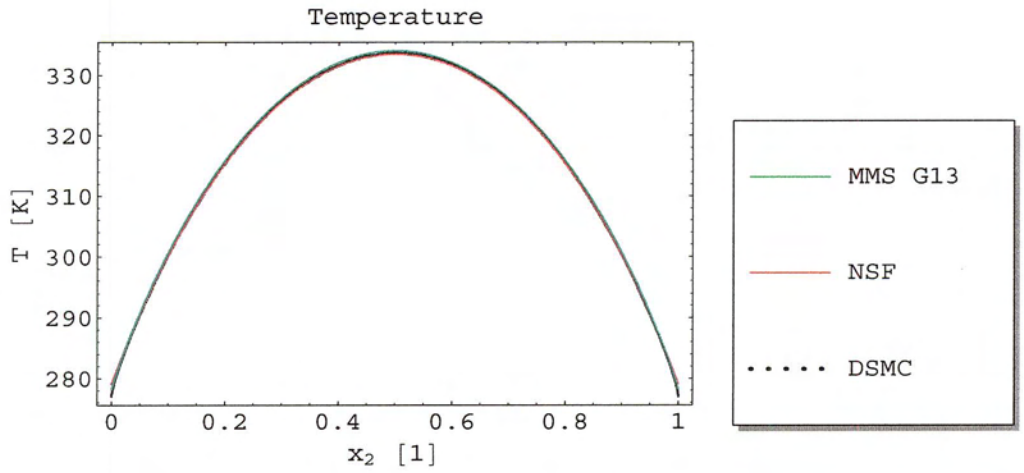

Figure 4-2a: Temperature at $Kn = 0.01$ and $\Delta v = 600\frac{\mathrm{m}}{\mathrm{s}}$

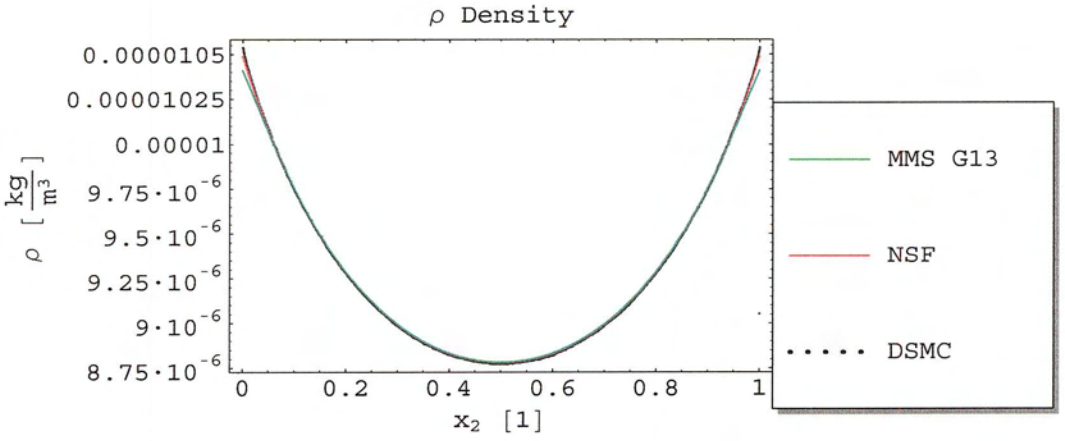

Figure 4-2b: Density at $Kn = 0.01$ and $\Delta v = 600\frac{\mathrm{m}}{\mathrm{s}}$

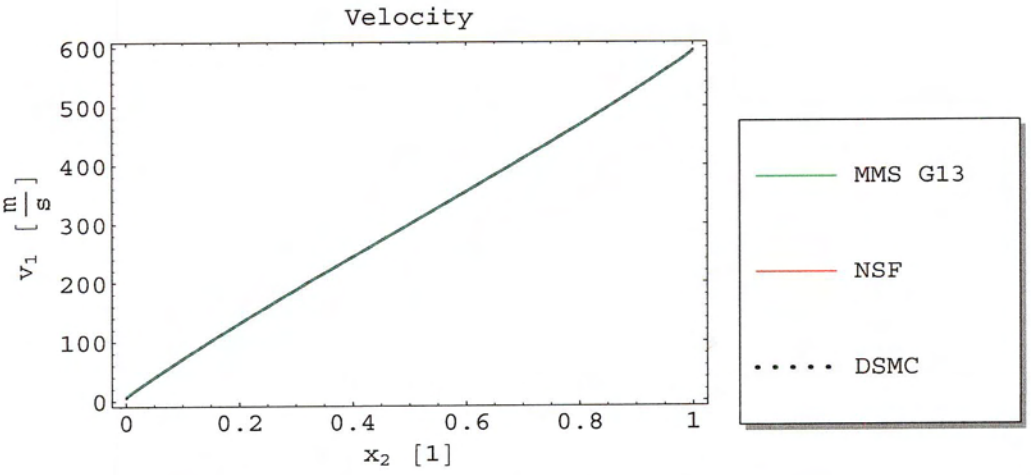

Figure 4-2c: Velocity v_1 at $Kn = 0.01$ and $\Delta v = 600\frac{\mathrm{m}}{\mathrm{s}}$

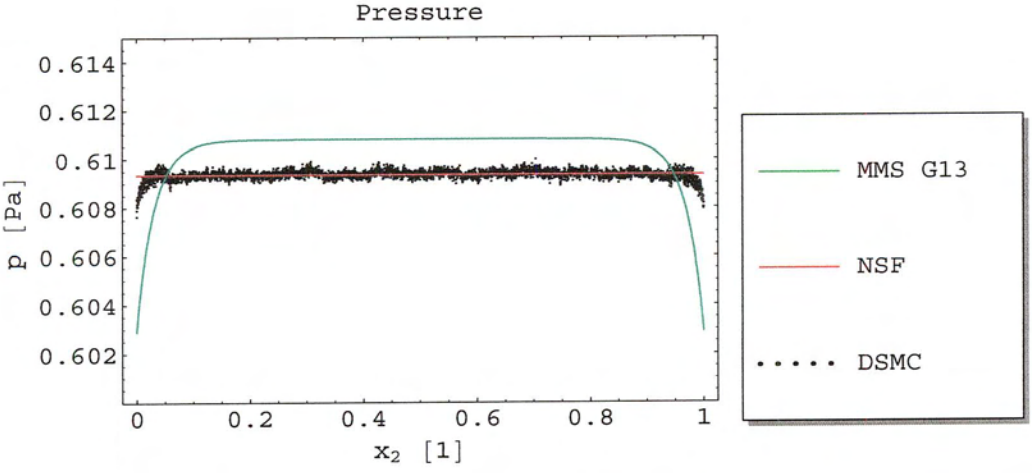

Figure 4-2d: Pressure at $Kn = 0.01$ and $\Delta v = 600\frac{\mathrm{m}}{\mathrm{s}}$

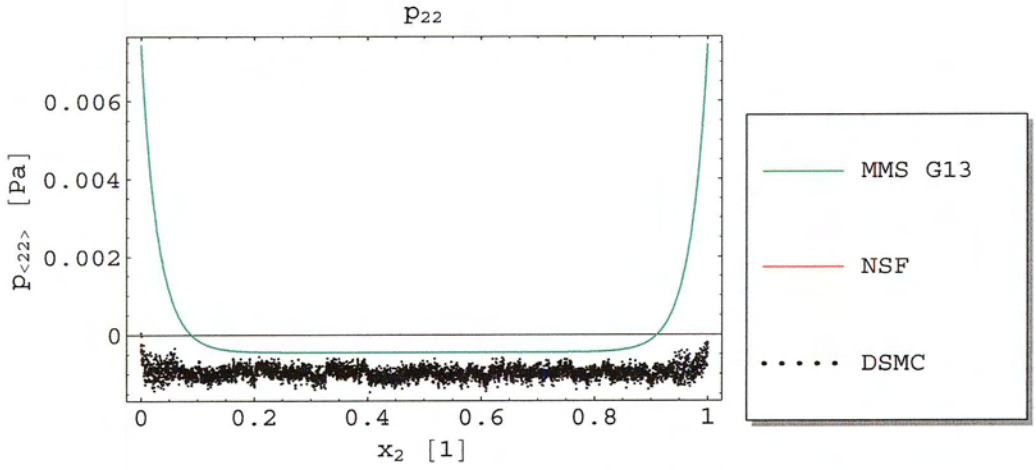

Figure 4-2e: $p_{<22>}$ at $Kn = 0.01$ and $\Delta v = 600\frac{\mathrm{m}}{\mathrm{s}}$

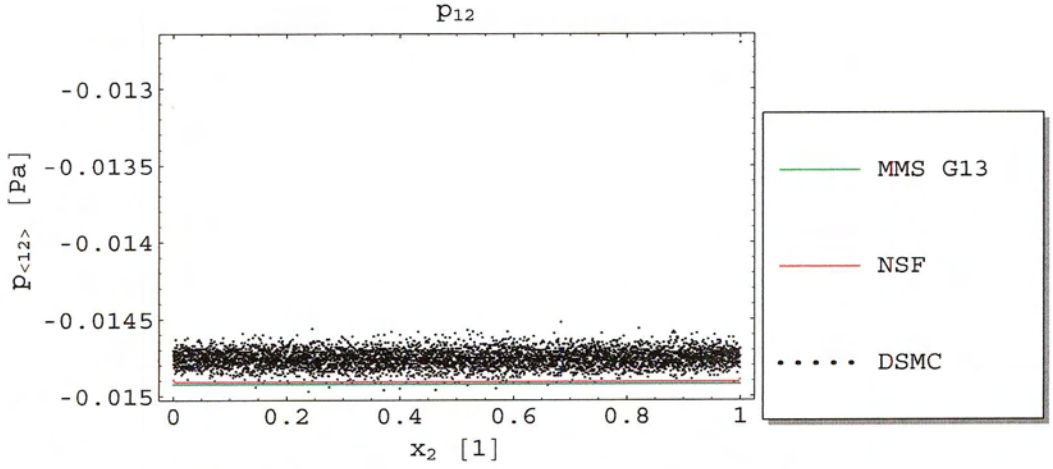

Figure 4-2f: $p_{<12>}$ at $Kn = 0.01$ and $\Delta v = 600\frac{\mathrm{m}}{\mathrm{s}}$

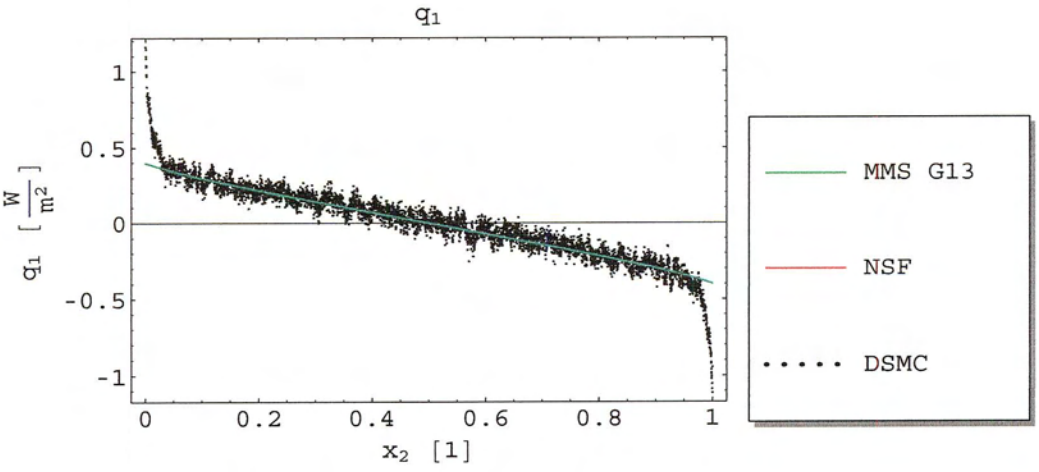

Figure 4-2g: q_1 at $Kn = 0.01$ and $\Delta v = 600\frac{\mathrm{m}}{\mathrm{s}}$

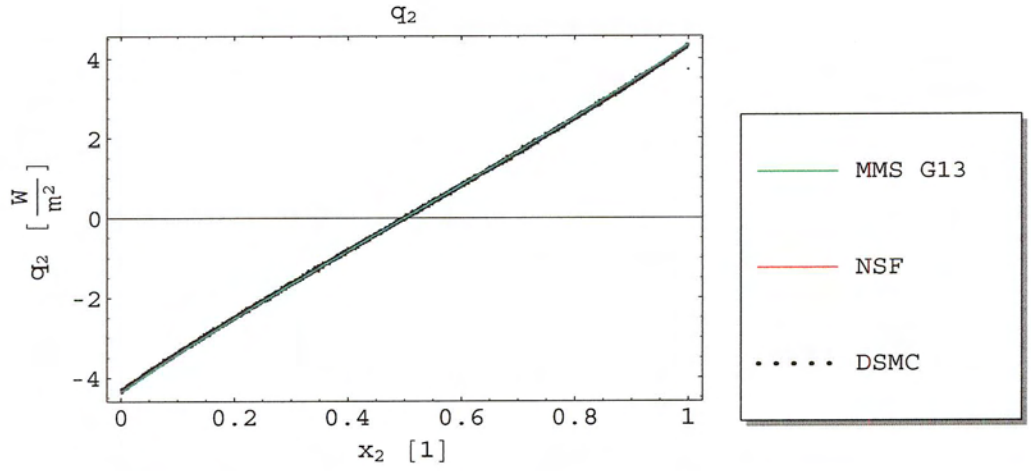

Figure 4-2h: q_2 at $Kn = 0.01$ and $\Delta v = 600\frac{\mathrm{m}}{\mathrm{s}}$

Looking at a higher Knudsen number $Kn = 0.05$ and back down to a lower velocity gradient $\Delta v = 300$, $M = 0.97$, the heat flux parallel to the plates q_1 becomes even more significant. The results thus are now compared to the Reduced Burnett equations as they add $p_{<22>}$ and q_1 contributions the the NSF results. These results are shown in Figs. 4-3a to 4-3h below. It becomes obvious that the reduced Burnett equations describe the gas in the bulk quite well, but cannot reproduce the Knudsen boundary layers, e.g., q_1 Fig. 4-3g. The

result for $p_{<22>}$, Fig. 4-3e, from the Grad 13 equations differs mostly in the Knudsen layers, which are more pronounced in the DSMC case. Note that the Grad 13 equations do not have linear Knudsen layers and the layers observed here are due to non-linear terms in the equations.

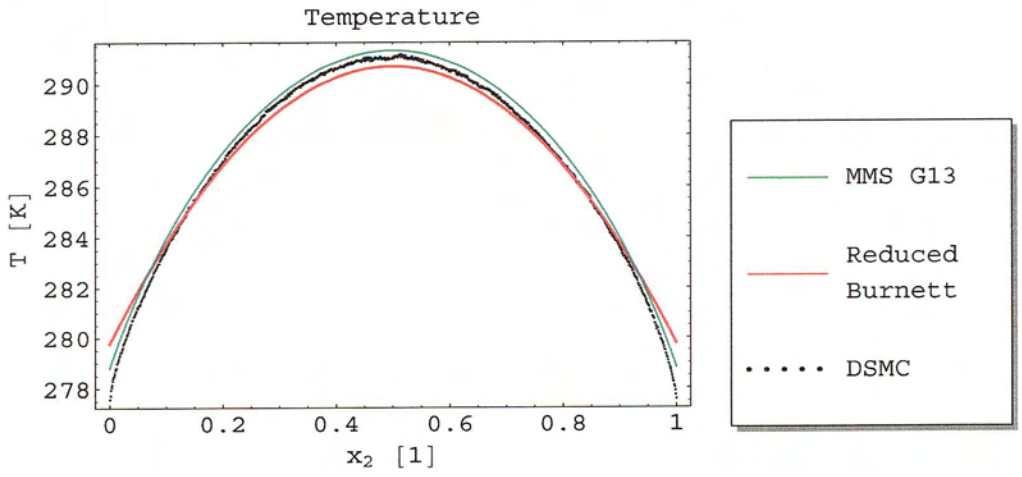

Figure 4-3a: Temperature at $Kn = 0.05$ and $\Delta v = 300\frac{\mathrm{m}}{\mathrm{s}}$

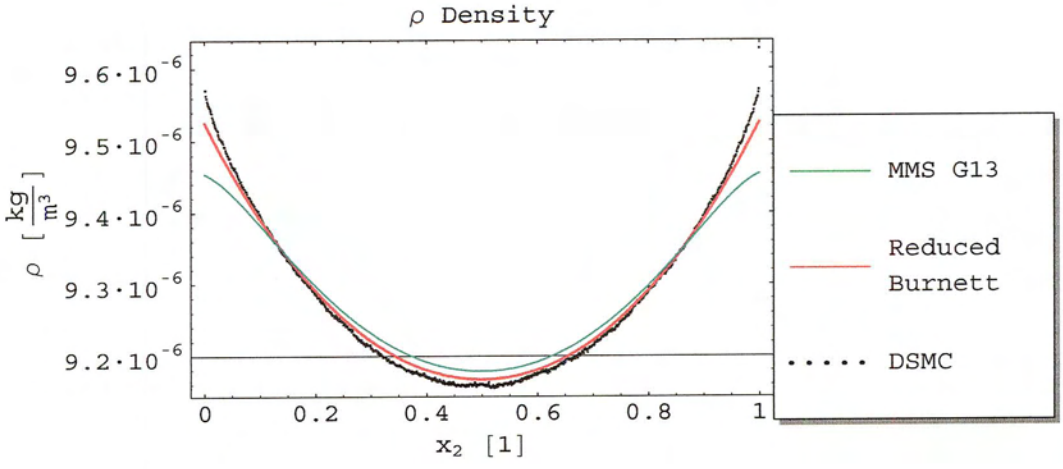

Figure 4-3b: Density at $Kn = 0.05$ and $\Delta v = 300\frac{\mathrm{m}}{\mathrm{s}}$

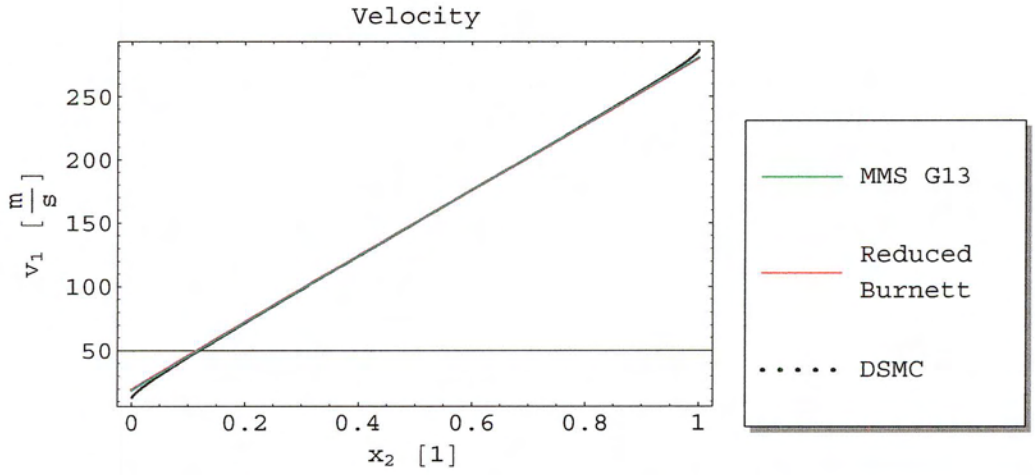

Figure 4-3c: Velocity v_1 at $Kn = 0.05$ and $\Delta v = 300\frac{\mathrm{m}}{\mathrm{s}}$

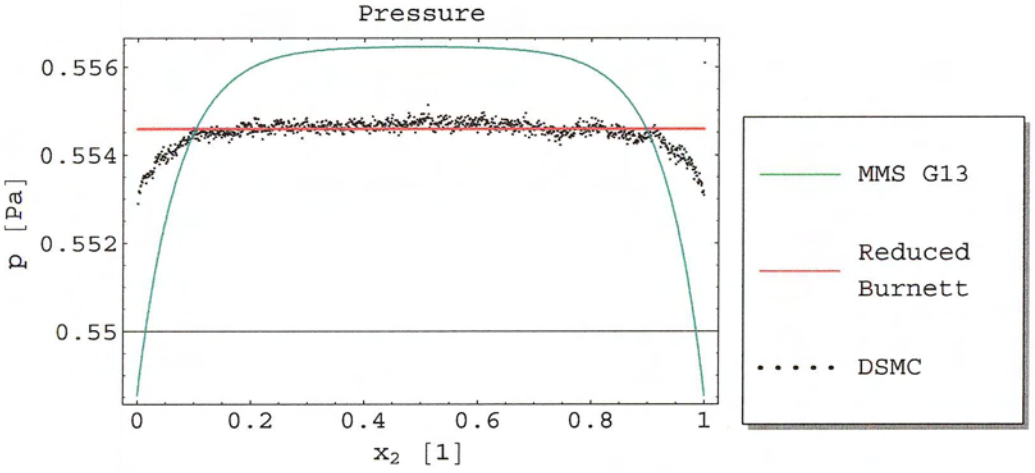

Figure 4-3d: Pressure at $Kn = 0.05$ and $\Delta v = 300\frac{\mathrm{m}}{\mathrm{s}}$

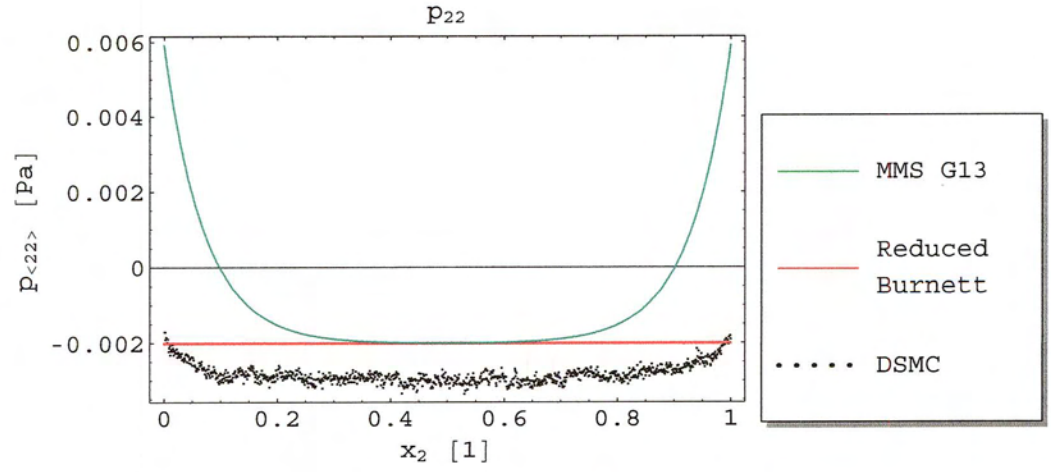

Figure 4-3e: $p_{<22>}$ at $Kn = 0.05$ and $\Delta v = 300\frac{\mathrm{m}}{\mathrm{s}}$

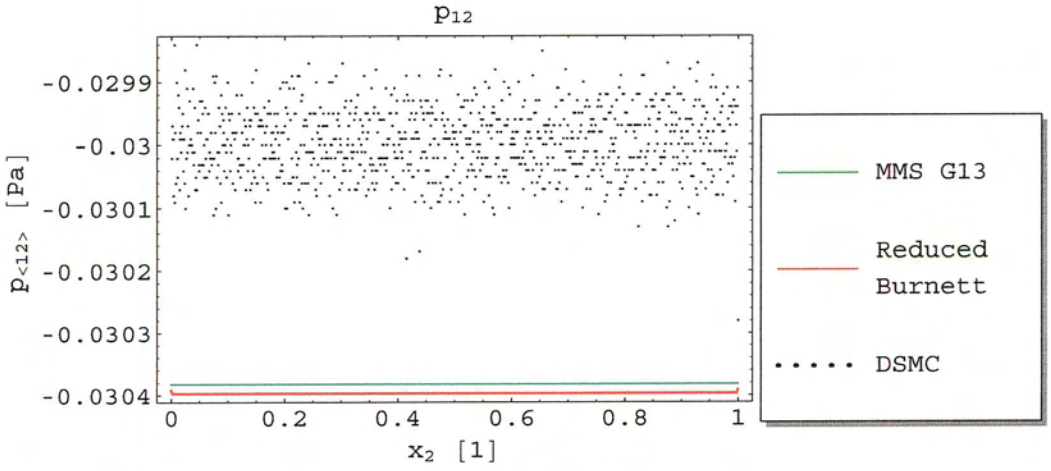

Figure 4-3f: $p_{<12>}$ at $Kn = 0.05$ and $\Delta v = 300\frac{\mathrm{m}}{\mathrm{s}}$

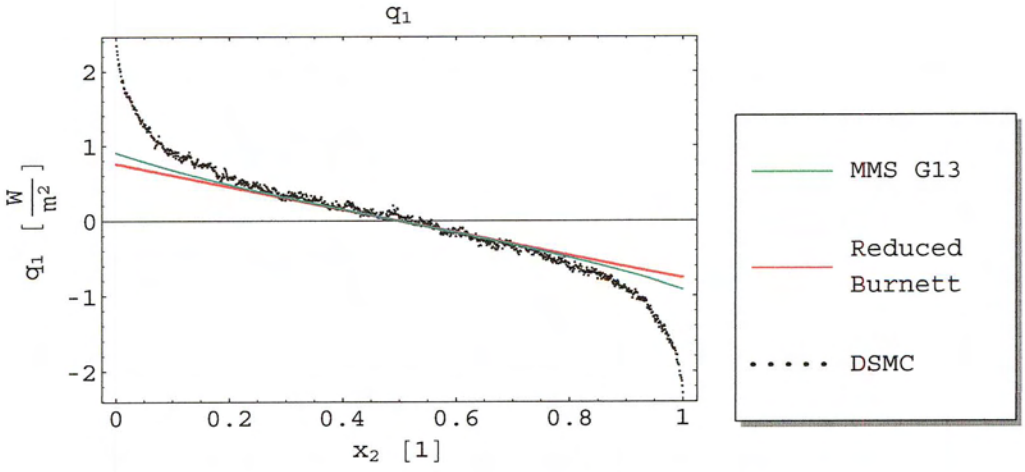

Figure 4-3g: q_1 at $Kn = 0.05$ and $\Delta v = 300\frac{\mathrm{m}}{\mathrm{s}}$

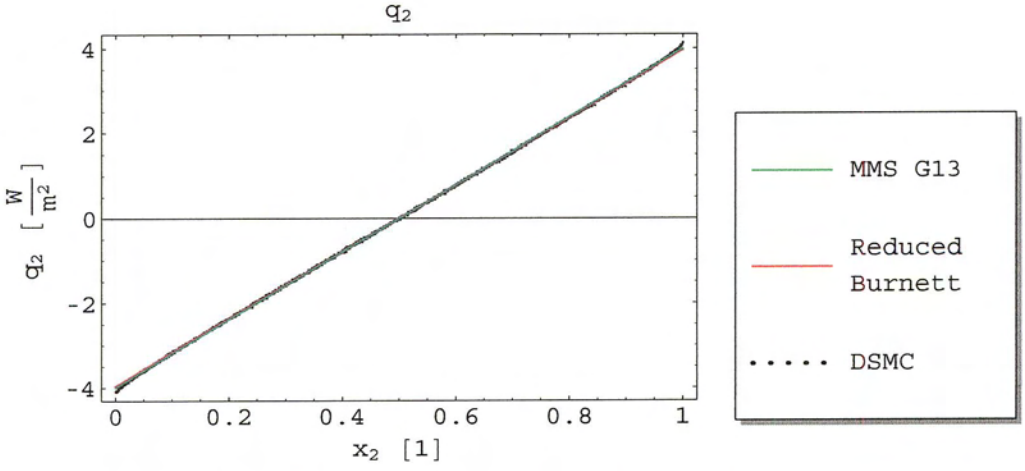

Figure 4-3h: q_2 at $Kn = 0.05$ and $\Delta v = 300\frac{\mathrm{m}}{\mathrm{s}}$

Results for $Kn = 0.05$ and $\Delta v = 800$ ($M = 2.6$) are shown below in Figs. 4-4a to 4-4h. These results show little extra about the nature of the flow and the Grad 13 equations. Close inspection of Figs. 4-4g and 4-4e, the q_1 and $p_{<22>}$ curves, shows the beginning of an error that could possibly be attributed to the numerical method. This error may however be inherent in the equations or the boundary conditions. This error is noticeable as the Reduced Burnett solution for these properties appears more accurate than the modified

MacCormack scheme Grad 13 solution.

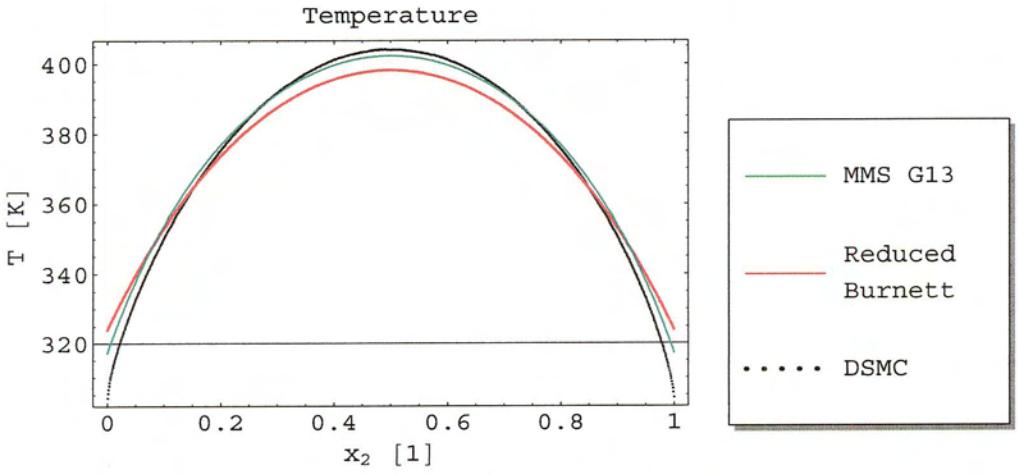

Figure 4-4a: Temperature at $Kn = 0.05$ and $\Delta v = 800\frac{\mathrm{m}}{\mathrm{s}}$

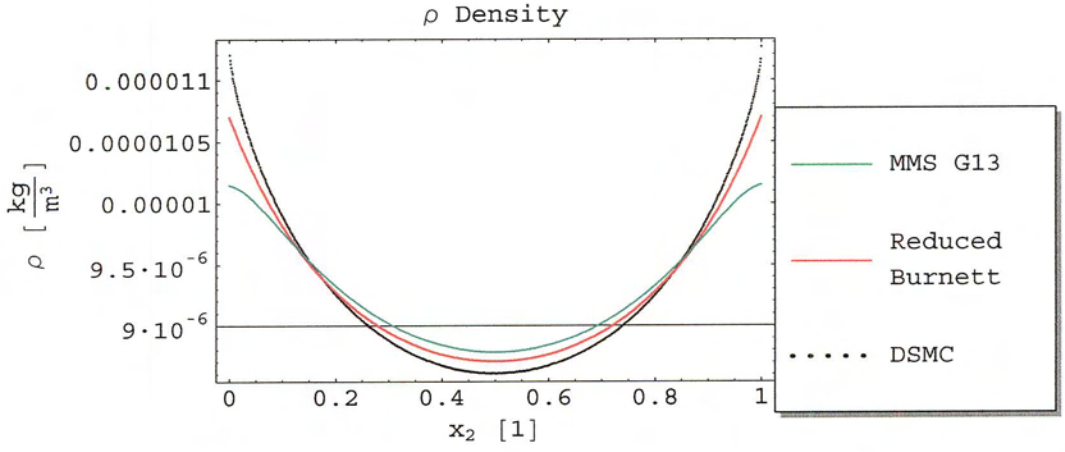

Figure 4-4b: Density at $Kn = 0.05$ and $\Delta v = 800\frac{\mathrm{m}}{\mathrm{s}}$

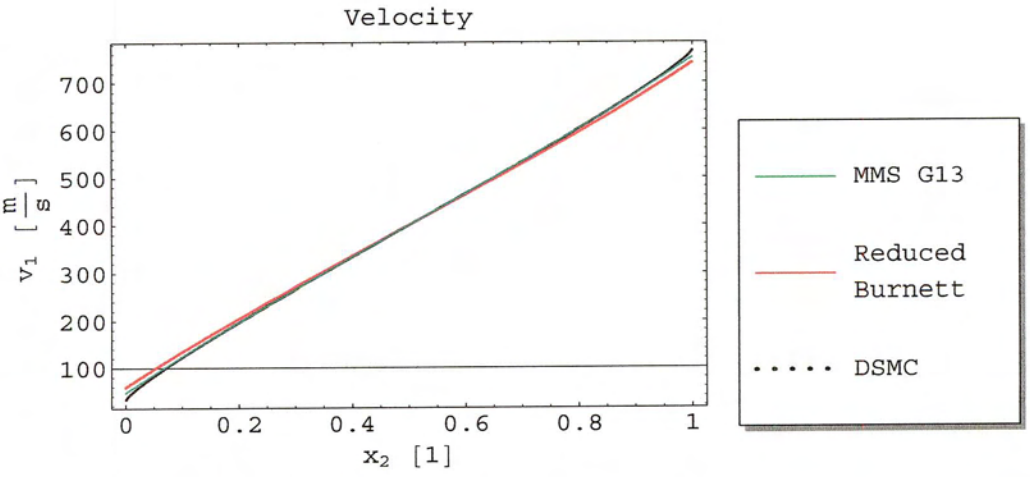

Figure 4-4c: Velocity v_1 at $Kn = 0.05$ and $\Delta v = 800\frac{\mathrm{m}}{\mathrm{s}}$

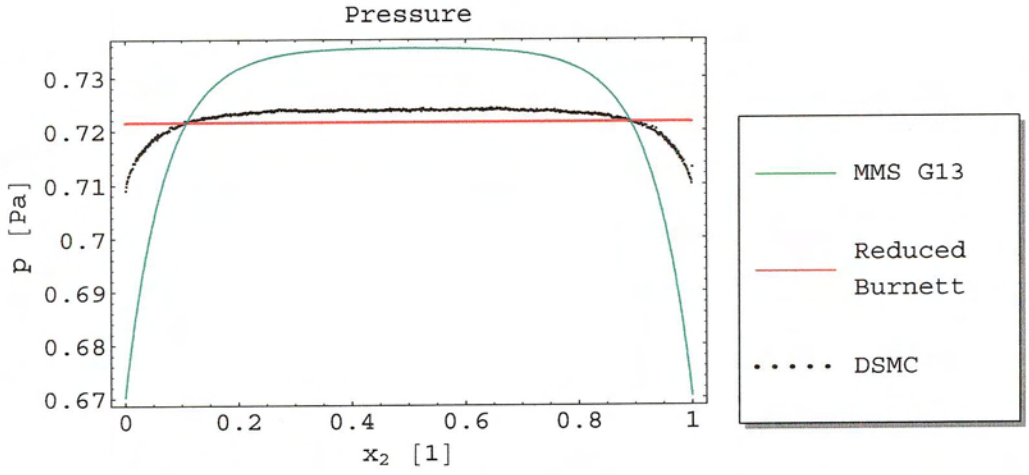

Figure 4-4d: Pressure at $Kn = 0.05$ and $\Delta v = 800\frac{\mathrm{m}}{\mathrm{s}}$

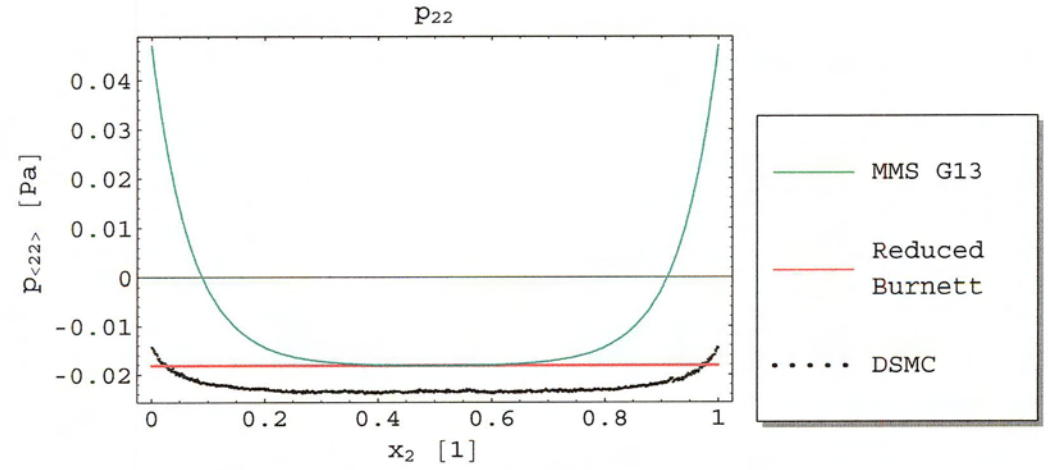

Figure 4-4e: $p_{<22>}$ at $Kn = 0.05$ and $\Delta v = 800\frac{\mathrm{m}}{\mathrm{s}}$

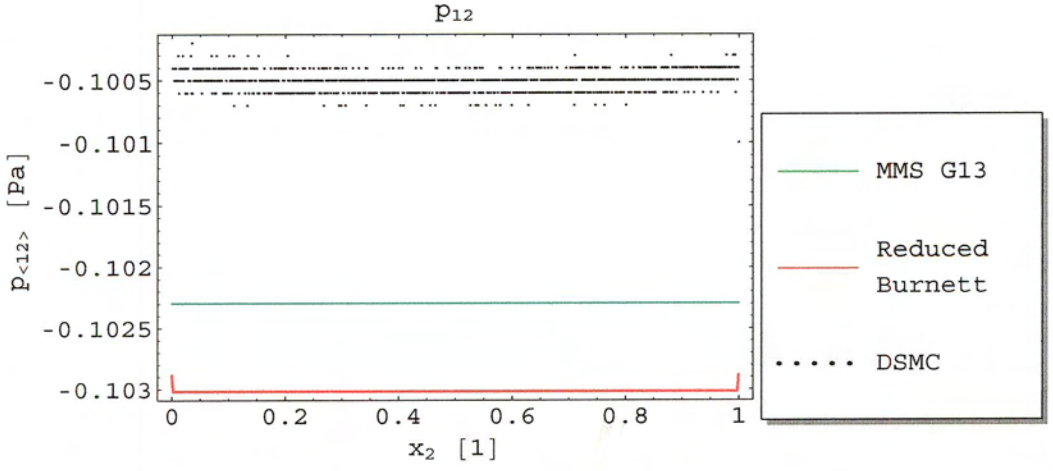

Figure 4-4f: $p_{<12>}$ at $Kn = 0.05$ and $\Delta v = 800\frac{\mathrm{m}}{\mathrm{s}}$

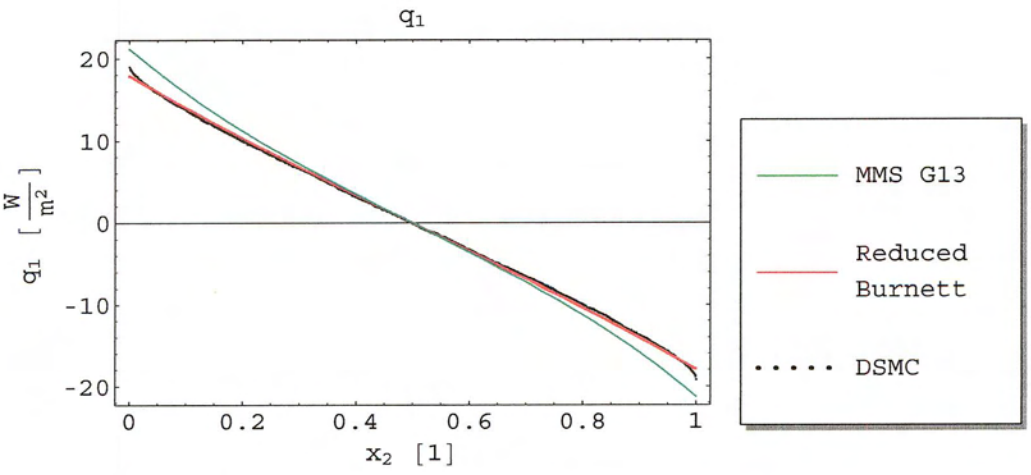

Figure 4-4g: q_1 at $Kn = 0.05$ and $\Delta v = 800\frac{\mathrm{m}}{\mathrm{s}}$

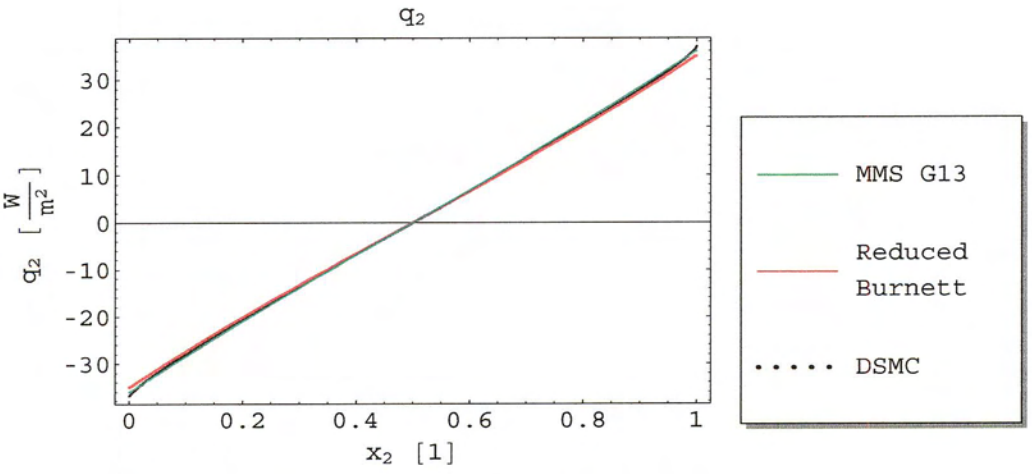

Figure 4-4h: q_2 at $Kn = 0.05$ and $\Delta v = 800\frac{\mathrm{m}}{\mathrm{s}}$

4.1.2 Early stages of transitional flow

In transitional flow regime of $0.1 \leq Kn < 10$ the NSF equations do not give good results. With the Grad 13 equations it will be shown that we can get some useful results, at least for the beginning stages of the regime $0.1 \leq Kn \leq 1.0$. This is promising as the beginning of this regime is exactly where there is a gap to fill. For larger Knudsen numbers compu-

tational times for DSMC simulations are significantly smaller, making continuum methods lose appeal at least for steady state situations.

We show results for $\Delta v = 300$, $M = 0.97$, but for a the Knudsen number of $Kn = 0.1$, shown in Figs. 4-5a to 4-5h below. This shows some definite promise for the Grad 13 equations, particularly in the temperature distribution of fig. 4-5a. The problem mentioned earlier of the $p_{<22>}$ distribution and carried through to the pressure and density distributions, Figs. 4-5e, 4-5d and 4-5b respectively, is becoming increasingly obvious. However, we do not know the magnitude of this effect and if the excessive nature of this effect in our results is inherent in the equations, due to our boundary conditions, the numerical method or a combination. Results for the Nessyahu-Tadmor method that will follow in the next section will suggest that this excessive nature is primarily an effect of the numerical method.

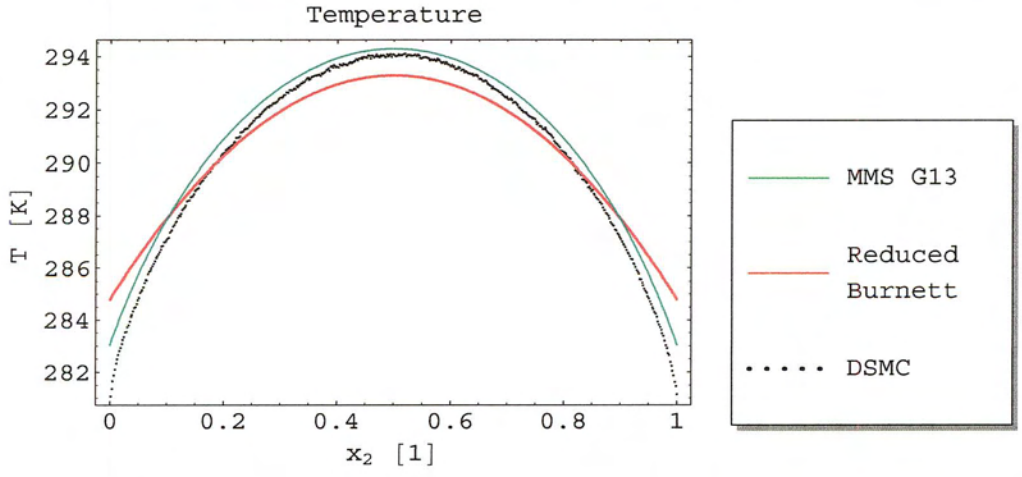

Figure 4-5a: Temperature at $Kn = 0.1$ and $\Delta v = 300\frac{\mathrm{m}}{\mathrm{s}}$

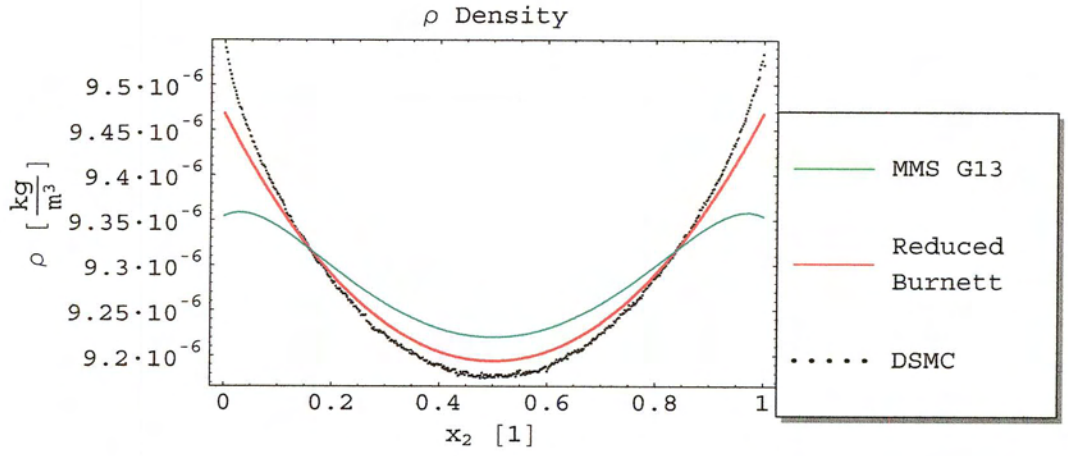

Figure 4-5b: Density at $Kn = 0.1$ and $\Delta v = 300\frac{\mathrm{m}}{\mathrm{s}}$

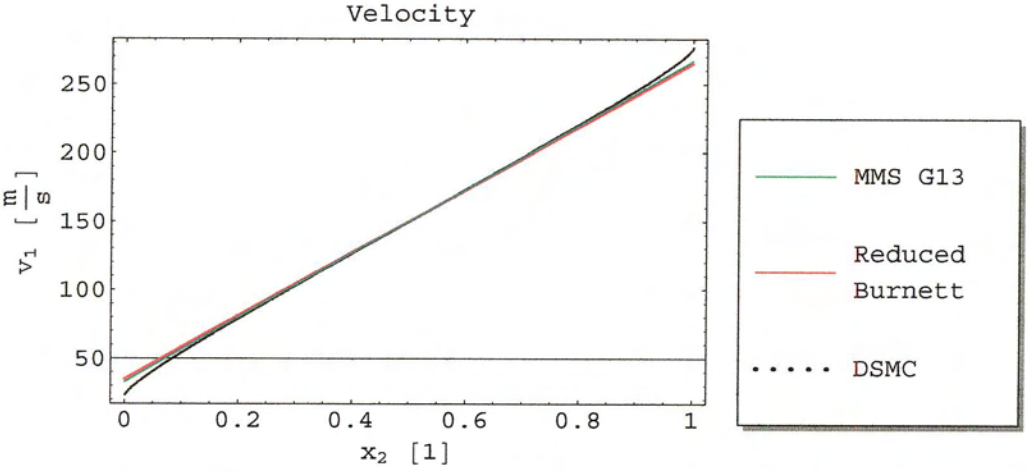

Figure 4-5c: Velocity v_1 at $Kn = 0.1$ and $\Delta v = 300\frac{\mathrm{m}}{\mathrm{s}}$

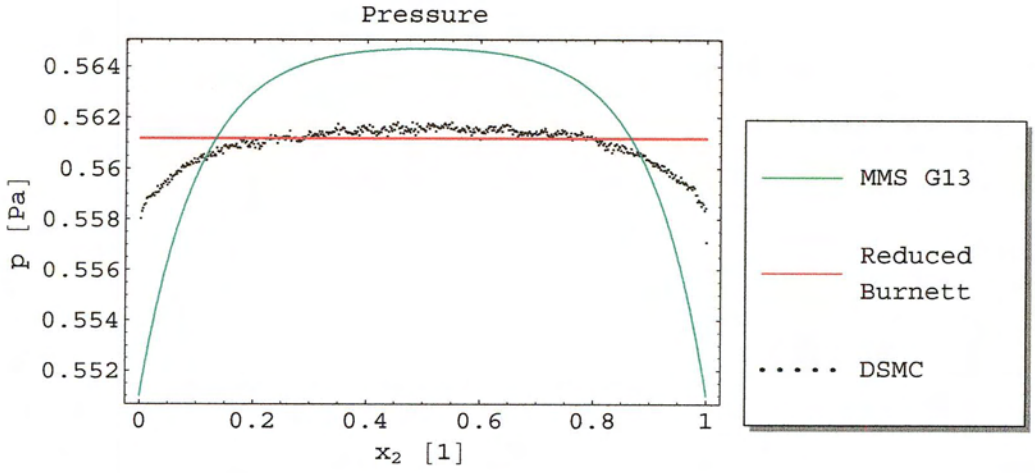

Figure 4-5d: Pressure at $Kn = 0.1$ and $\Delta v = 300\frac{\mathrm{m}}{\mathrm{s}}$

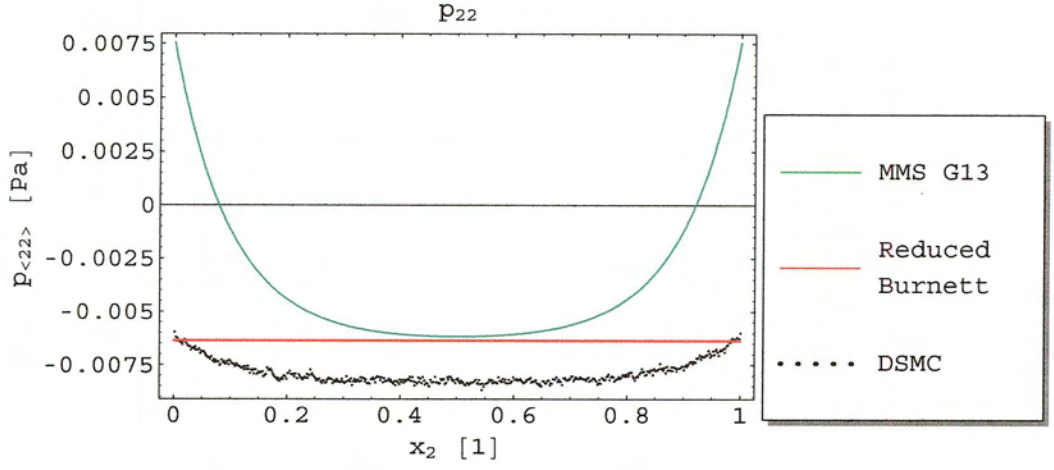

Figure 4-5e: $p_{<22>}$ at $Kn = 0.1$ and $\Delta v = 300\frac{\mathrm{m}}{\mathrm{s}}$

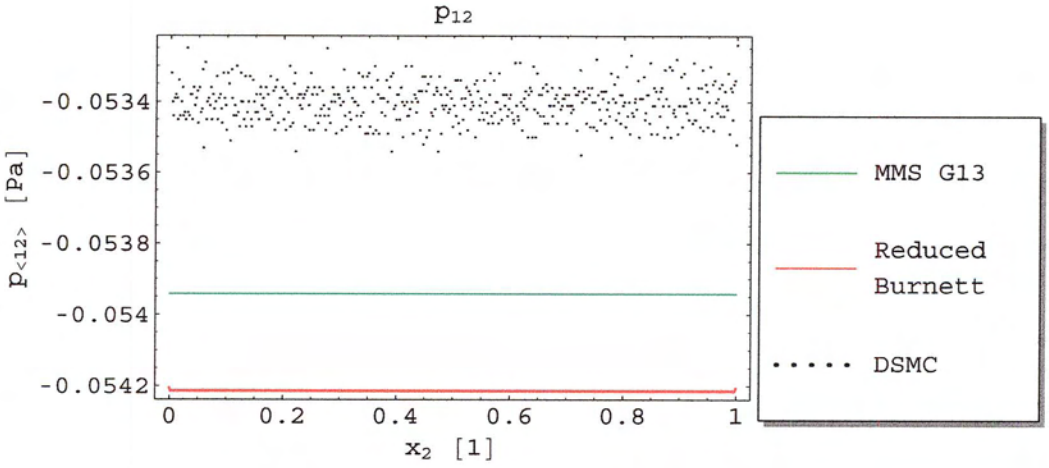

Figure 4-5f: $p_{<12>}$ at $Kn = 0.1$ and $\Delta v = 300\frac{\mathrm{m}}{\mathrm{s}}$

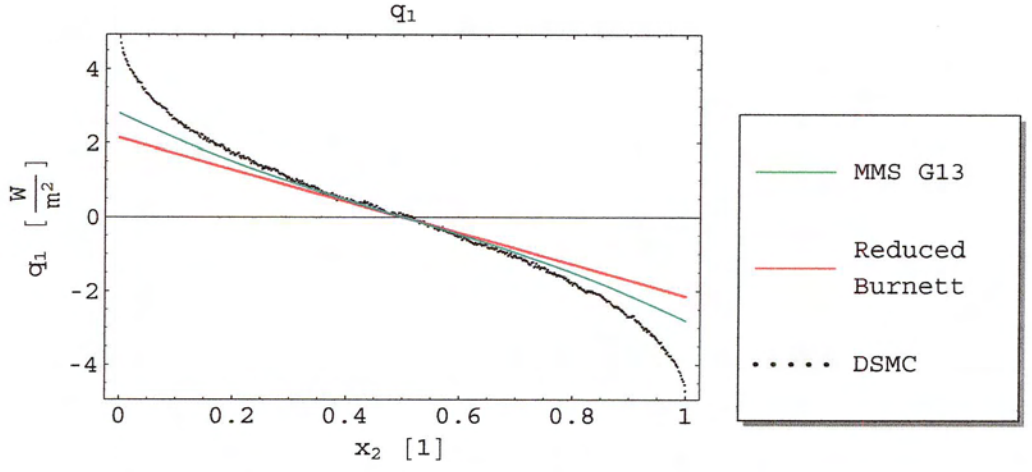

Figure 4-5g: q_1 at $Kn = 0.1$ and $\Delta v = 300\frac{\mathrm{m}}{\mathrm{s}}$

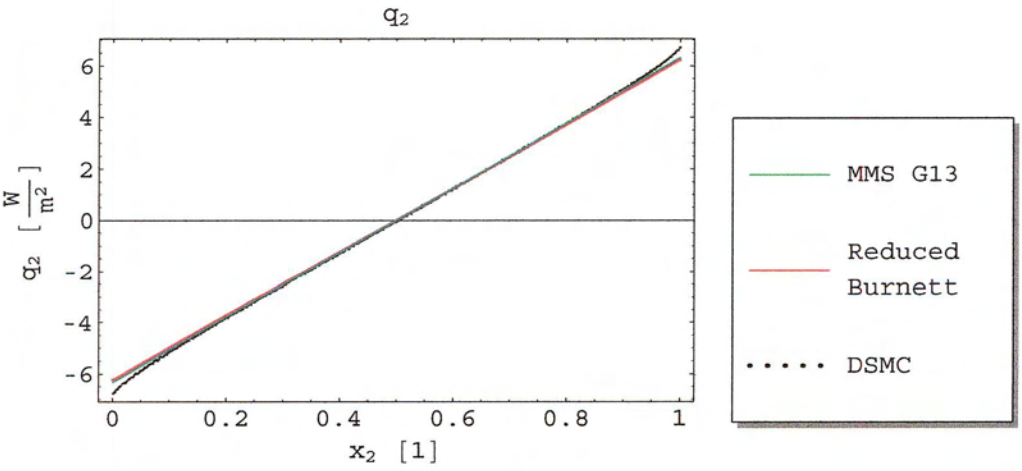

Figure 4-5h: q_2 at $Kn = 0.1$ and $\Delta v = 300\frac{\mathrm{m}}{\mathrm{s}}$

The case of $Kn = 0.1$ and $\Delta v = 300\frac{\mathrm{m}}{\mathrm{s}}$ is also used here to demonstrate that steady state in the solution of the modified MacCormack's scheme has reached steady state. Figure 4-6 below shows the variation of the central(grid point) value of temperature with time or number of iterations. It is clear that steady state has been reached.

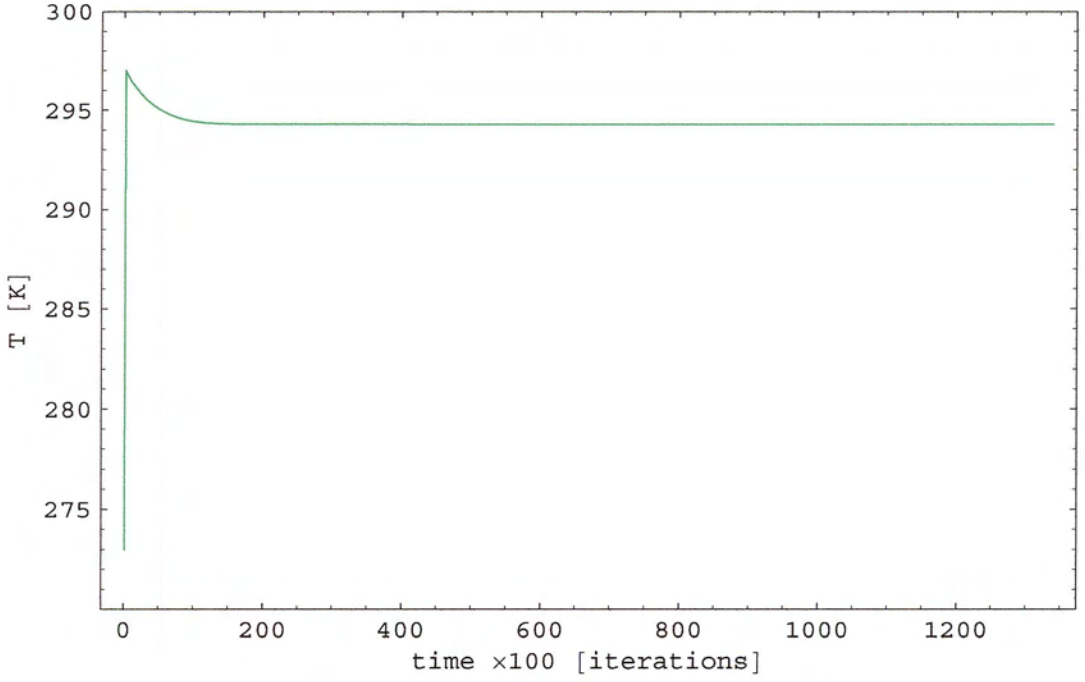

Figure 4-6: Central point temperature at $Kn = 0.1$ and $\Delta v = 300\frac{\mathrm{m}}{\mathrm{s}}$

Results for $Kn = 0.1$, $\Delta v = 800$, and $M = 2.6$, below in Figs. 4-7a to 4-7h, show more of the same error discussed previously. Now that the relative velocity of the plates has been increased, the effect is apparent in the q_1 distribution of Fig. 4-7g as well.

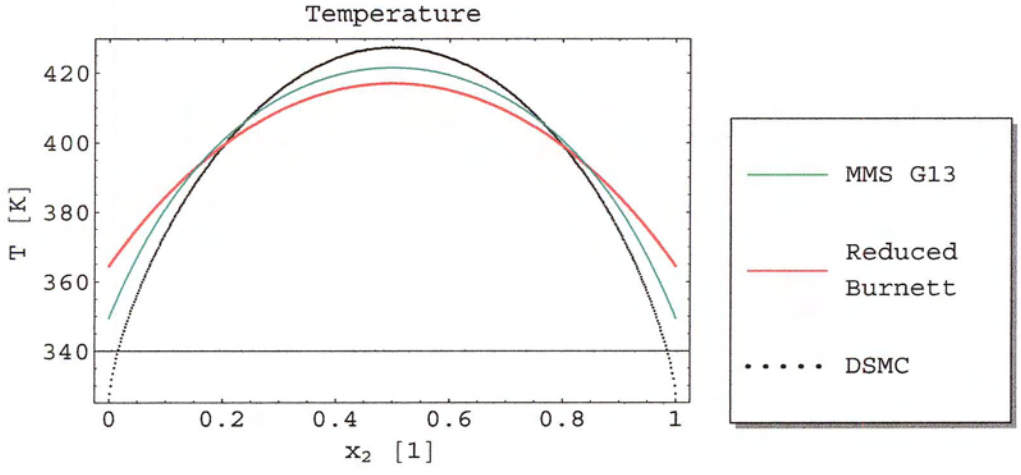

Figure 4-7a: Temperature at $Kn = 0.1$ and $\Delta v = 800\frac{\mathrm{m}}{\mathrm{s}}$

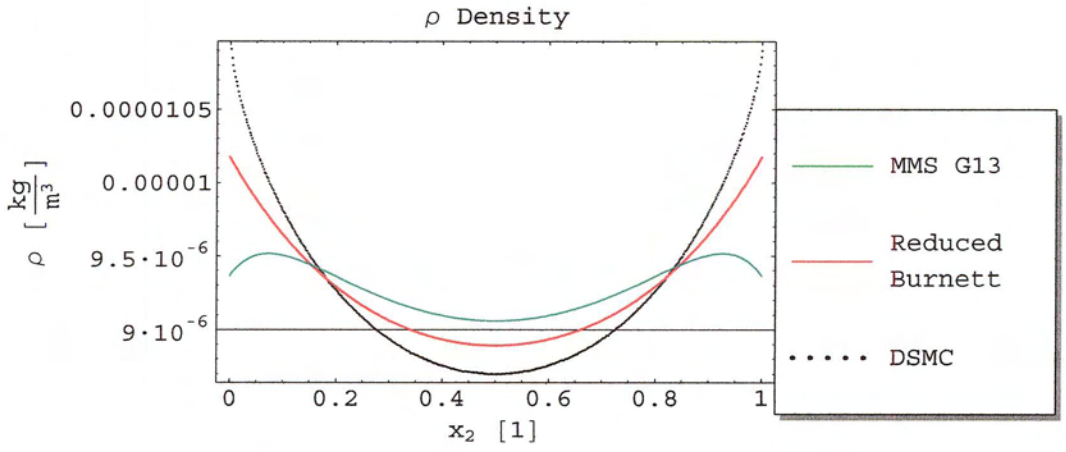

Figure 4-7b: Density at $Kn = 0.1$ and $\Delta v = 800\frac{\mathrm{m}}{\mathrm{s}}$

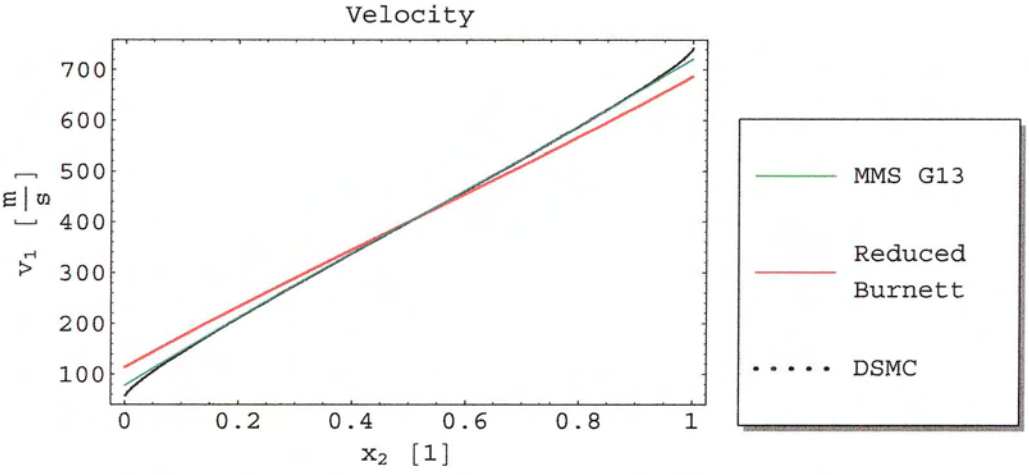

Figure 4-7c: Velocity v_1 at $Kn = 0.1$ and $\Delta v = 800\frac{\mathrm{m}}{\mathrm{s}}$

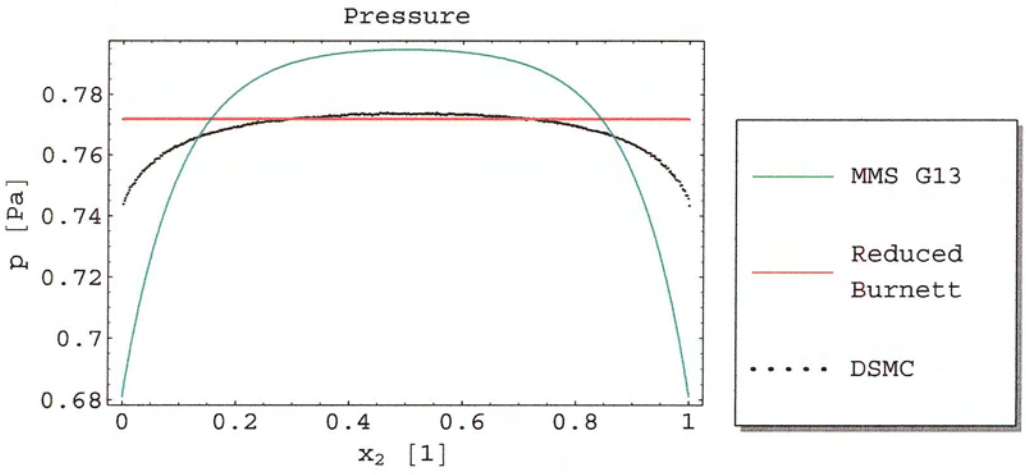

Figure 4-7d: Pressure at $Kn = 0.1$ and $\Delta v = 800\frac{\mathrm{m}}{\mathrm{s}}$

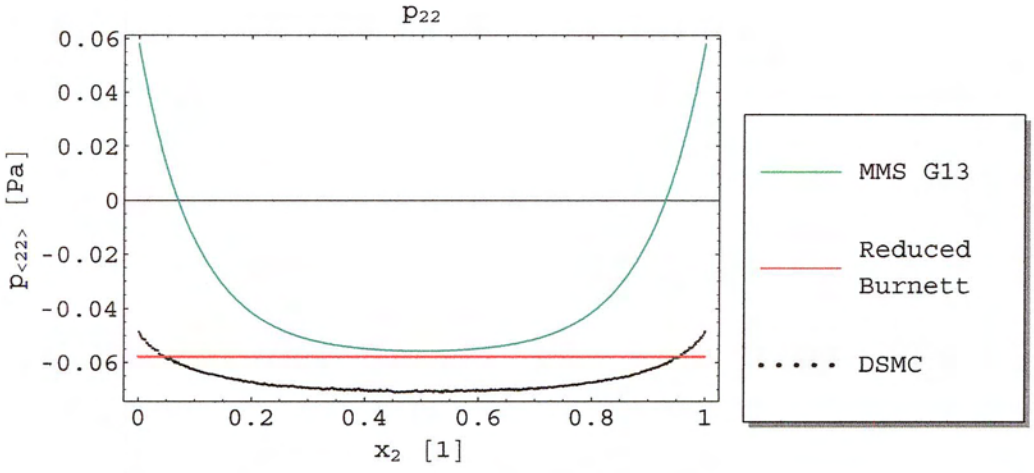

Figure 4-7e: $p_{<22>}$ at $Kn = 0.1$ and $\Delta v = 800\frac{\mathrm{m}}{\mathrm{s}}$

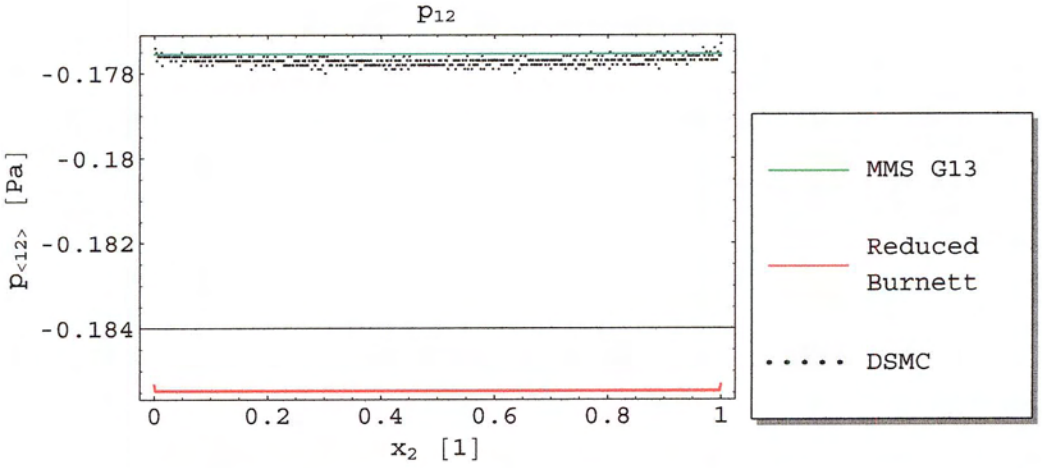

Figure 4-7f: $p_{<12>}$ at $Kn = 0.1$ and $\Delta v = 800\frac{\mathrm{m}}{\mathrm{s}}$

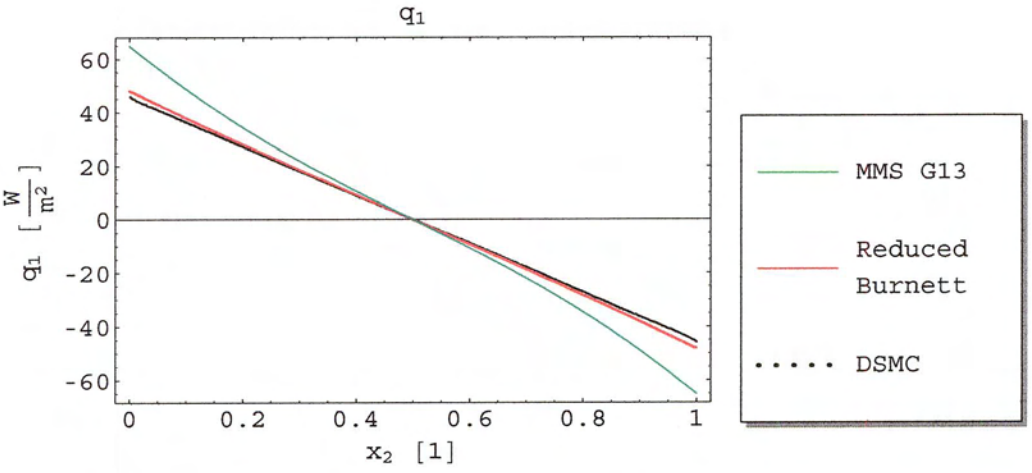

Figure 4-7g: q_1 at $Kn = 0.1$ and $\Delta v = 800\frac{\mathrm{m}}{\mathrm{s}}$

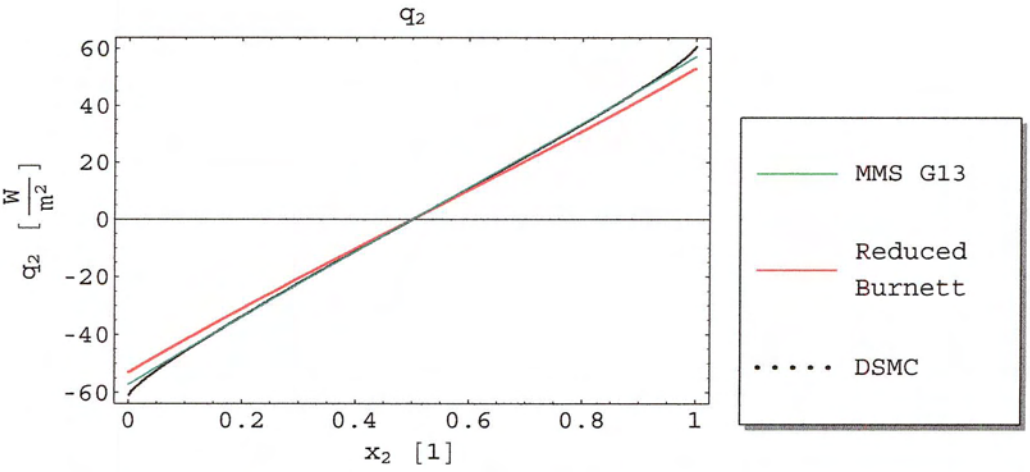

Figure 4-7h: q_2 at $Kn = 0.1$ and $\Delta v = 800\frac{\mathrm{m}}{\mathrm{s}}$

Results for $Kn = 0.25$, $\Delta v = 300$, and $M = 0.97$ below in Figs. 4-8a to 4-8h follow the same lines. Notice especially that the temperature distribution of the NSF and Reduced Burnett in Fig. 4-8a are becoming increasingly different from the DSMC benchmark. It is also now painstakingly obvious that the MMS results for $p_{<22>}$(Fig. 4-8g) does not match the DSMC results. The error in $p_{<22>}$ leads to the inverted density profile in Fig. 4-8b. A similar behavior is observed in solutions of the Burnett equations with the boundary condition $p_{<22>} = 0$ [7]. Obviously, the BC has a marked influence on the result for $p_{<22>}$ and thus for density as $\rho = \frac{p}{T} = \frac{p_\alpha - p_{<22>}}{T}$. This result puts the boundary condition Eqn. (2.84) into question.

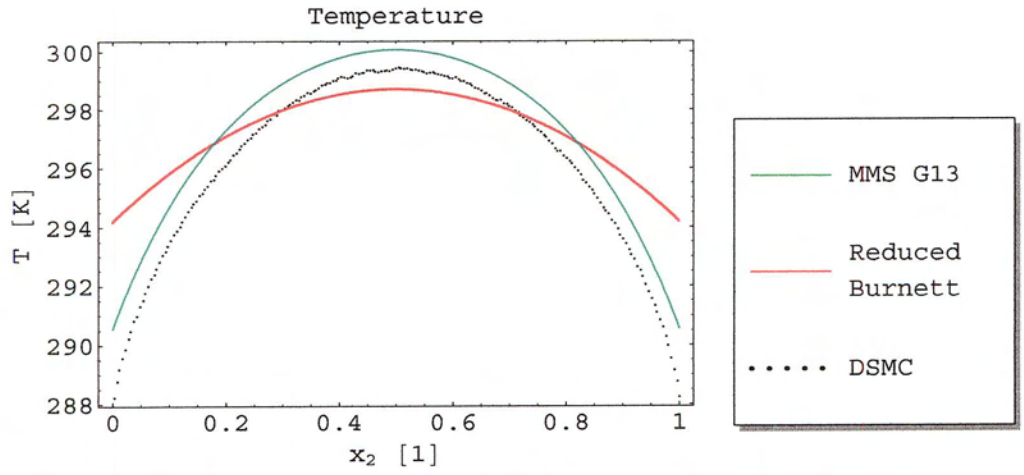

Figure 4-8a: Temperature at $Kn = 0.25$ and $\Delta v = 300\frac{\mathrm{m}}{\mathrm{s}}$

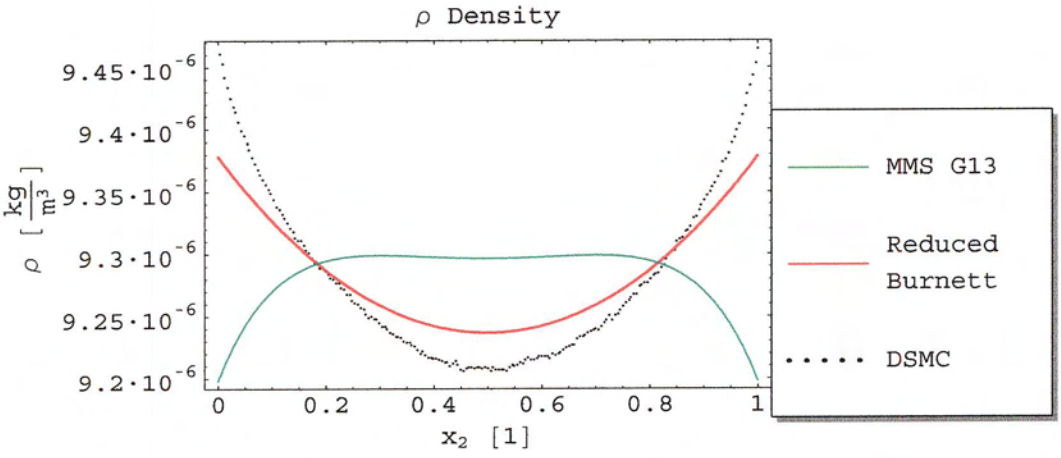

Figure 4-8b: Density at $Kn = 0.25$ and $\Delta v = 300\frac{\mathrm{m}}{\mathrm{s}}$

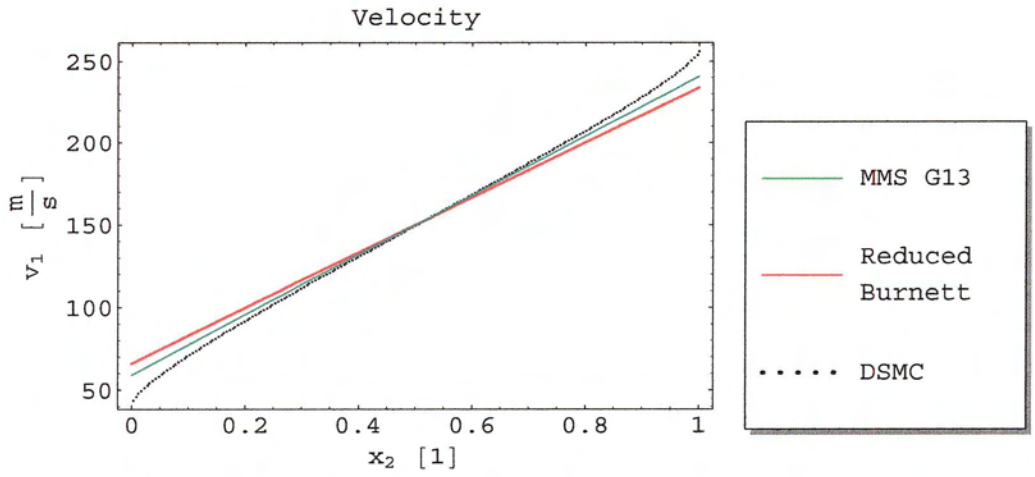

Figure 4-8c: Velocity v_1 at $Kn = 0.25$ and $\Delta v = 300\frac{\text{m}}{\text{s}}$

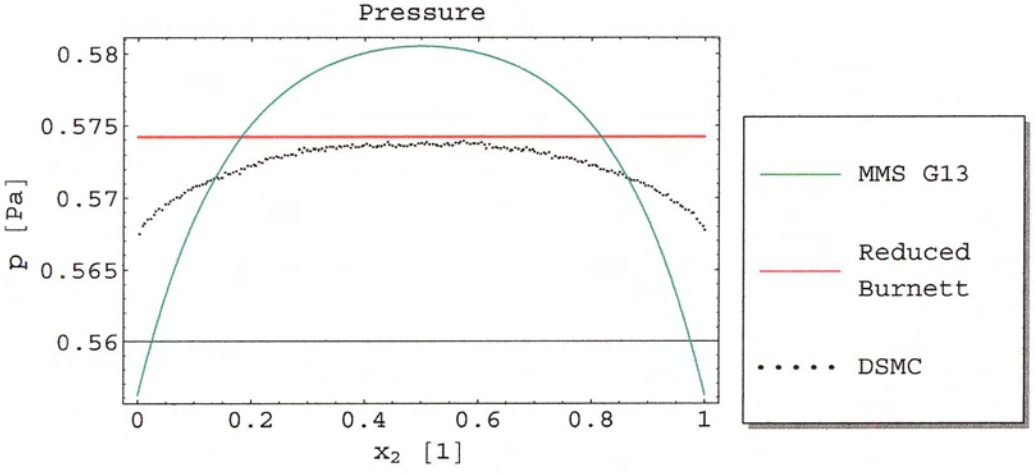

Figure 4-8d: Pressure at $Kn = 0.25$ and $\Delta v = 300\frac{\text{m}}{\text{s}}$

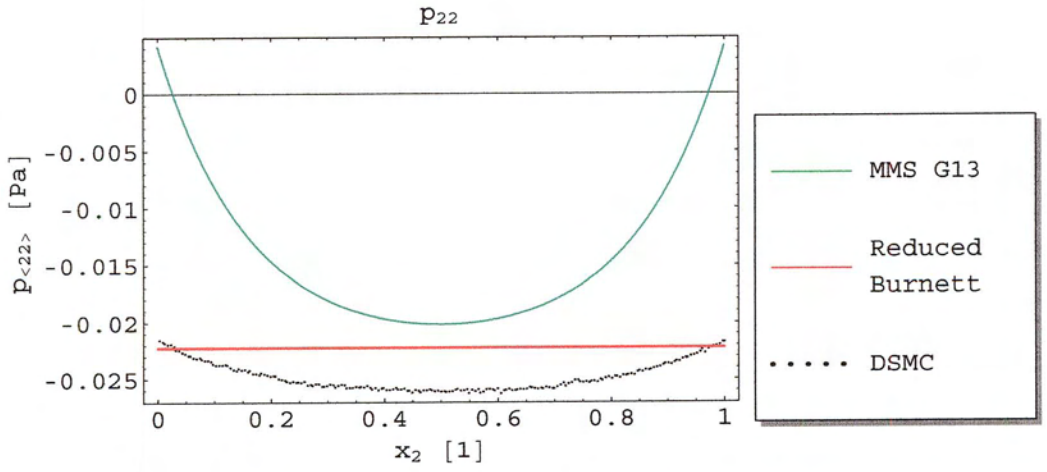

Figure 4-8e: $p_{<22>}$ at $Kn = 0.25$ and $\Delta v = 300\frac{\mathrm{m}}{\mathrm{s}}$

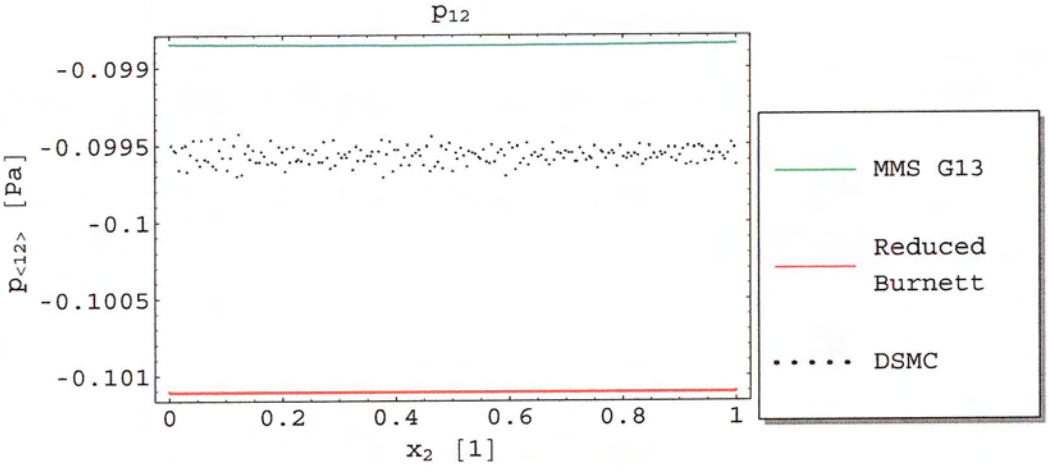

Figure 4-8f: $p_{<12>}$ at $Kn = 0.25$ and $\Delta v = 300\frac{\mathrm{m}}{\mathrm{s}}$

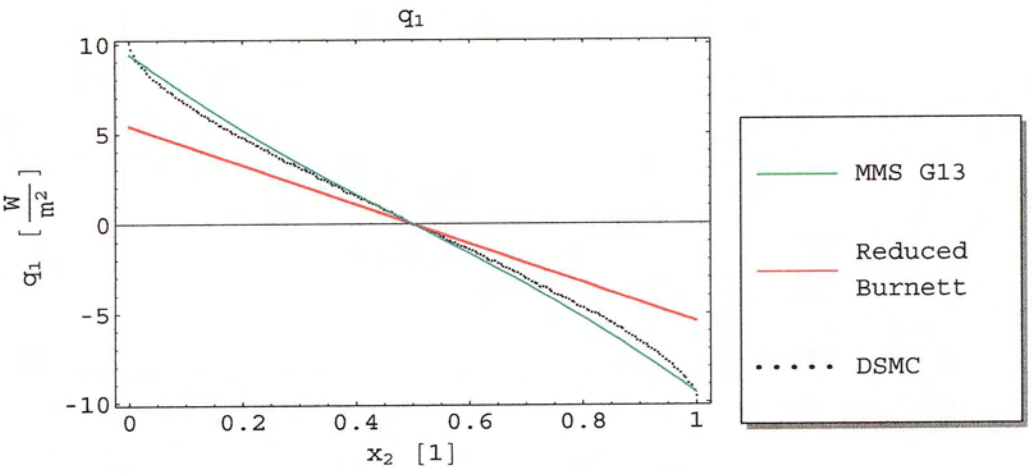

Figure 4-8g: q_1 at $Kn = 0.25$ and $\Delta v = 300\frac{\mathrm{m}}{\mathrm{s}}$

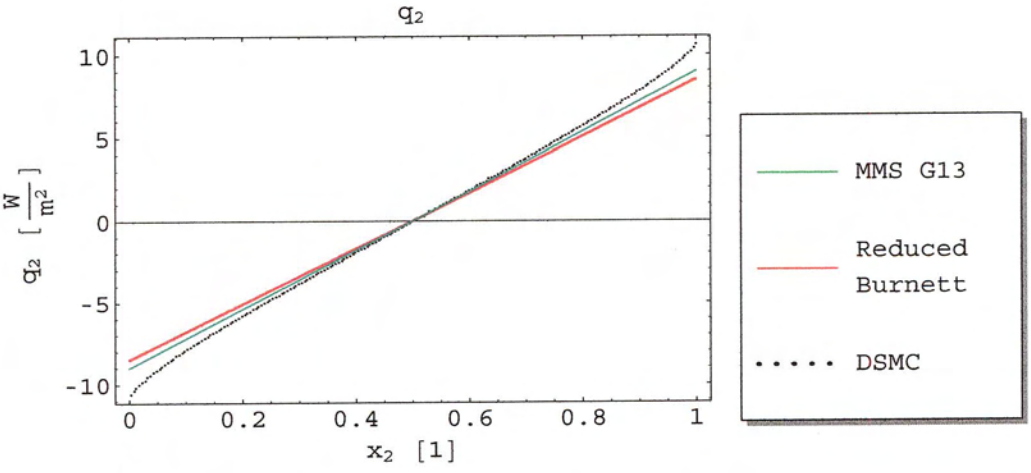

Figure 4-8h: q_2 at $Kn = 0.25$ and $\Delta v = 300\frac{\mathrm{m}}{\mathrm{s}}$

Results for $Kn = 0.5$, $\Delta v = 300$, and $M = 0.97$ below in Fig.s 4-9a to 4-9h shows more of the same. These results have been included to show that the MMS method will work at these Knudsen numbers, but has some problems. These problems could be of the method or of the equations.

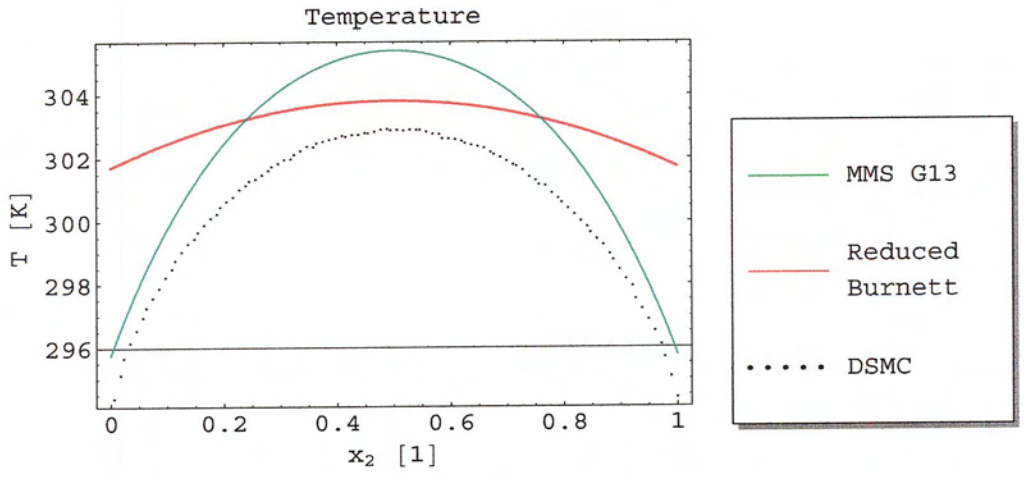

Figure 4-9a: Temperature at $Kn = 0.5$ and $\Delta v = 300\frac{\mathrm{m}}{\mathrm{s}}$

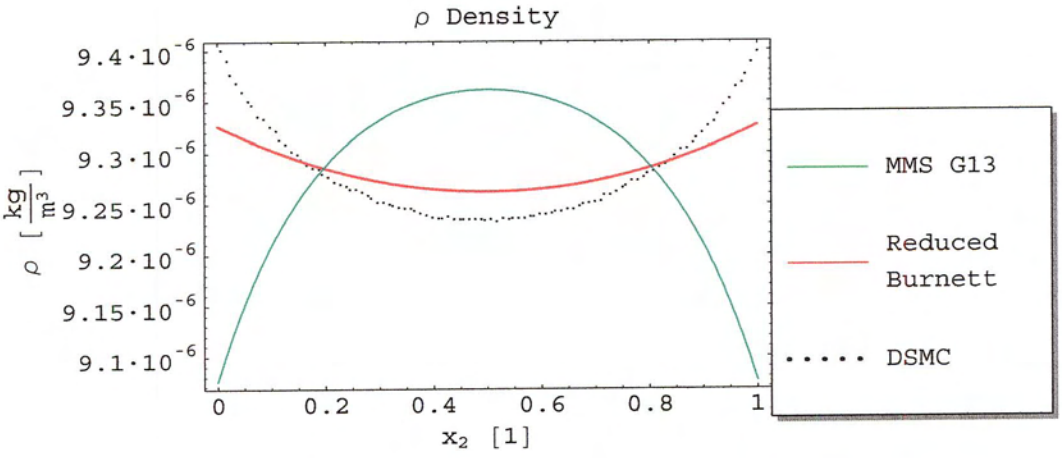

Figure 4-9b: Density at $Kn = 0.5$ and $\Delta v = 300\frac{\mathrm{m}}{\mathrm{s}}$

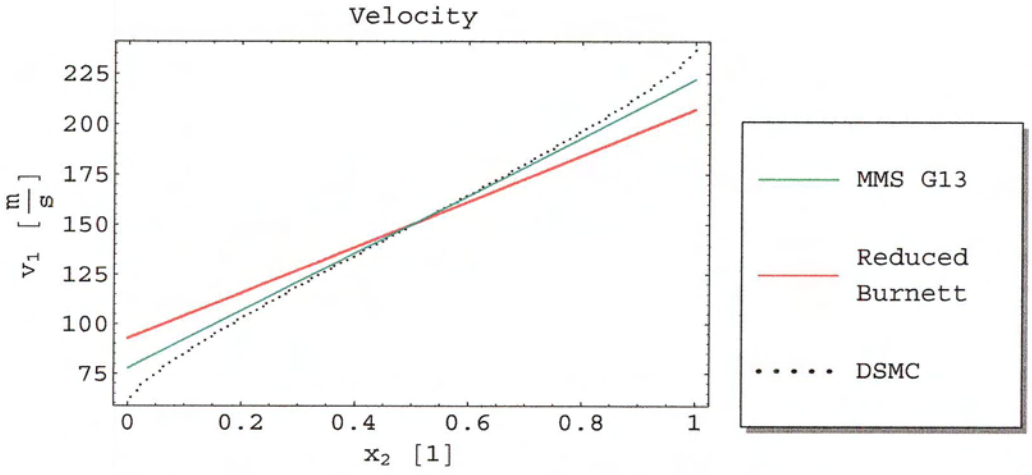

Figure 4-9c: Velocity v_1 at $Kn = 0.5$ and $\Delta v = 300\frac{\mathrm{m}}{\mathrm{s}}$

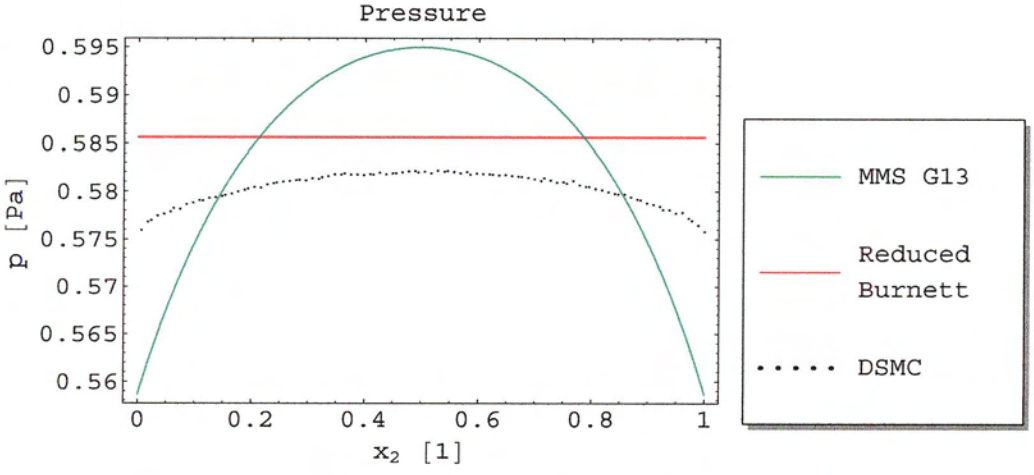

Figure 4-9d: Pressure at $Kn = 0.5$ and $\Delta v = 300\frac{\mathrm{m}}{\mathrm{s}}$

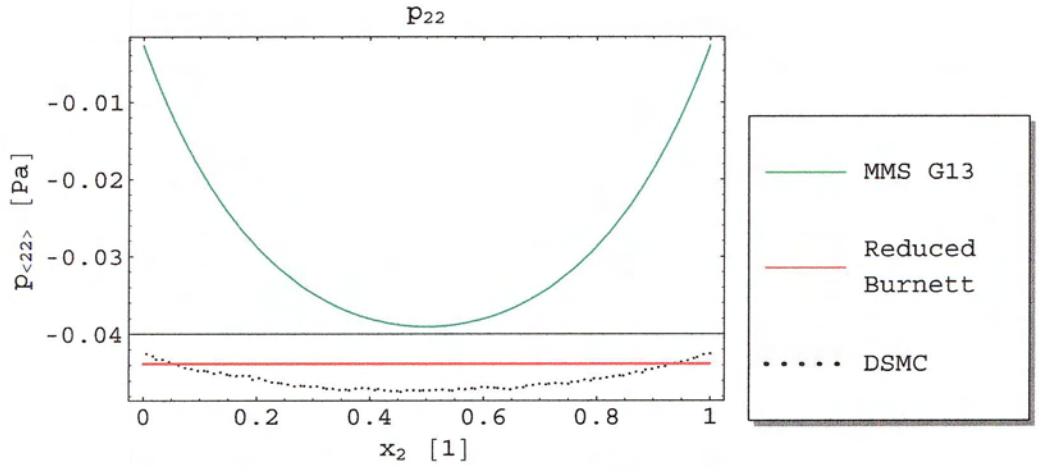

Figure 4-9e: $p_{<22>}$ at $Kn = 0.5$ and $\Delta v = 300\frac{\mathrm{m}}{\mathrm{s}}$

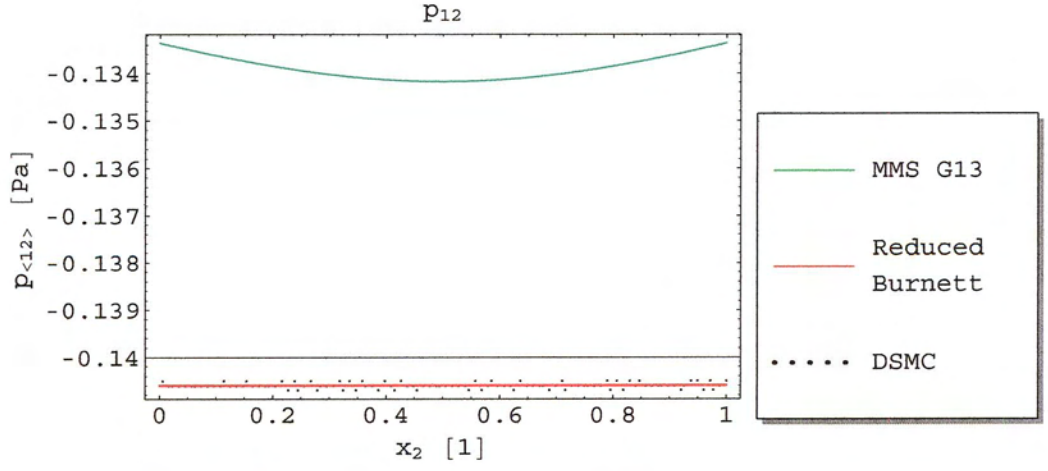

Figure 4-9f: $p_{<12>}$ at $Kn = 0.5$ and $\Delta v = 300\frac{\mathrm{m}}{\mathrm{s}}$

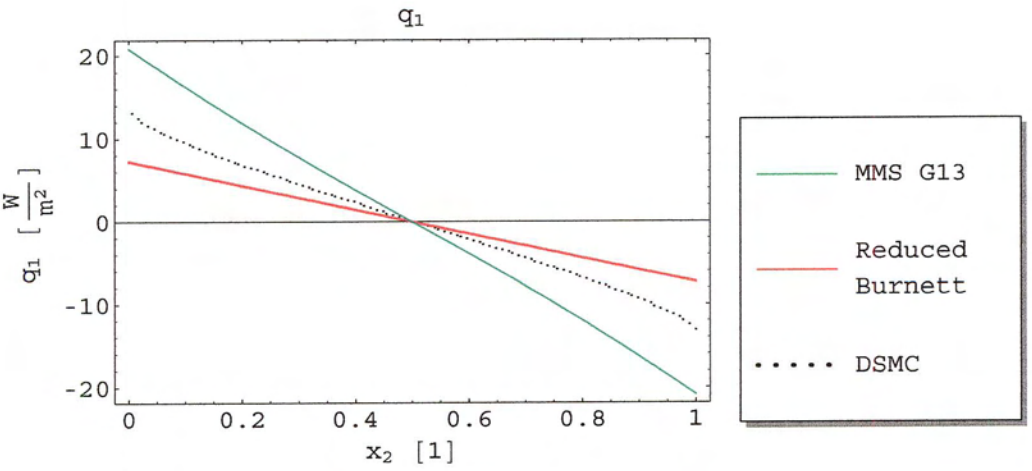

Figure 4-9g: q_1 at $Kn = 0.5$ and $\Delta v = 300\frac{\mathrm{m}}{\mathrm{s}}$

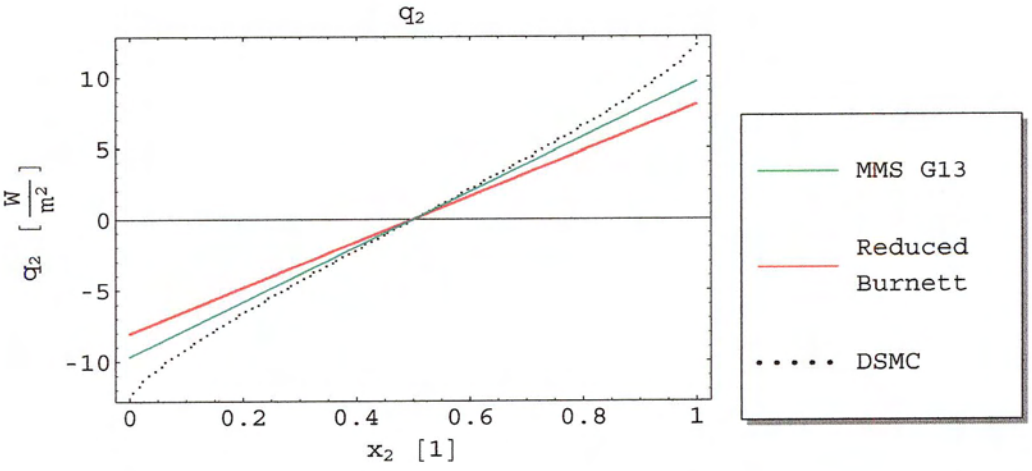

Figure 4-9h: q_2 at $Kn = 0.5$ and $\Delta v = 300\frac{\mathrm{m}}{\mathrm{s}}$

It is interesting to note that the errors that are seen in the previous results in the q_1 and $p_{<22>}$ distributions can be greatly reduced by increasing the amount of numerical damping. This addition of numerical damping however introduces numerical heat dissipation that is reflected in the temperature distribution. Shown below in Fig.s 4-10a to 4-10h are results at $Kn = 0.1$, $\Delta v = 300$, and $M = 0.97$ with ten times as much damping applied by reducing the time step by a factor of ten.

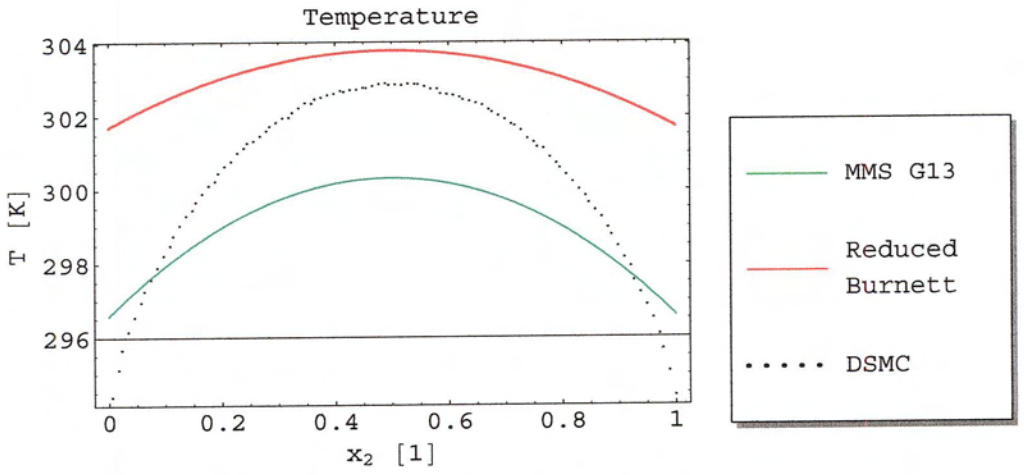

Figure 4-10a: Temperature at $Kn = 0.5$, $\Delta v = 300_D \frac{\mathrm{m}}{\mathrm{s}}$ and $\Delta t = \frac{\Delta t}{10}$

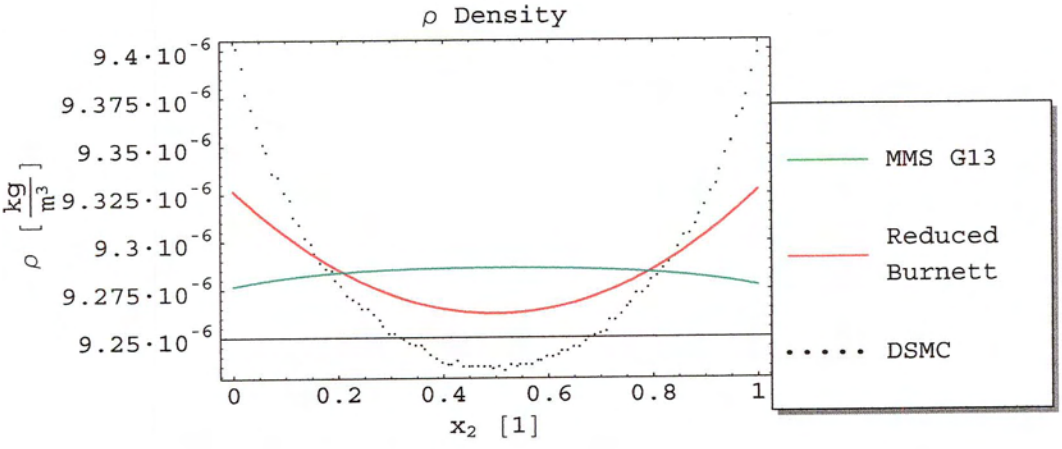

Figure 4-10b: Density at $Kn = 0.5$, $\Delta v = 300_D \frac{\mathrm{m}}{\mathrm{s}}$ and $\Delta t = \frac{\Delta t}{10}$

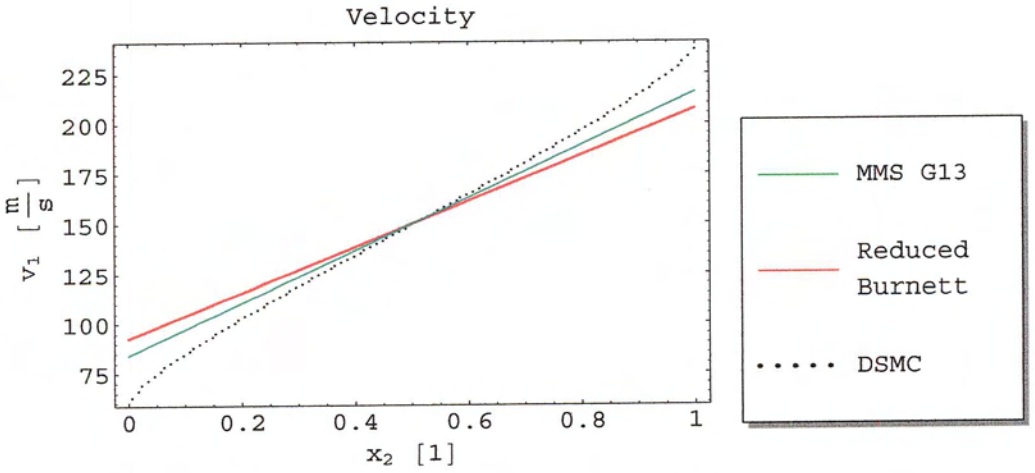

Figure 4-10c: Velocity v_1 at $Kn = 0.5$, $\Delta v = 300_D \frac{\mathrm{m}}{\mathrm{s}}$ and $\Delta t = \frac{\Delta t}{10}$

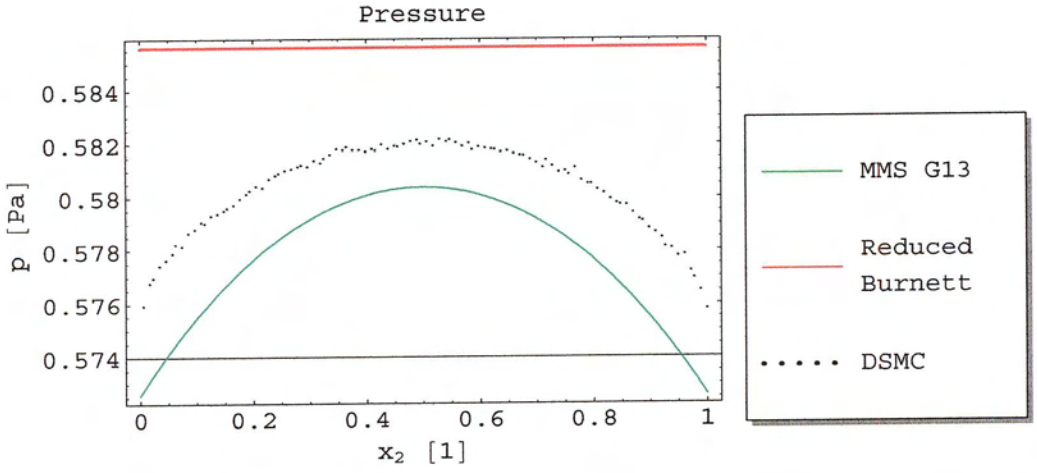

Figure 4-10d: Pressure at $Kn = 0.5$, $\Delta v = 300_D \frac{\mathrm{m}}{\mathrm{s}}$ and $\Delta t = \frac{\Delta t}{10}$

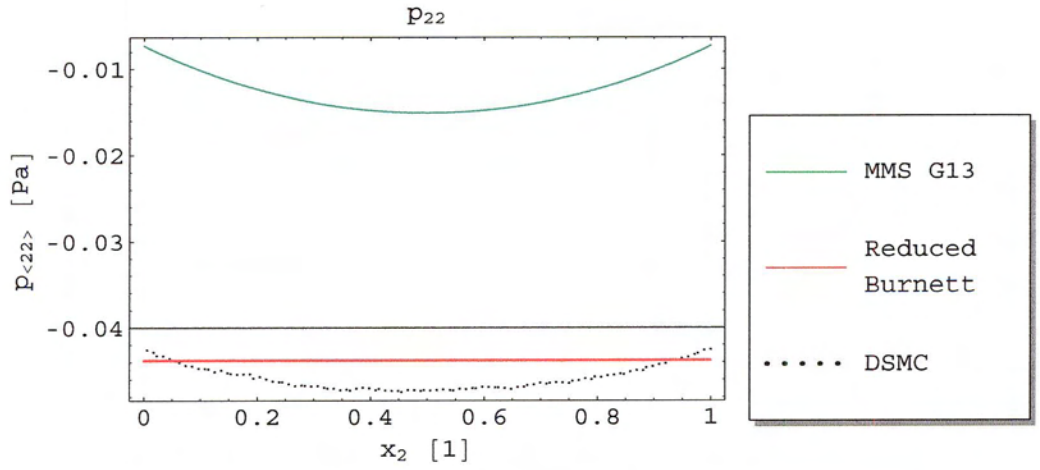

Figure 4-10e: $p_{<22>}$ at $Kn = 0.5$, $\Delta v = 300_D \frac{\mathrm{m}}{\mathrm{s}}$ and $\Delta t = \frac{\Delta t}{10}$

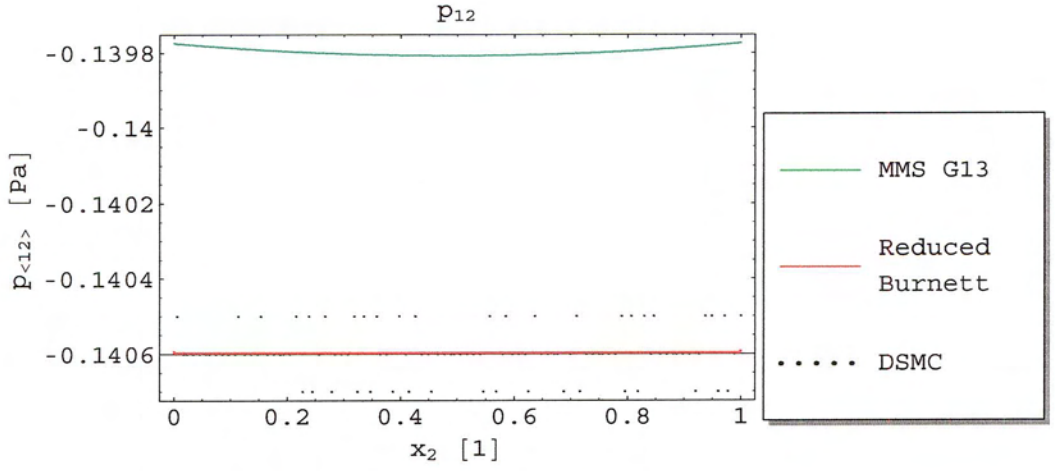

Figure 4-10f: $p_{<12>}$ at $Kn = 0.5$, $\Delta v = 300_D \frac{\mathrm{m}}{\mathrm{s}}$ and $\Delta t = \frac{\Delta t}{10}$

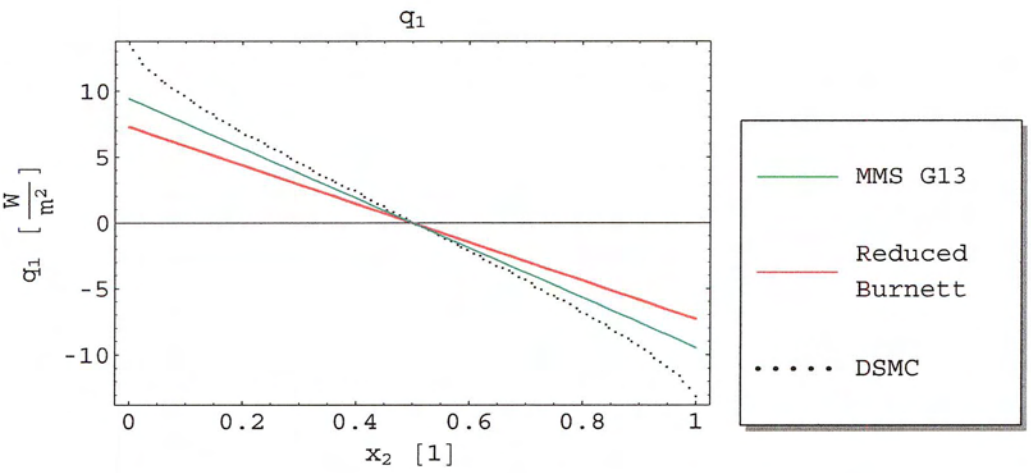

Figure 4-10g: q_1 at $Kn = 0.5$, $\Delta v = 300_D \frac{\mathrm{m}}{\mathrm{s}}$ and $\Delta t = \frac{\Delta t}{10}$

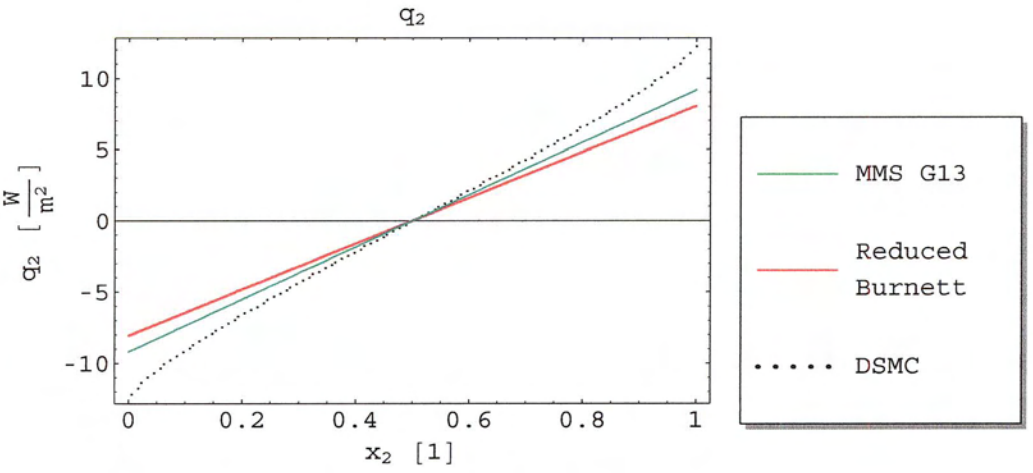

Figure 4-10h: q_2 at $Kn = 0.5$, $\Delta v = 300_D \frac{\mathrm{m}}{\mathrm{s}}$ and $\Delta t = \frac{\Delta t}{10}$

4.2 Nessyahu-Tadmor scheme results

The results previously shown for the modified MacCormack's scheme are somewhat dependent on the amount of numerical damping. The Nessyahu-Tadmor scheme was attempted in order to overcome this problem. The dependence on the time step and the side effects of

the numerical damping have been avoided. Other problems however are now encountered.

The primary problem encountered with the Nessyahu-Tadmor results is a lack of perfect symmetry in the results. The cause of this has not been identified. It appears that a numerical error likely introduced at the boundary is propagating inwards, in some cases causing instability.

As suggested in [35] time steps for the Nessyahu-Tadmor method are chosen as the largest possible that provide for stable results.

Results in this section for the Nessyahu-Tadmor scheme will not be presented in such an exhaustive fashion as they were in the previous section. Below Figs. 4-11a to 4-11i, are results at $Kn = 0.01$, $\Delta v = 300\frac{\mathrm{m}}{\mathrm{s}}$ and a maximum Mach number of $M = 0.97$. These low Knudsen number results show strong agreement with the Reduced-Burnett/NSF results. The asymmetry is not yet apparent.

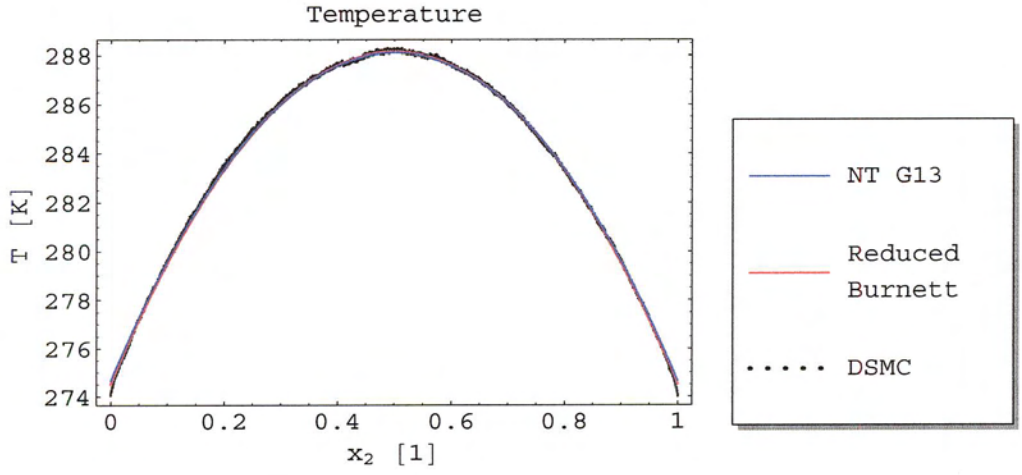

Figure 4-11a: Temperature at $Kn = 0.01$ and $\Delta v = 300\frac{\mathrm{m}}{\mathrm{s}}$

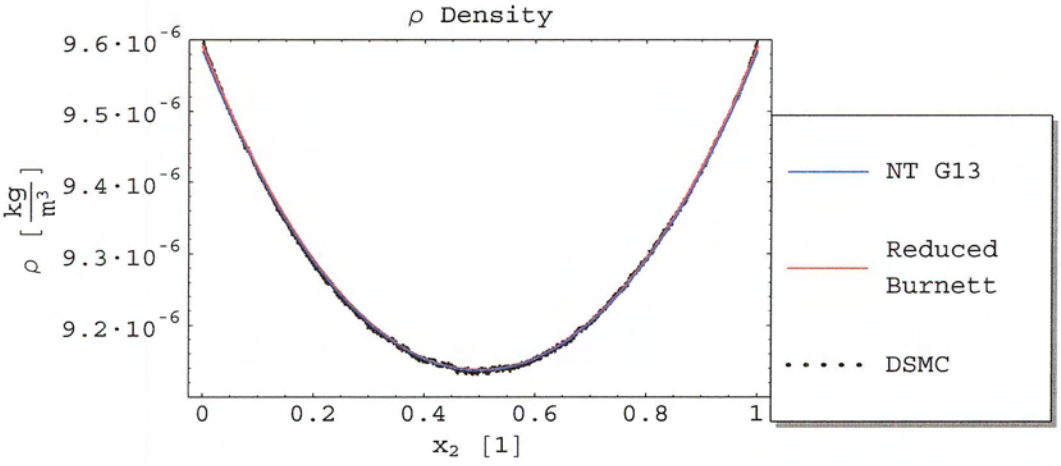

Figure 4-11b: Density at $Kn = 0.01$ and $\Delta v = 300\frac{\mathrm{m}}{\mathrm{s}}$

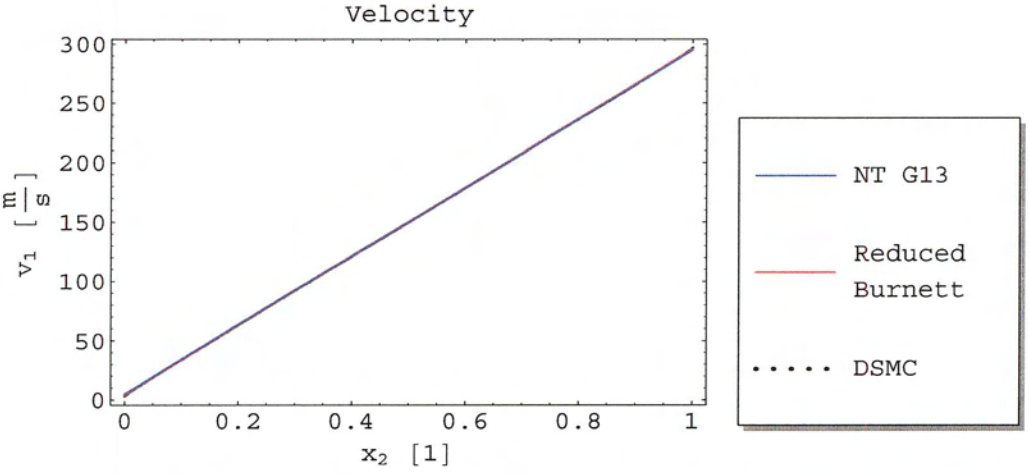

Figure 4-11c: Velocity v_1 parallel to the wall at $Kn = 0.01$ and $\Delta v = 300\frac{\mathrm{m}}{\mathrm{s}}$

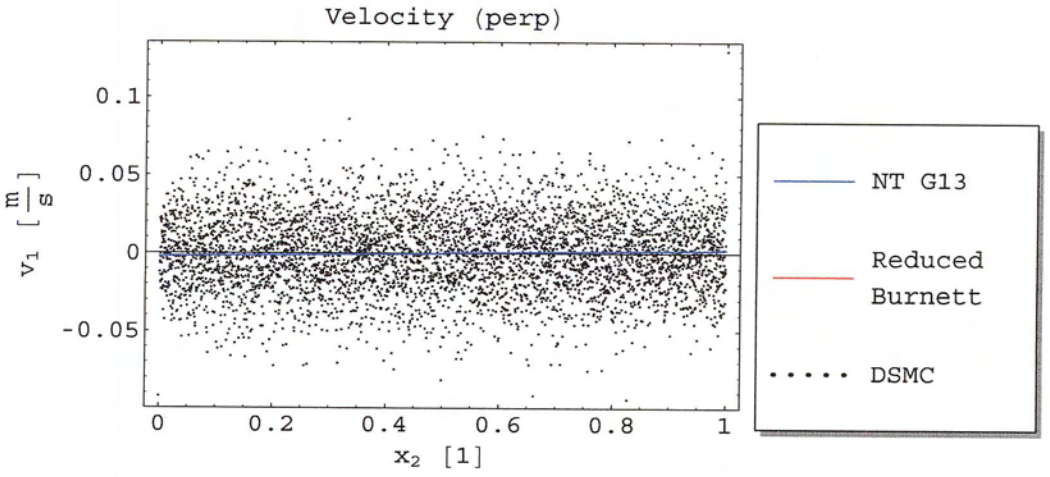

Figure 4-11d: Velocity v_2 perpendicular to the wall at $Kn = 0.01$ and $\Delta v = 300\frac{\mathrm{m}}{\mathrm{s}}$

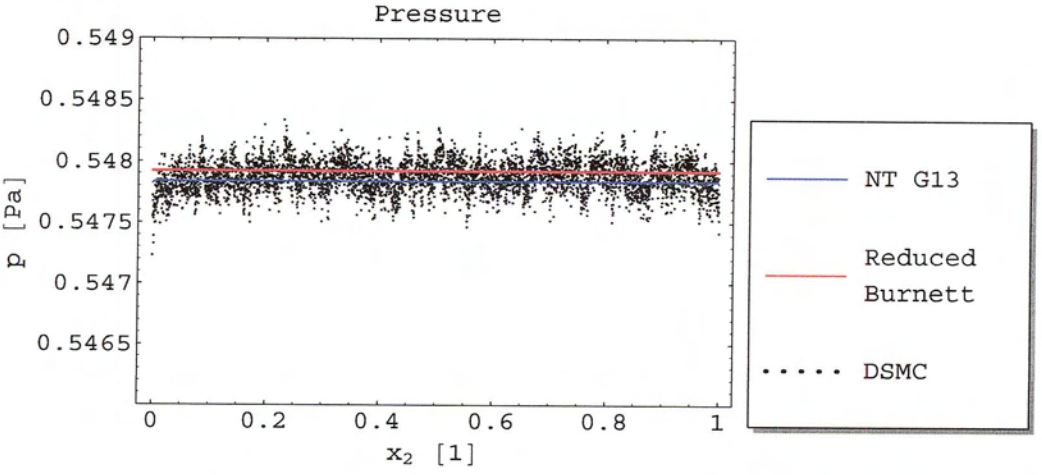

Figure 4-11e: Pressure at $Kn = 0.01$ and $\Delta v = 300\frac{\mathrm{m}}{\mathrm{s}}$

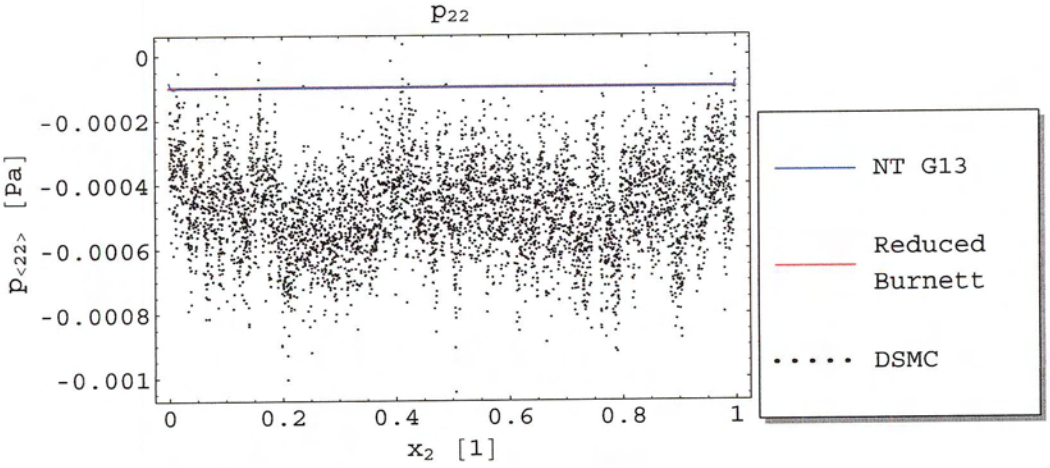

Figure 4-11f: $p_{<22>}$ at $Kn = 0.01$ and $\Delta v = 300\frac{\mathrm{m}}{\mathrm{s}}$

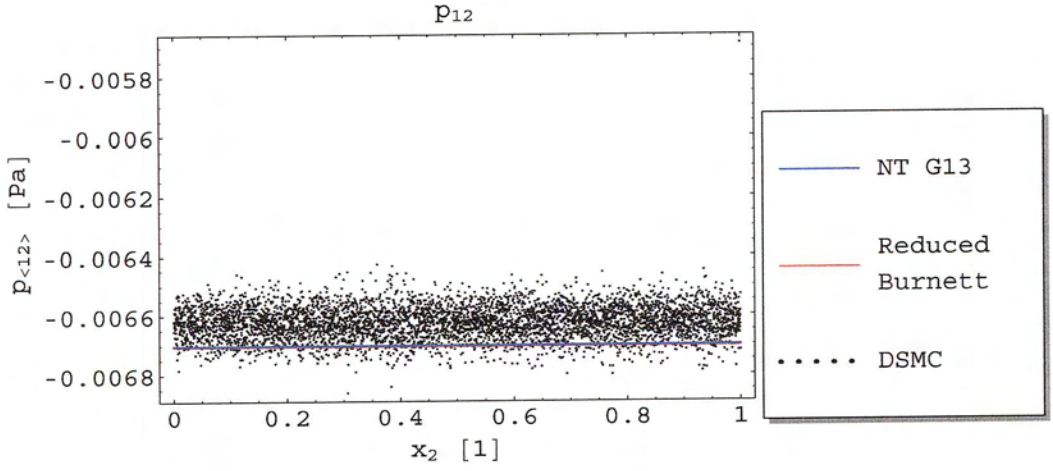

Figure 4-11g: $p_{<12>}$ at $Kn = 0.01$ and $\Delta v = 300\frac{\mathrm{m}}{\mathrm{s}}$

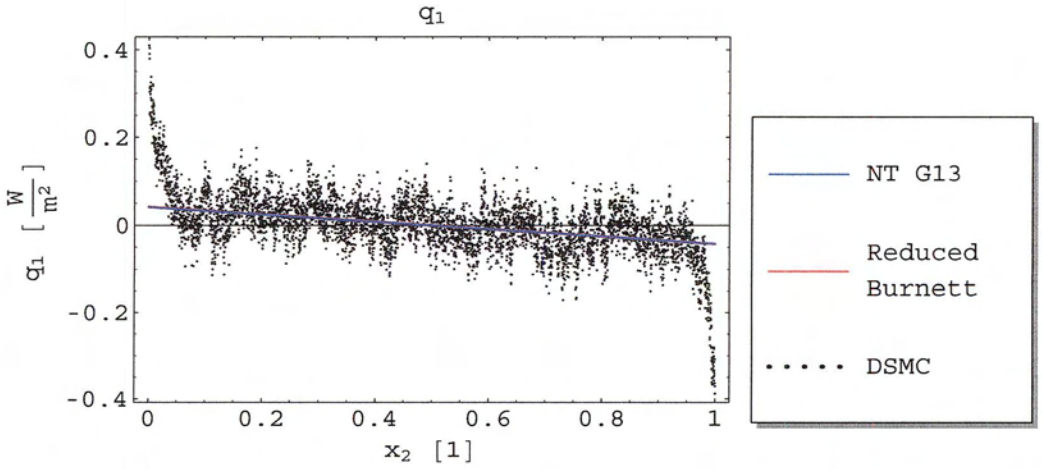

Figure 4-11h: q_1 at $Kn = 0.01$ and $\Delta v = 300\frac{\mathrm{m}}{\mathrm{s}}$

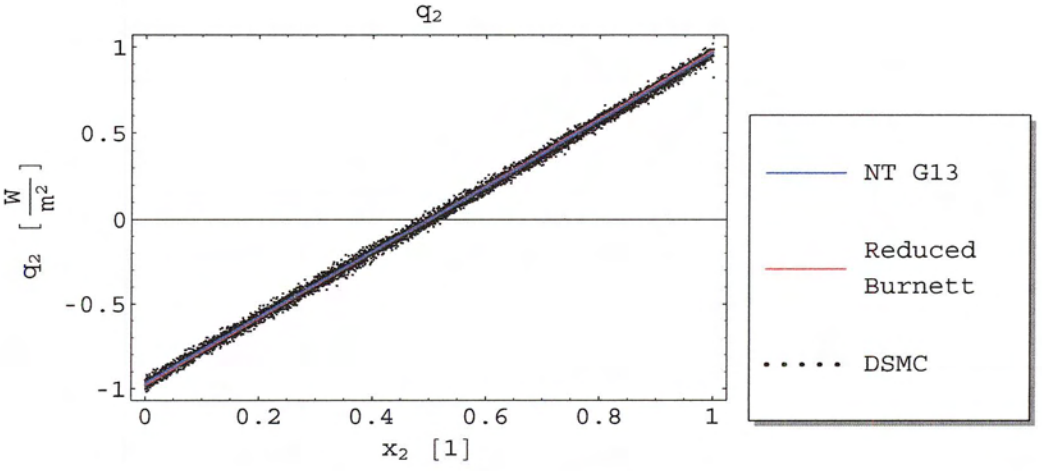

Figure 4-11i: q_2 at $Kn = 0.01$ and $\Delta v = 300\frac{\mathrm{m}}{\mathrm{s}}$

Figures 4-12a to 4-12i below are results at $Kn = 0.05$, $\Delta v = 300\frac{\mathrm{m}}{\mathrm{s}}$ and a wall Mach number of $Ma = 0.97$. Very good agreement with both DSMC results and the reduced Burnett is still present. Beginnings of asymmetry can be detected at the boundaries in the $p_{<22>}$ and v_2 distributions of Figs. 4-12f and 4-12d respectively.

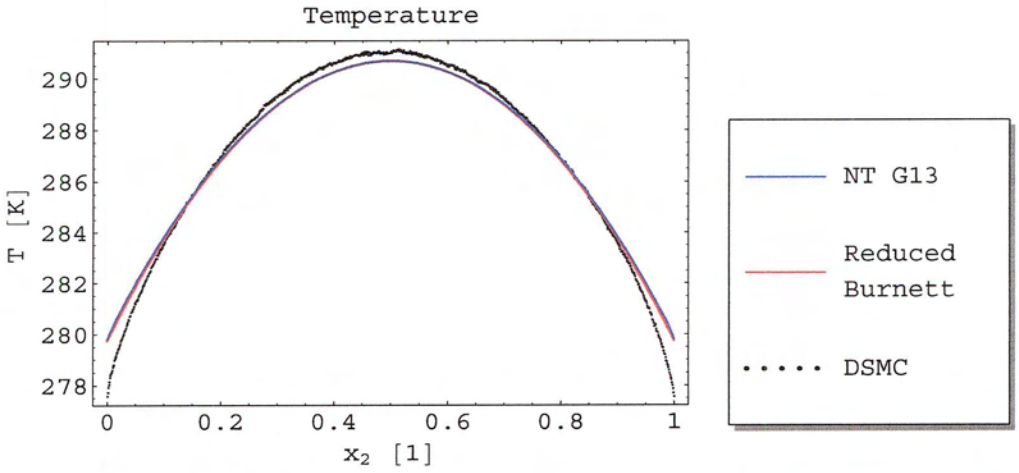

Figure 4-12a: Temperature at $Kn = 0.05$ and $\Delta v = 300\frac{\mathrm{m}}{\mathrm{s}}$

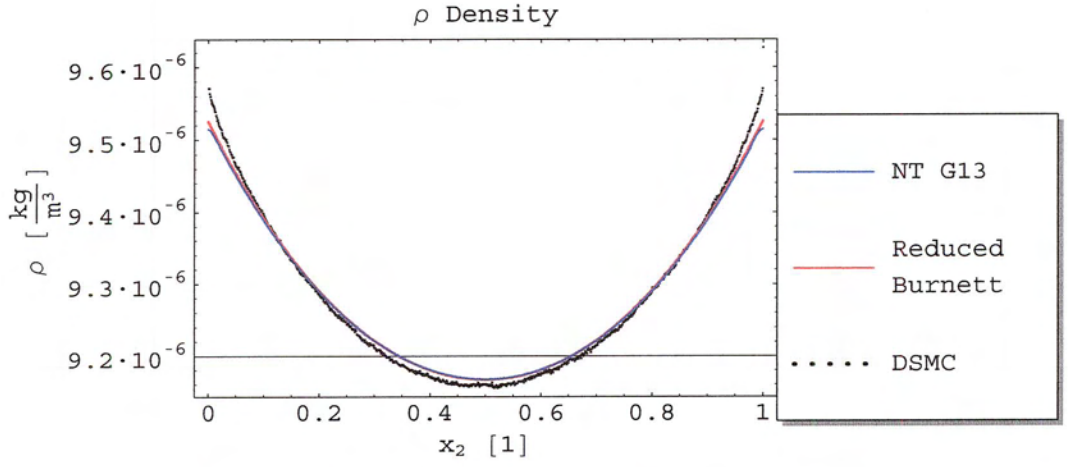

Figure 4-12b: Density at $Kn = 0.05$ and $\Delta v = 300\frac{\mathrm{m}}{\mathrm{s}}$

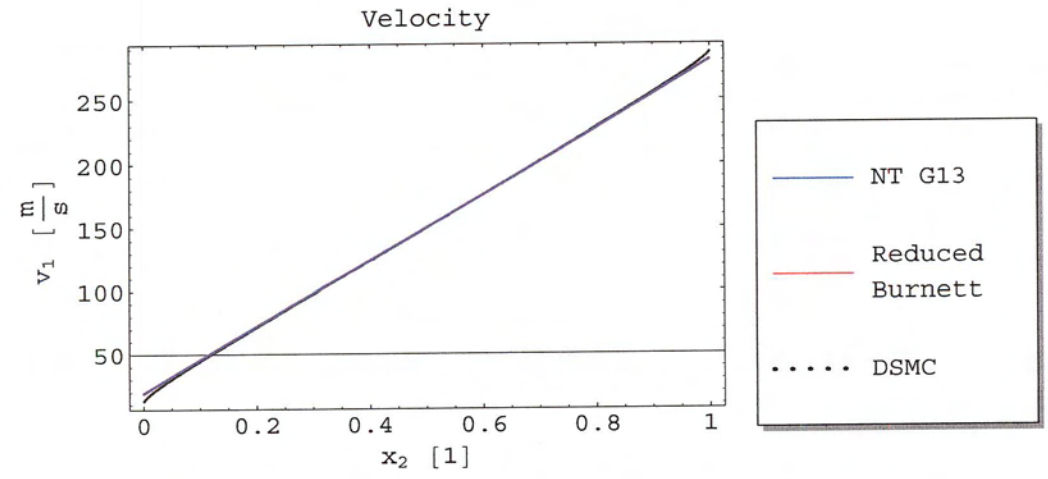

Figure 4-12c: Velocity v_1 parallel to the wall at $Kn = 0.05$ and $\Delta v = 300\frac{\mathrm{m}}{\mathrm{s}}$

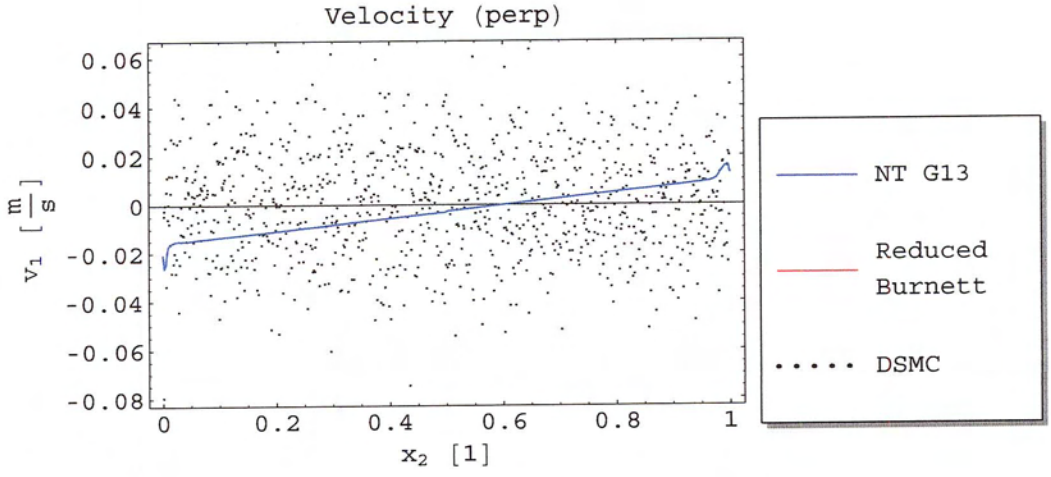

Figure 4-12d: Velocity v_2 perpendicular to the wall at $Kn = 0.05$ and $\Delta v = 300\frac{\mathrm{m}}{\mathrm{s}}$

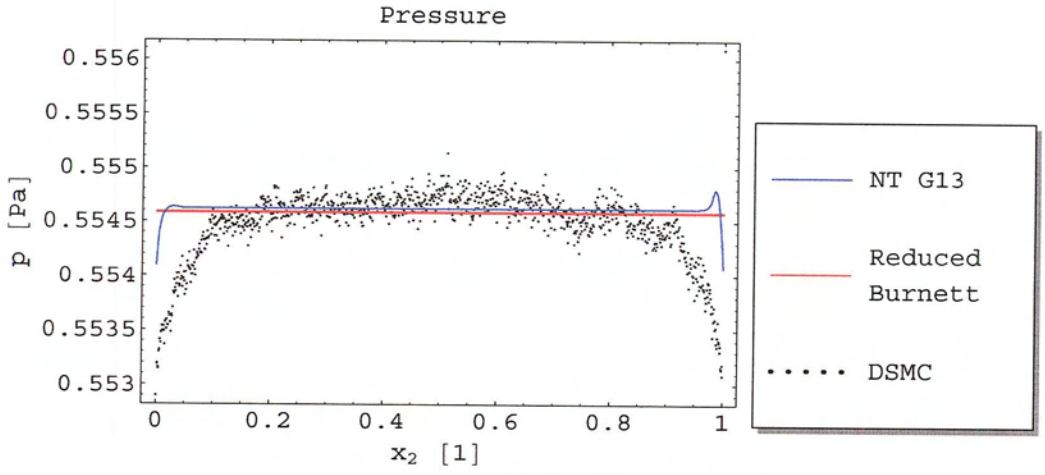

Figure 4-12e: Pressure at $Kn = 0.05$ and $\Delta v = 300\frac{\mathrm{m}}{\mathrm{s}}$

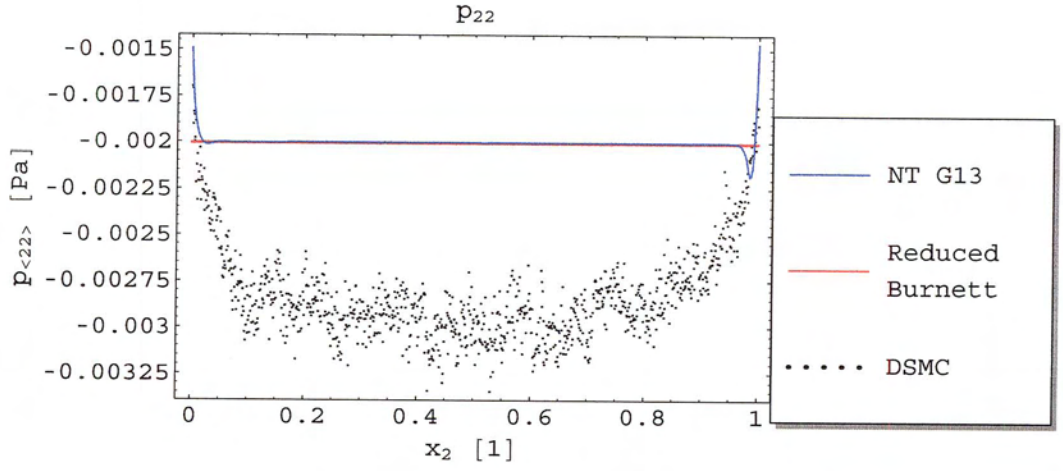

Figure 4-12f: $p_{<22>}$ at $Kn = 0.05$ and $\Delta v = 300\frac{\mathrm{m}}{\mathrm{s}}$

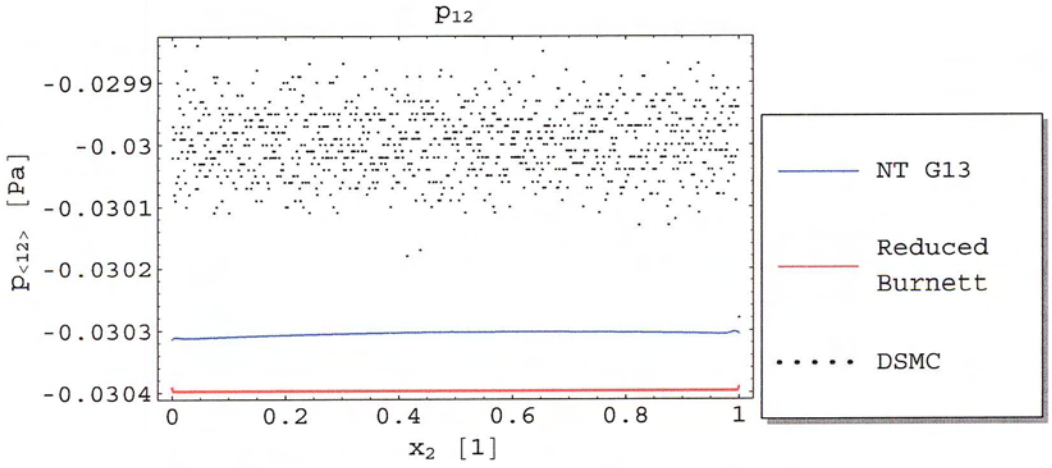

Figure 4-12g: $p_{<12>}$ at $Kn = 0.05$ and $\Delta v = 300\frac{\mathrm{m}}{\mathrm{s}}$

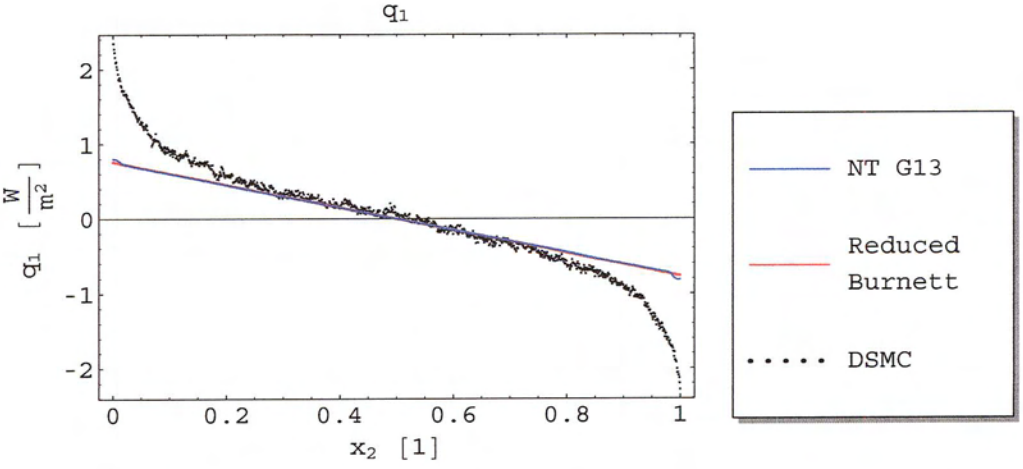

Figure 4-12h: q_1 at $Kn = 0.05$ and $\Delta v = 300\frac{\mathrm{m}}{\mathrm{s}}$

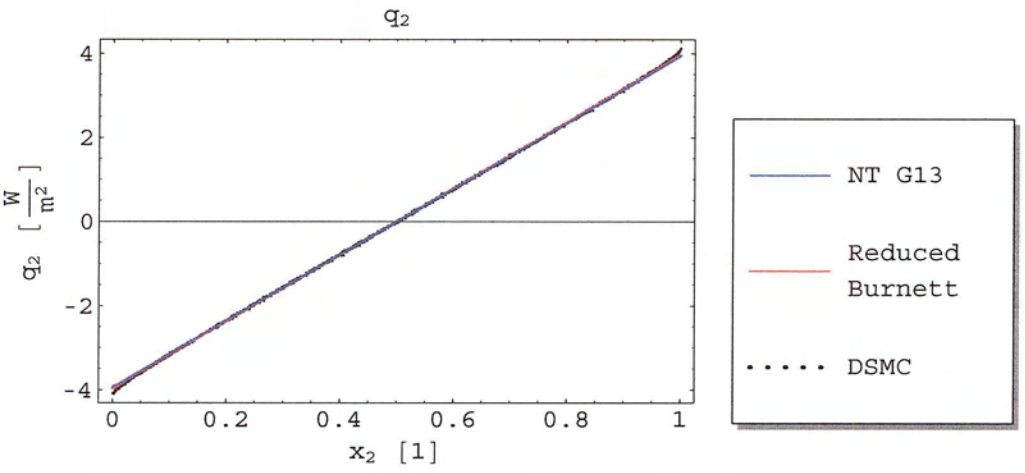

Figure 4-12i: q_2 at $Kn = 0.05$ and $\Delta v = 300\frac{\mathrm{m}}{\mathrm{s}}$

In Fig.s 4-13a to 4-13i the Knudsen number has been increased to $Kn = 0.1$. The velocity difference remains at $\Delta v = 300$ giving a maximum Mach number of $M = 0.97$. The symmetry problems are now becoming significant.

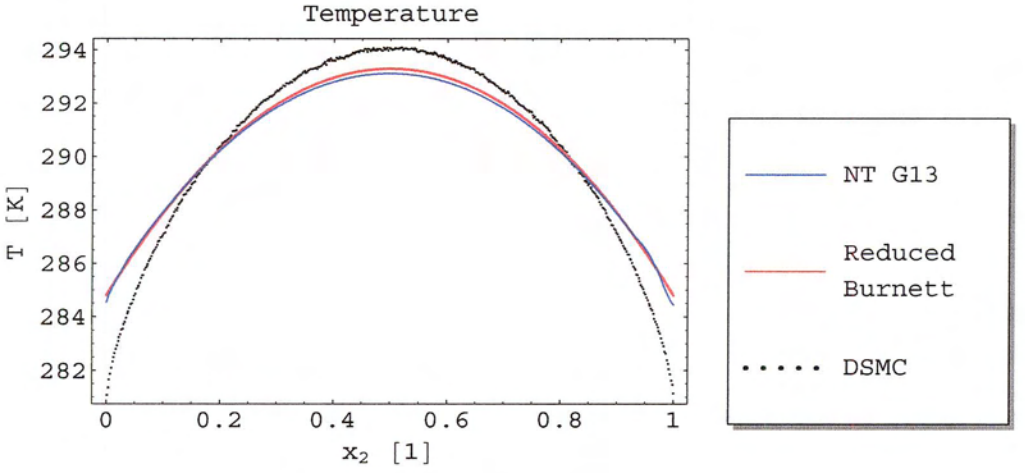

Figure 4-13a: Temperature at $Kn = 0.1$ and $\Delta v = 300\frac{\mathrm{m}}{\mathrm{s}}$

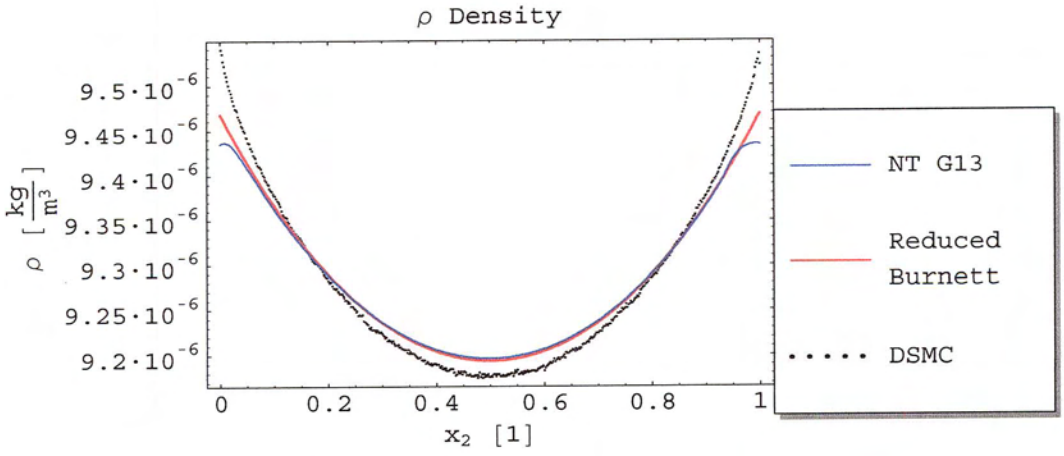

Figure 4-13b: Density at $Kn = 0.1$ and $\Delta v = 300\frac{\mathrm{m}}{\mathrm{s}}$

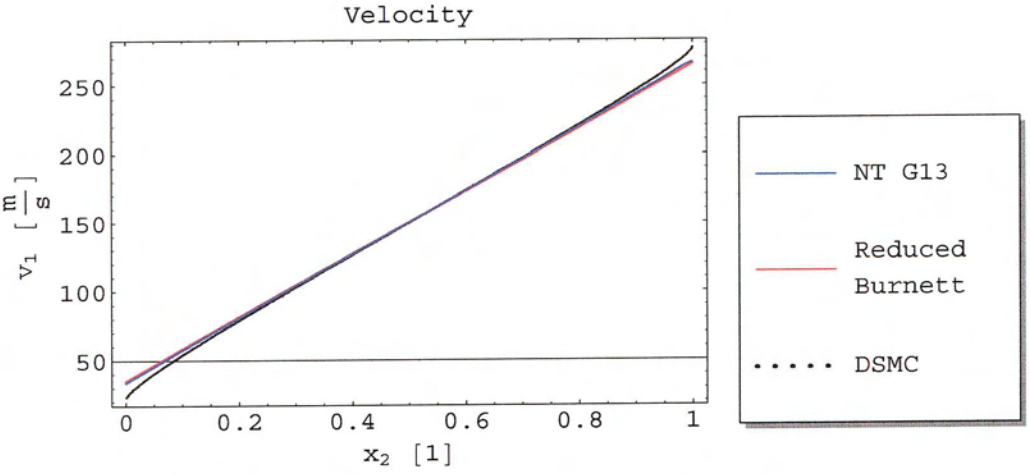

Figure 4-13c: Velocity v_1 parallel to the wall at $Kn = 0.1$ and $\Delta v = 300\frac{\mathrm{m}}{\mathrm{s}}$

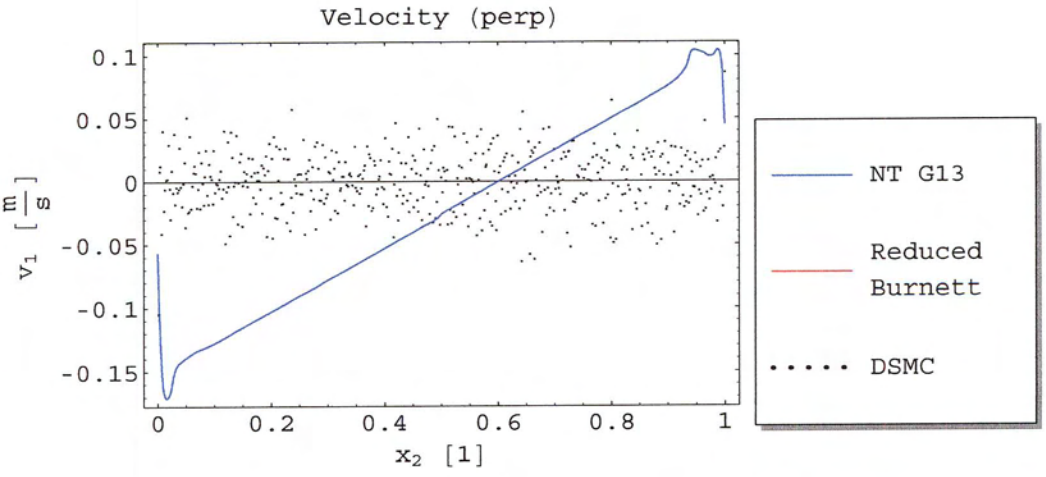

Figure 4-13d: Velocity v_2 perpendicular to the wall at $Kn = 0.1$ and $\Delta v = 300\frac{\mathrm{m}}{\mathrm{s}}$

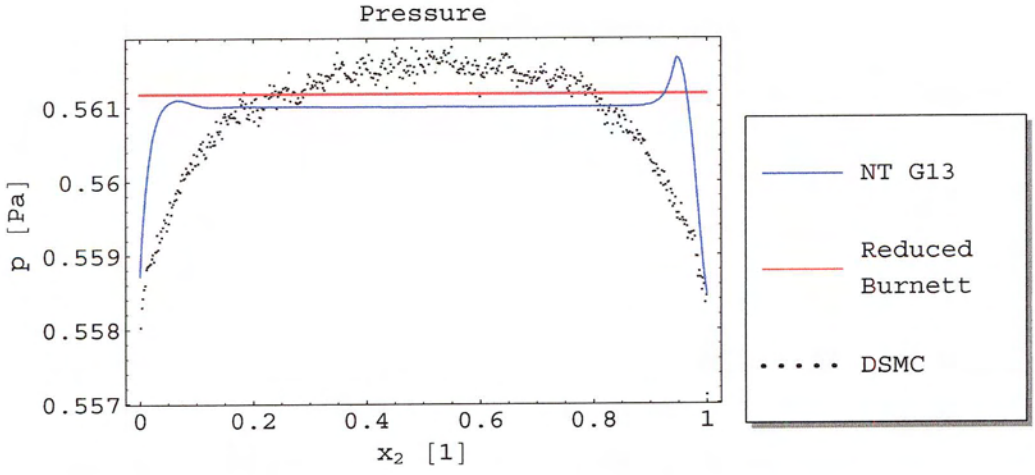

Figure 4-13e: Pressure at $Kn = 0.1$ and $\Delta v = 300\frac{\mathrm{m}}{\mathrm{s}}$

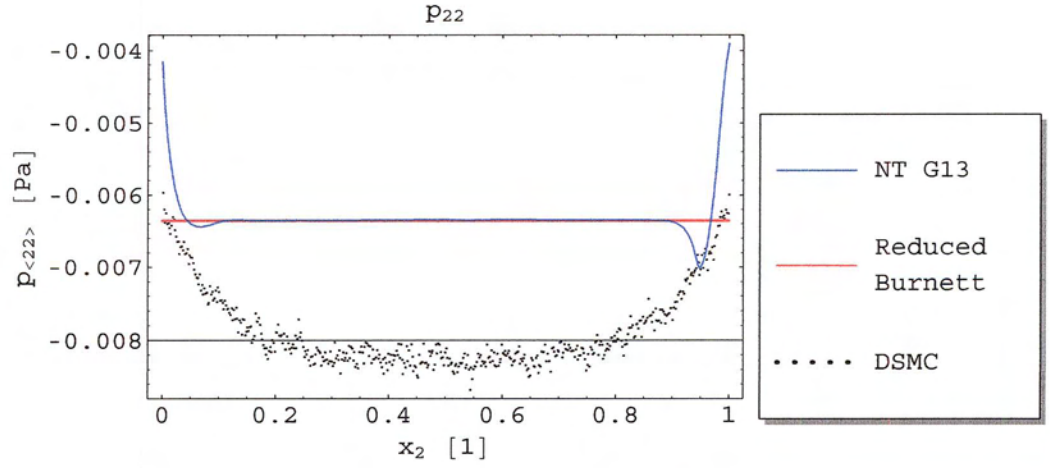

Figure 4-13f: $p_{<22>}$ at $Kn = 0.1$ and $\Delta v = 300\frac{\mathrm{m}}{\mathrm{s}}$

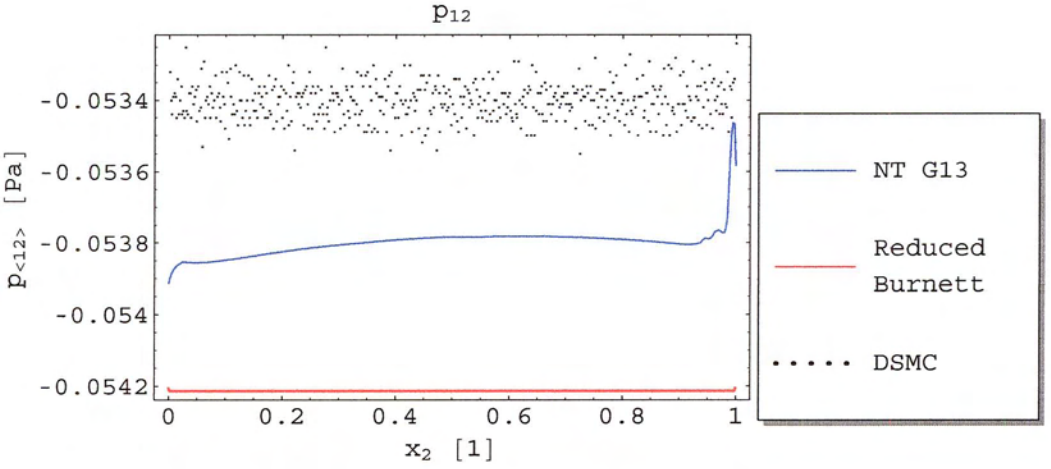

Figure 4-13g: $p_{<12>}$ at $Kn = 0.1$ and $\Delta v = 300\frac{\mathrm{m}}{\mathrm{s}}$

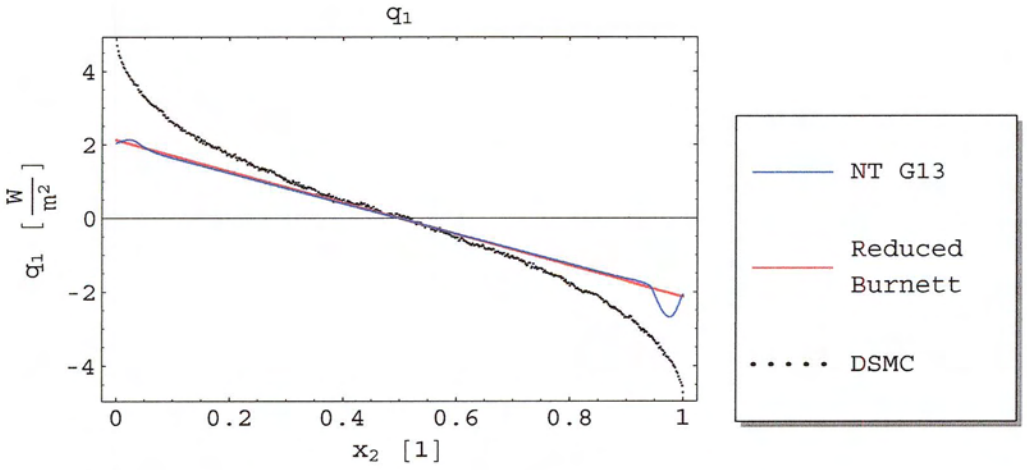

Figure 4-13h: q_1 at $Kn = 0.1$ and $\Delta v = 300\frac{\mathrm{m}}{\mathrm{s}}$

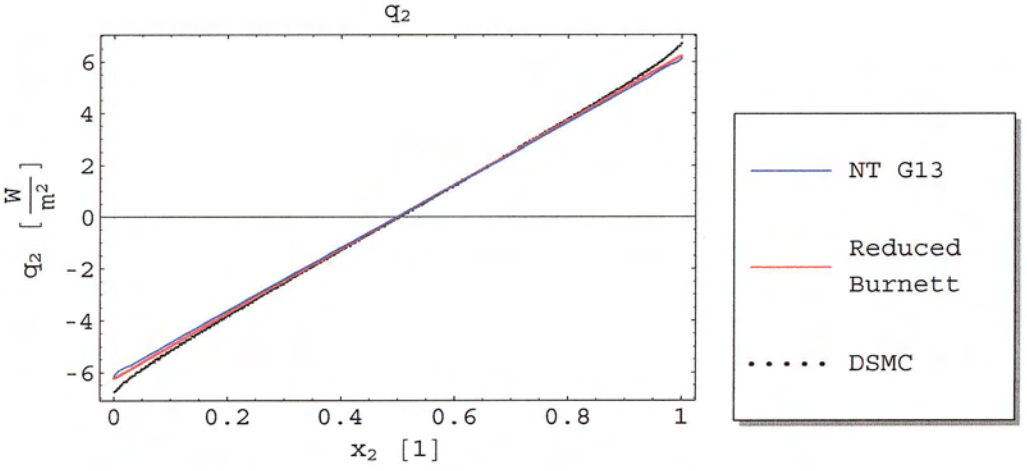

Figure 4-13i: q_2 at $Kn = 0.1$ and $\Delta v = 300\frac{\mathrm{m}}{\mathrm{s}}$

The case of $Kn = 0.1$ and $\Delta v = 300\frac{\mathrm{m}}{\mathrm{s}}$ is also used here to demonstrate that steady state in the solution of the Nessyahu-Tadmor scheme has reached steady state. Figure 4-14 below shows the variation of the central(grid point) value of temperature with time or number of iterations. It is clear that steady state has been reached.

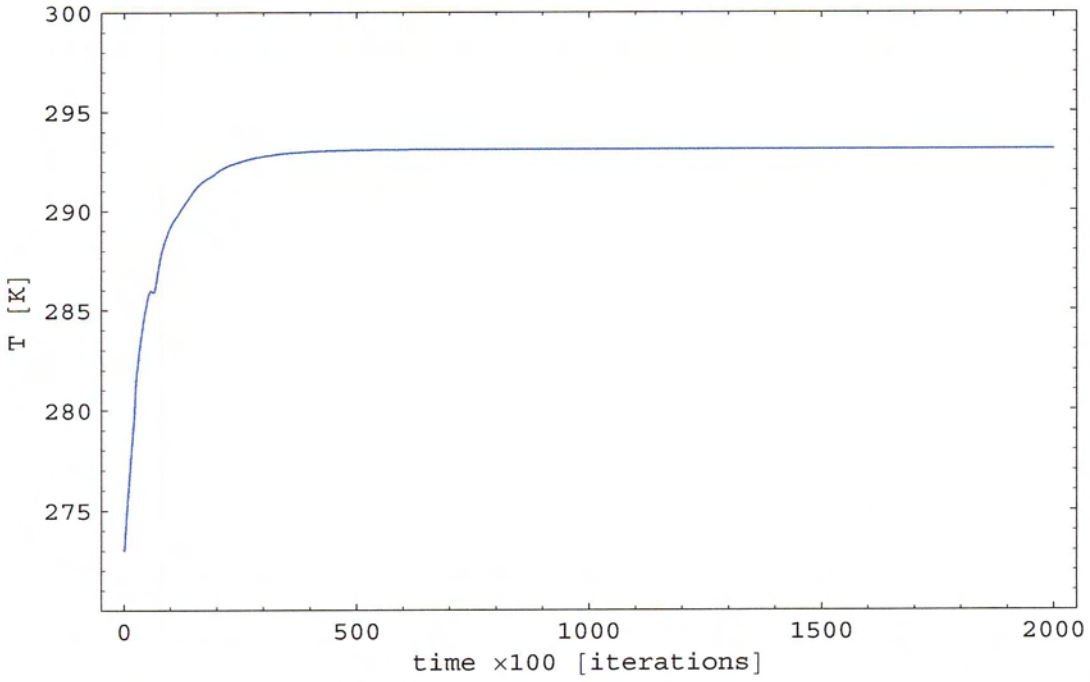

Figure 4-14: Central point temperature at $Kn = 0.1$ and $\Delta v = 300\frac{\mathrm{m}}{\mathrm{s}}$

An increased velocity difference, Fig.s 4-15a and 4-15b below, shows that the symmetry error does not increase significantly with a corresponding increased velocity.

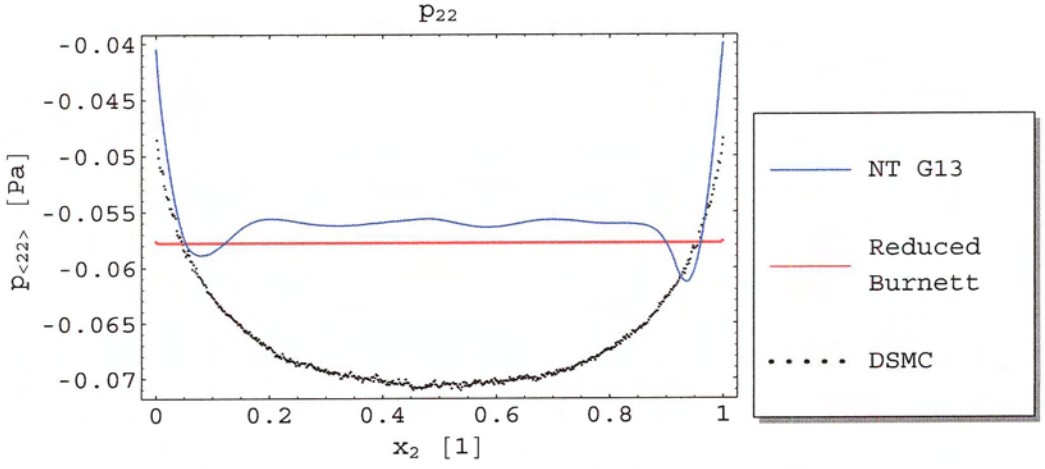

Figure 4-15a: $p_{<22>}$ at $Kn = 0.1$ and $\Delta v = 800\frac{\mathrm{m}}{\mathrm{s}}$

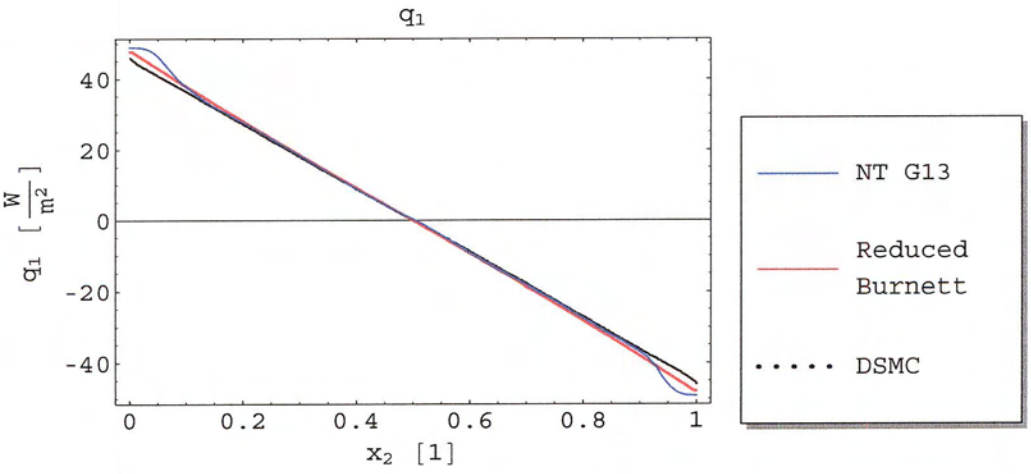

Figure 4-15b: q_1 at $Kn = 0.1$ and $\Delta v = 800\frac{\mathrm{m}}{\mathrm{s}}$

Once the Knudsen number is increased beyond $Kn = 0.1$ the symmetry problems at the boundaries are so significant that the results are no longer reliable.

4.3 Compared results

To complete the results we show a comparison of the two schemes, Figs. 4-16a to 4-16i below. The scheme are compared at $Kn = 0.1$, $\Delta v = 300$ and $M = 0.97$ as it is sufficiently rarefied to have microscale effects and yet still well within the ideal range of the two schemes. It can be seen here that the Nessyahu-Tadmor scheme appears more accurate. However when choosing a scheme, one must decide what regions of the flow and flow regimes are of interest and what flow characteristics are of interest. The Nessyahu-Tadmor scheme gives a more precise representation of the flow overall, but the NSF equations in combination with the Reduced Burnett equations are almost as precise and are much easier to work with. The modified MacCormack's scheme, however, provides a more precise model of temperature and shows the boundary region effects in the $p_{<22>}$ and pressure profiles, albeit theses effects are exaggerated. The computational time of the Nessyahu-Tadmor method is just under an order of magnitude more than the modified MacCormack's method.

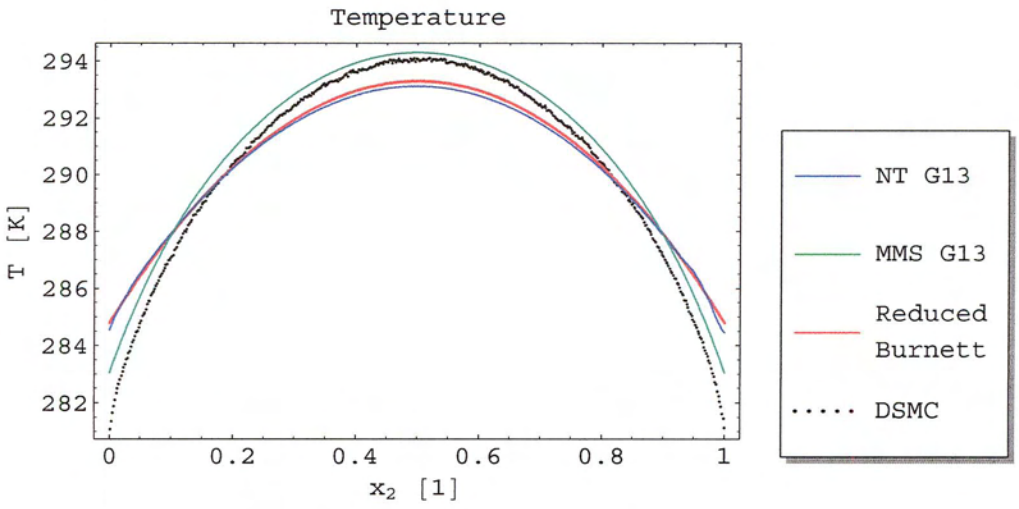

Figure 4-16a: Temperature at $Kn = 0.1$ and $\Delta v = 300 \frac{\mathrm{m}}{\mathrm{s}}$

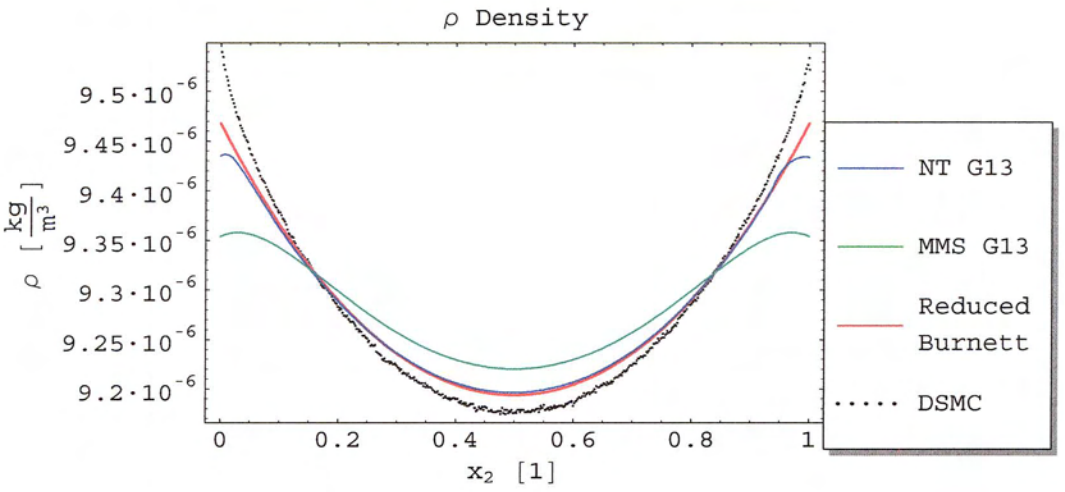

Figure 4-16b: Density at $Kn = 0.1$ and $\Delta v = 300 \frac{\mathrm{m}}{\mathrm{s}}$

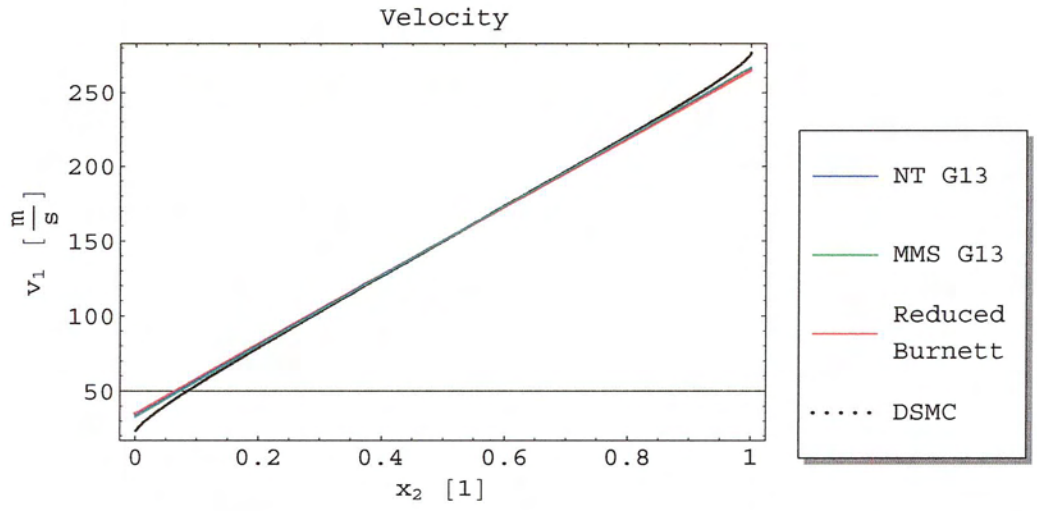

Figure 4-16c: Velocity v_1 parallel to the wall at $Kn = 0.1$ and $\Delta v = 300\frac{\mathrm{m}}{\mathrm{s}}$

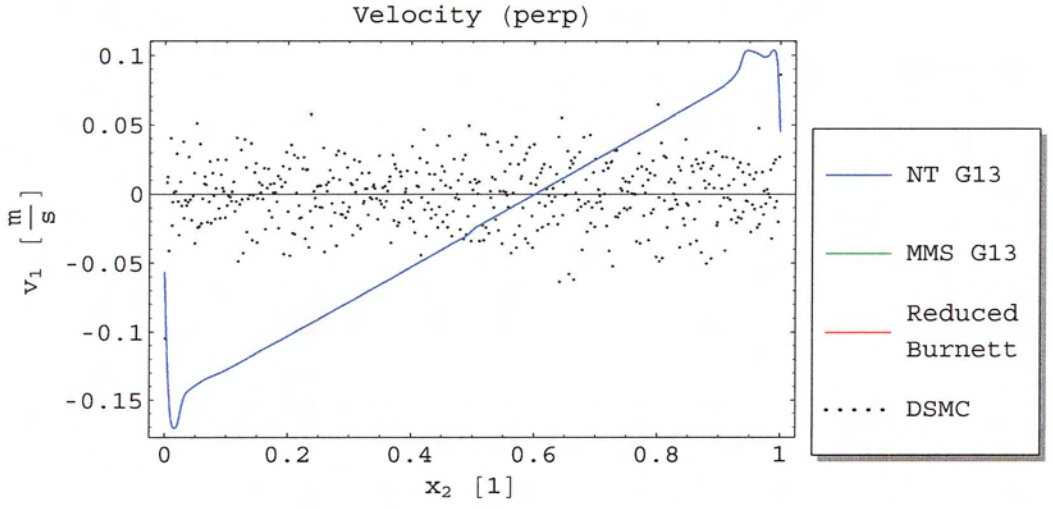

Figure 4-16d: Velocity v_2 perpendicular to the wall at $Kn = 0.1$ and $\Delta v = 300\frac{\mathrm{m}}{\mathrm{s}}$

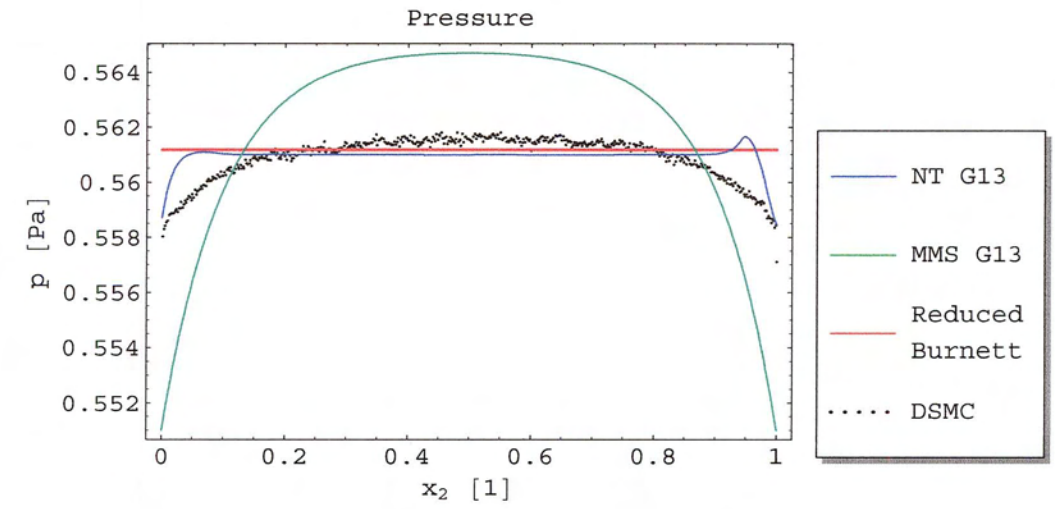

Figure 4-16e: Pressure at $Kn = 0.1$ and $\Delta v = 300\frac{\mathrm{m}}{\mathrm{s}}$

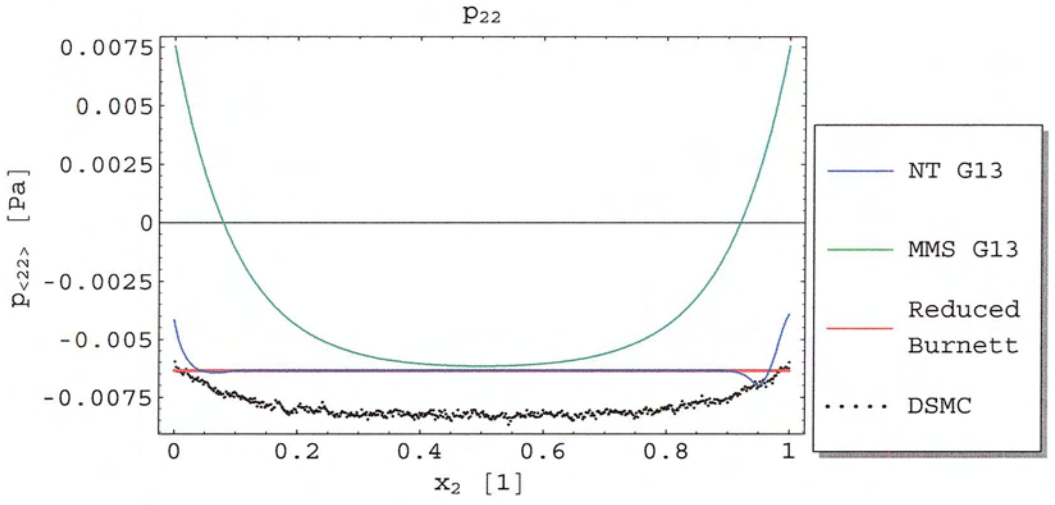

Figure 4-16f: $p_{<22>}$ at $Kn = 0.1$ and $\Delta v = 300\frac{\mathrm{m}}{\mathrm{s}}$

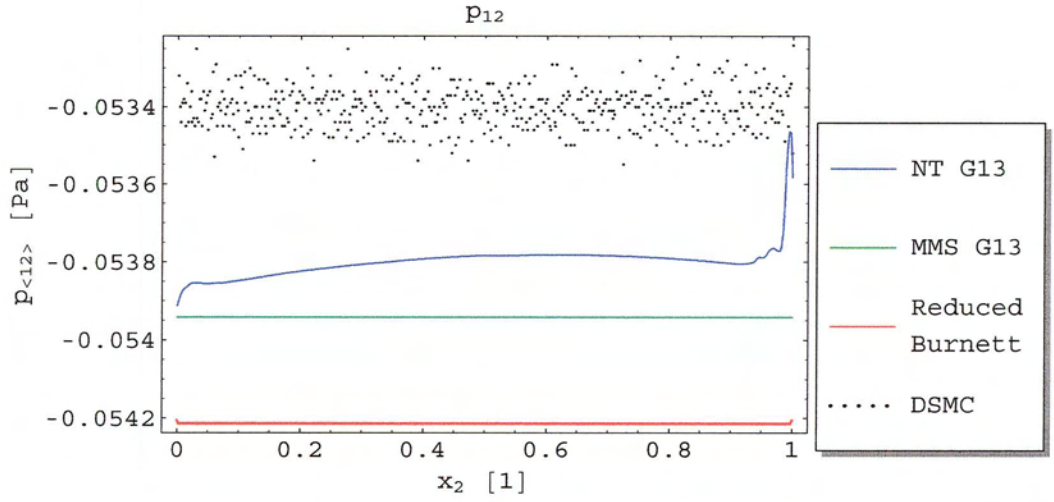

Figure 4-16g: $p_{<12>}$ at $Kn = 0.1$ and $\Delta v = 300\frac{\mathrm{m}}{\mathrm{s}}$

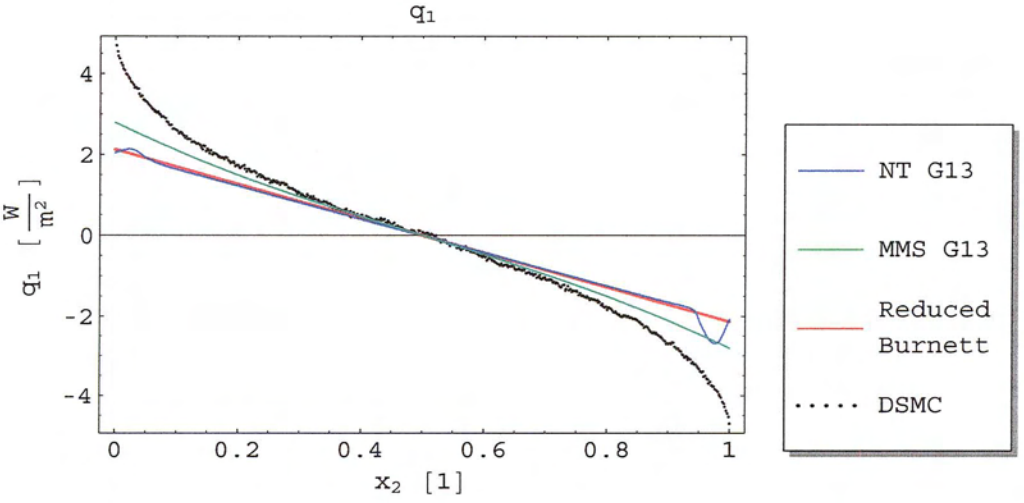

Figure 4-16h: q_1 at $Kn = 0.1$ and $\Delta v = 300\frac{\mathrm{m}}{\mathrm{s}}$

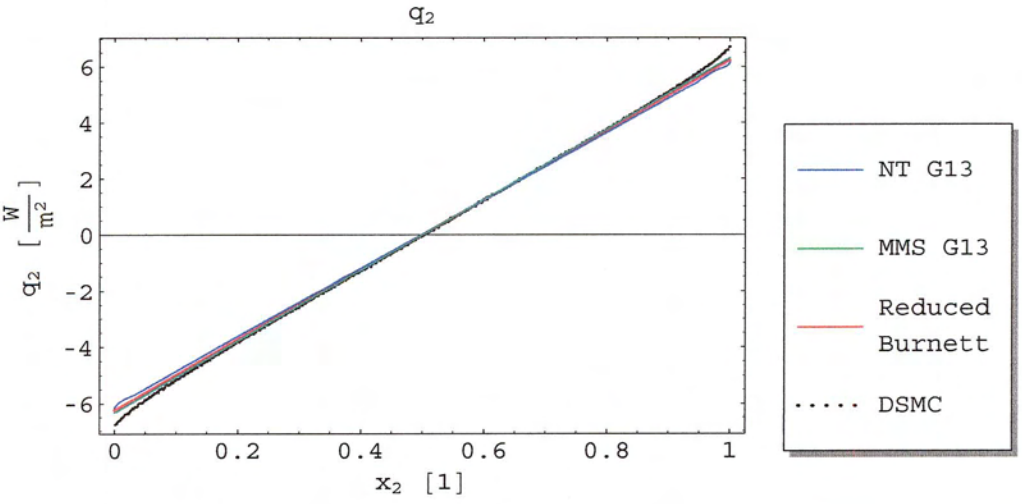

Figure 4-16i: q_2 at $Kn = 0.1$ and $\Delta v = 300\frac{\mathrm{m}}{\mathrm{s}}$

Chapter 5

Regularized Grad 13 equations

5.1 Superpositions

An alternative way to look at the Grad 13 equations is given through the regularization of Grad's 13 moment equations (R13 equations) [11][13][14][36]. The regularization method of Ref. [11] gives a modification of the Grad 13 equations with additional terms due to a Chapman-Enskog expansion of the moment equations for higher moments. The R13 equations can also be derived independent of Grad's closure method, by isolating the order of magnitude of all moments and the influence of their respective terms on the conservation laws [13]. It is shown in Ref.s [11][13][14] that the R13 equations are stable equations that contain the Navier-Stokes, Burnett and super-Burnett equations in their respective limits of the Knudsen number.

What interests us here is that when linearized and simplified for the steady state Couette flow, the R13 equations provide solutions for $p_{<22>}$ and q_1 that can be solved analytically [36].

The linear non-conservative R13 equations for heat flux and pressure tensor from Ref. [36] read

$$\frac{\partial p_{<ij>}}{\partial t} + \frac{4}{5}\frac{\partial q_{<i}}{\partial x_{j>}} + 2\frac{\partial v_{<i}}{\partial x_{j>}} - 2Kn\frac{\partial}{\partial x_k}\frac{\partial p_{<ij>}}{\partial x_k} = -\frac{1}{Kn}p_{<ij>}, \tag{5.1}$$

$$\frac{\partial q_i}{\partial t} + \frac{5}{2}\frac{\partial T}{\partial x_i} + \frac{\partial p_{<ik>}}{\partial x_k} - \frac{12}{5}Kn\frac{\partial}{\partial x_k}\frac{\partial q_{<i}}{\partial x_{k>}} - 2Kn\frac{\partial}{\partial x_i}\frac{\partial q_k}{\partial x_k} = -\frac{2}{3}\frac{1}{Kn}q_i. \tag{5.2}$$

Now considering Couette flow, steady state and linear dimensionless flow, we find Eqn.s

(2.36) and (2.37) reduce to

$$\frac{\partial p_{<12>}}{\partial x_2} = 0 \tag{5.3}$$

and

$$\frac{\partial q_2}{\partial x_2} = -p_{<12>}\frac{\partial v_1}{\partial x_2}. \tag{5.4}$$

Now combined with Eqn.s (5.1) and (5.2) the flow is described by,

$$\frac{\partial v_1}{\partial x_2} + \frac{2}{5}\frac{\partial q_1}{\partial x_2} = -\frac{p_{<12>}}{Kn}, \tag{5.5}$$

$$\frac{5}{2}\frac{\partial T}{\partial x_2} + \frac{\partial p_{<22>}}{\partial x_2} = -\frac{2}{3}\frac{q_2}{Kn}, \tag{5.6}$$

$$p_{<22>} = \frac{6}{5}Kn^2\frac{\partial^2 p_{<22>}}{\partial x_2^2}, \tag{5.7}$$

and

$$q_1 = \frac{9}{5}Kn^2\frac{\partial^2 q_1}{\partial x_2^2}. \tag{5.8}$$

Integrating these equations with respect to x_2 we find

$$v_1(x_2) = v_0 - \frac{p_{12}}{Kn}x - \frac{2}{5}q_1(x) \tag{5.9}$$

where

$$q_1(x) = A\sinh\left(\sqrt{\frac{5}{9}}\frac{x-\frac{1}{2}}{Kn}\right) + B\cosh\left(\sqrt{\frac{5}{9}}\frac{x-\frac{1}{2}}{Kn}\right) \tag{5.10}$$

and

$$T(x) = T_0 - \frac{4}{15}\frac{q_2}{Kn}x - \frac{2}{5}p_{<22>}(x) \tag{5.11}$$

where

$$p_{<22>}(x) = C\sinh\left(\sqrt{\frac{5}{6}}\frac{x-\frac{1}{2}}{Kn}\right) + D\cosh\left(\sqrt{\frac{5}{6}}\frac{x-\frac{1}{2}}{Kn}\right). \tag{5.12}$$

v_0, T_0, A, B, C and D are constants of integration to be determined from the boundary conditions. It follows that the R13 equations yield linear contributions to q_1 and $p_{<22>}$. This sets them apart from the Navier-Stokes and Fourier (NSF) equations which just yield $q_1 = p_{<22>} = 0$, and the Grad 13 equations, which give only non-linear contributions, as expressed in the reduced Burnett Eqn.s (2.94) and (2.96). These linear contributions

have the form of Knudsen layers, and by comparing to the DSMC results we can see that $B = C = 0$ should hold.

An approximation of solutions of the R13 equations can be obtained by superposition of the linear Knudsen layers, Eqn.s (5.10) and (5.12) and the full nonlinear solutions of the reduced Burnett equations, Eqn.s (2.36), (2.37), (2.88), (2.91), (2.94) and (2.96) with boundary conditions, Eqn.s (2.78) and (2.80) of Ch. 2. Such a superposition of linear boundary layer and bulk solution has been used successfully for the solution of the full Burnett equations [37]. The reduced Burnett equations are chosen, since the R13 equations have been shown to contain the Burnett equations [13] and thus contain the reduced Burnett equations as well. Boundary conditions for $\hat{q}_1$ and $\hat{p}_{<22>}$ under the R13 equations have yet to be found and are beyond the scope of this work. The boundary conditions for velocity jump and temperature slip are as presented earlier in Sec. 2.5, but to find v_0, T_0 we need $\hat{q}_1$ and $\hat{p}_{<22>}$ at the boundary.

5.2 Regularized Grad13 results

The reduced Burnett equations are solved as in Sec. 3.4 of Ch. 3.4. Results for the solution have been calculated and plotted with the help of Mathematica®. Early stages of the transition regime ($Kn = 0.1$) proves a good representation of both the capabilities and the limitations of these linear results. It can be seen below, Fig.s 5-1a to 5-1h, that the basic properties of the flow are well represented. The constants for the R13 solution are obtained by fitting the $p_{<22>}$ and q_1 solutions to the DSMC results, i.e. by fitting the constants A and D. No extra boundary conditions have been provided. The $p_{<12>}$ and q_2 results do not differ between the reduced Burnett and R13 solutions.

The results for the reduced Burnett/R13 superpositions are remarkably good and are superior to the results from the Grad 13 and the NSF equations.

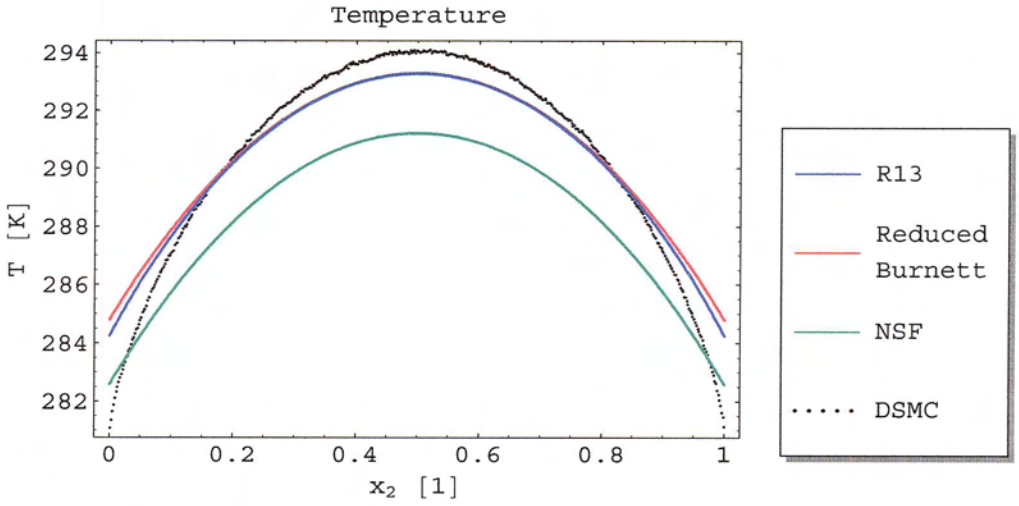

Figure 5-1a: Temperature at $Kn = 0.1$ and $\Delta v = 300\frac{\mathrm{m}}{\mathrm{s}}$

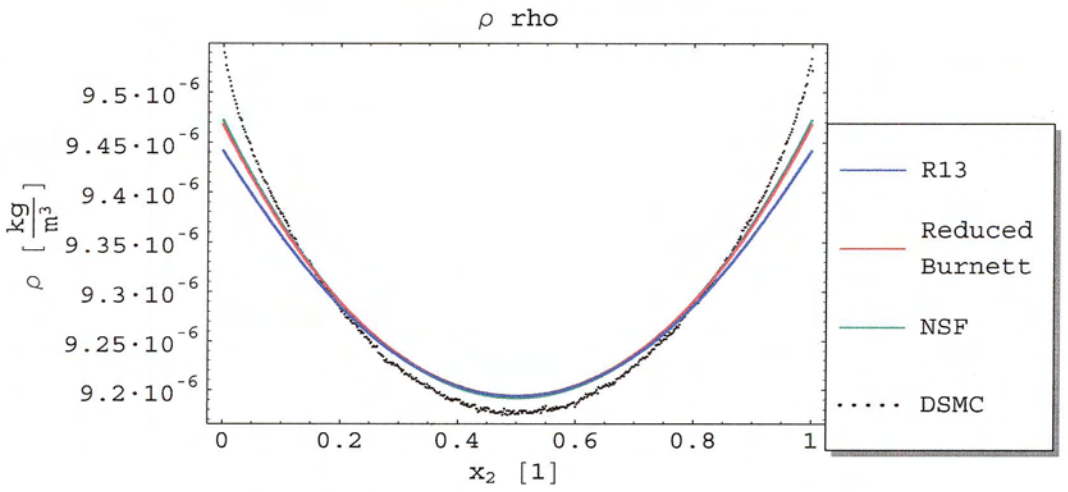

Figure 5-1b: Density at $Kn = 0.1$ and $\Delta v = 300\frac{\mathrm{m}}{\mathrm{s}}$

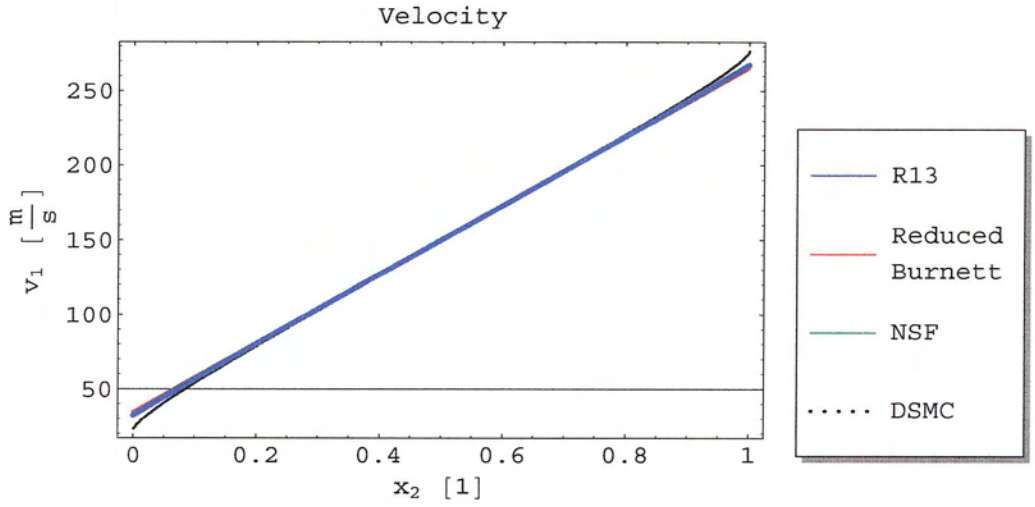

Figure 5-1c: Velocity v_1 at $Kn = 0.1$ and $\Delta v = 300\frac{\mathrm{m}}{\mathrm{s}}$

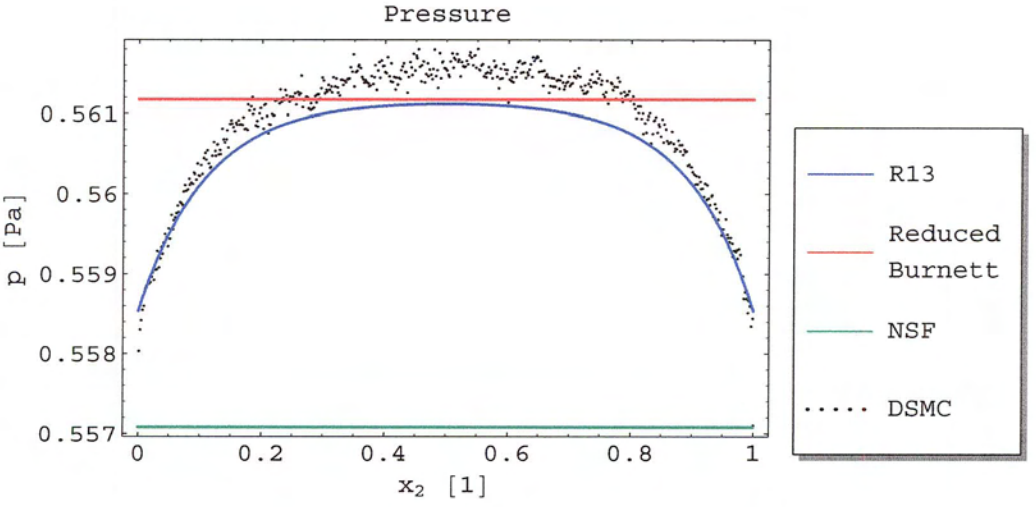

Figure 5-1d: Pressure at $Kn = 0.1$ and $\Delta v = 300\frac{\mathrm{m}}{\mathrm{s}}$

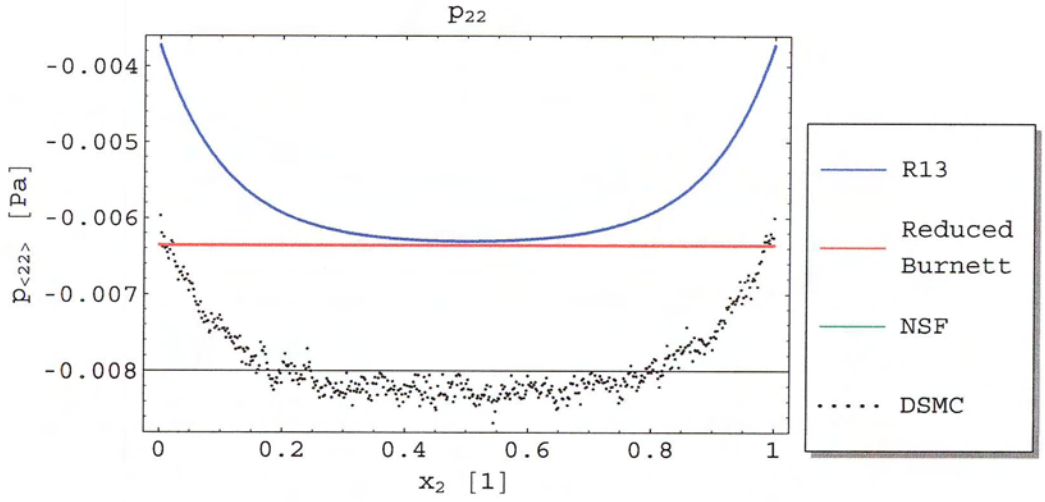

Figure 5-1e: $p_{<22>}$ at $Kn = 0.1$ and $\Delta v = 300\frac{\mathrm{m}}{\mathrm{s}}$

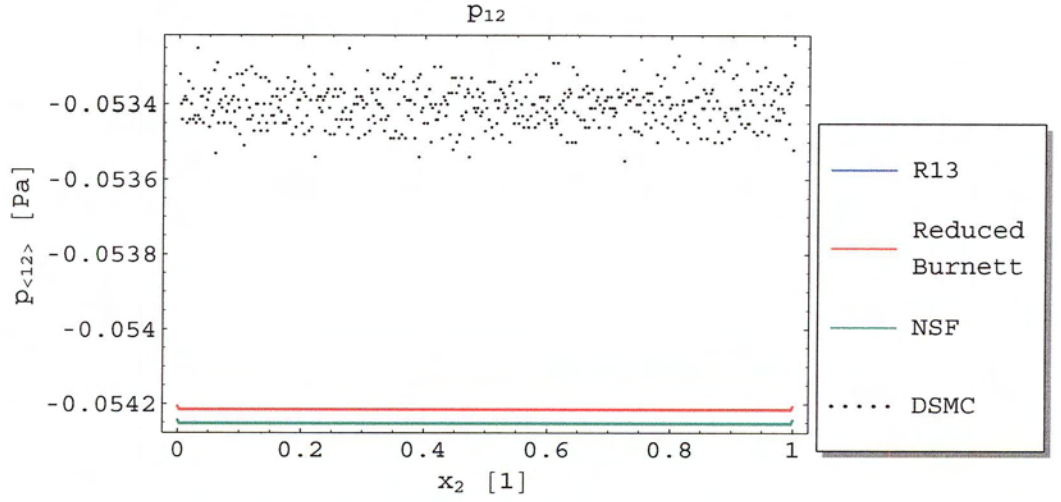

Figure 5-1f: $p_{<12>}$ at $Kn = 0.1$ and $\Delta v = 300\frac{\mathrm{m}}{\mathrm{s}}$

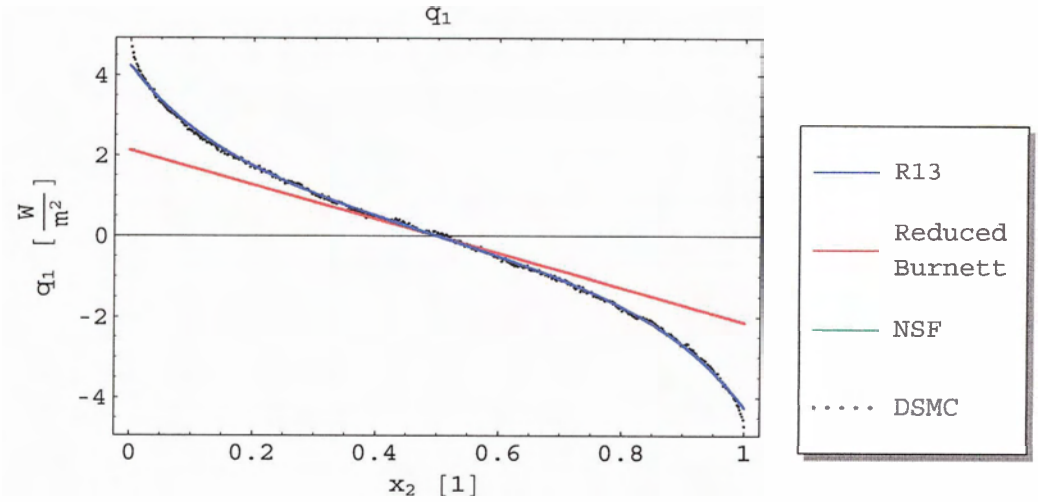

Figure 5-1g: q_1 at $Kn = 0.1$ and $\Delta v = 300\frac{\mathrm{m}}{\mathrm{s}}$

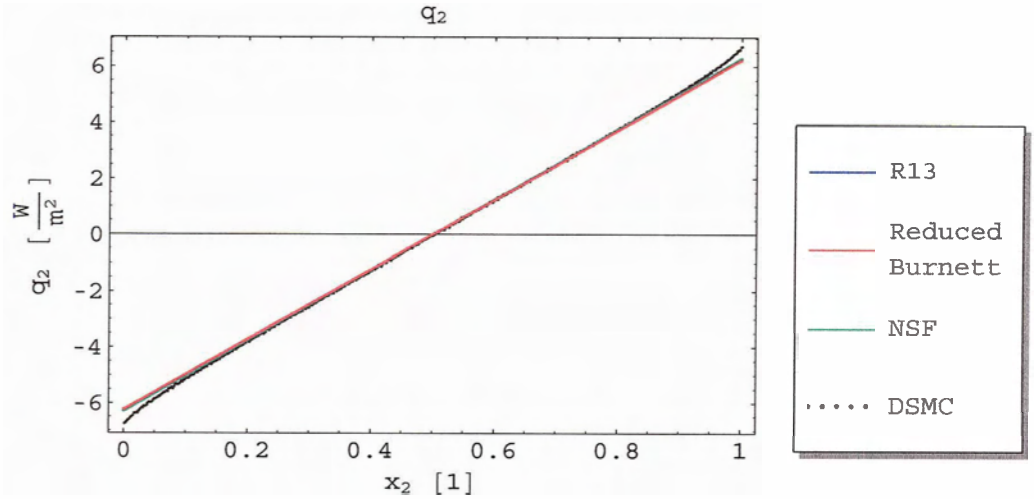

Figure 5-1h: q_2 at $Kn = 0.1$ and $\Delta v = 300\frac{\mathrm{m}}{\mathrm{s}}$

Notice that the NSF equations are shown with here without the non-linear contribution of the square of the slip velocity, V^2, in the temperature jump (Eqn. 2.80), as is common in the application of the NSF equations for microscale flow [2][3]. Note that this term is quadratic in the Knudsen number, since the slip velocity is proportional to Kn. Since the NSF equations are of first order, this second order term is normally not considered. The

contribution to the temperature jump is significant as becomes clear from Fig. 5-1a and Fig. 5-2a (below).

Figures 5-2a to 5-2h below, show the superposition of reduced Burnett and R13 boundary layers at $Kn = 0.1$ and $\Delta v = 600\frac{\mathrm{m}}{\mathrm{s}}$. It can be seen, that also at the higher Mach numbers the superposition gives very good results.

At larger Knudsen numbers (not shown), however, the quality is not really satisfactory. This is probably because non-linear third order effects that are not described by the reduced Burnett equations become important.

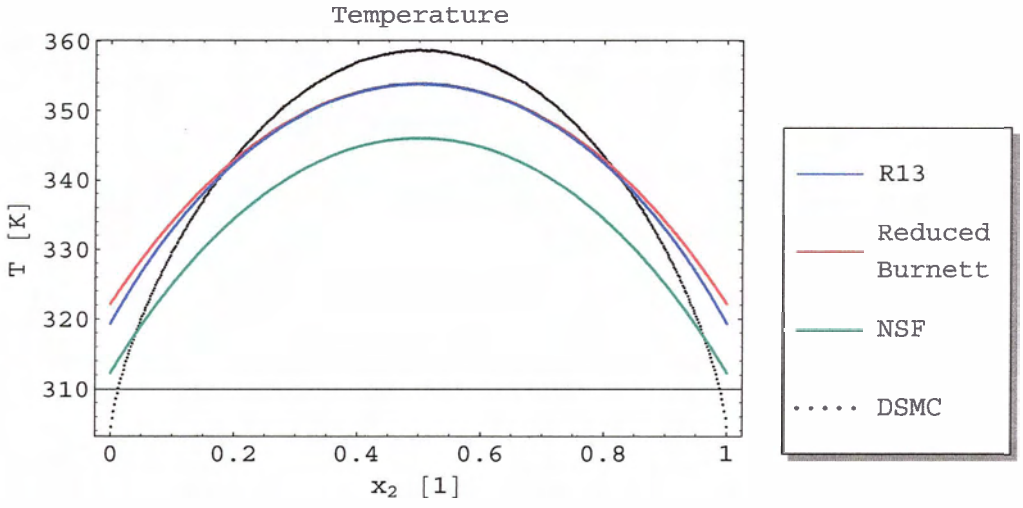

Figure 5-2a: Temperature at $Kn = 0.1$ and $\Delta v = 600\frac{\mathrm{m}}{\mathrm{s}}$

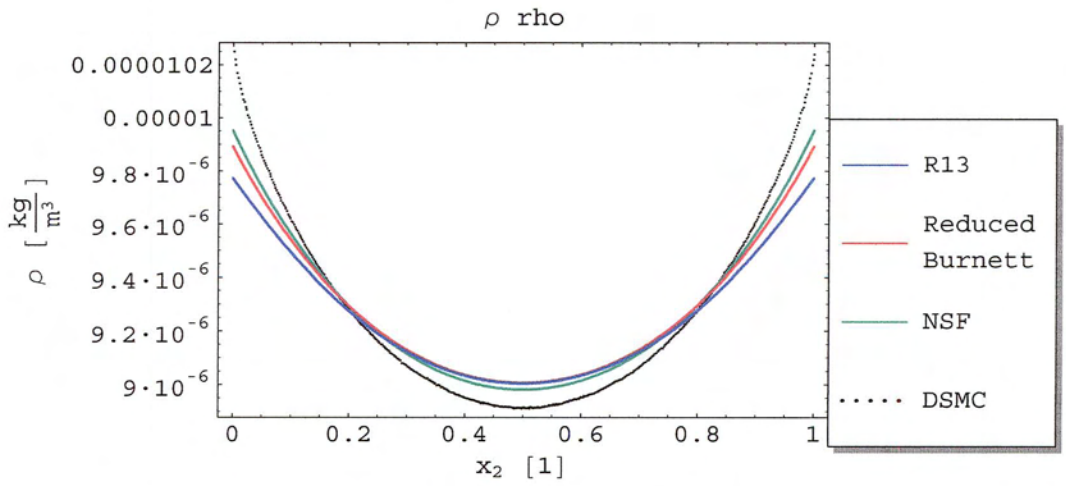

Figure 5-2b: Density at $Kn = 0.1$ and $\Delta v = 600\frac{\mathrm{m}}{\mathrm{s}}$

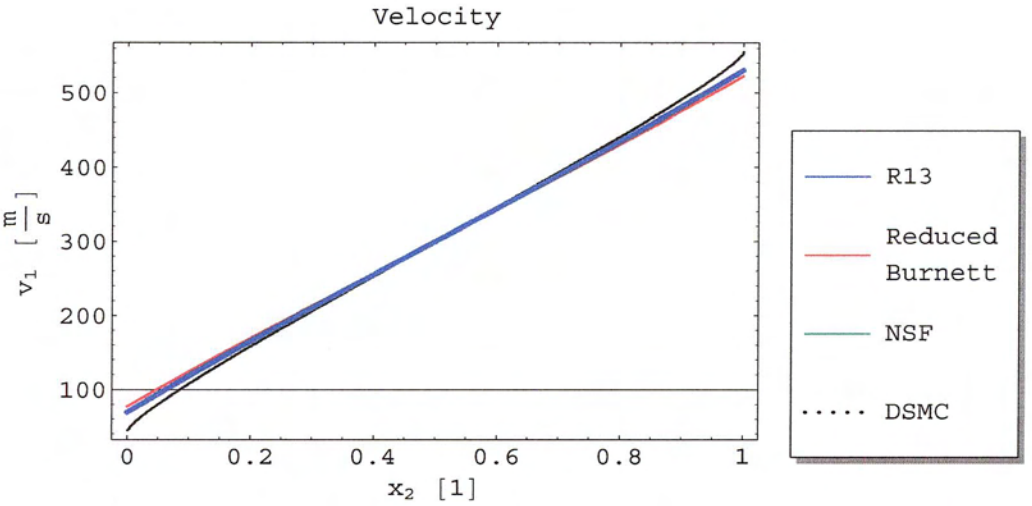

Figure 5-2c: Velocity v_1 at $Kn = 0.1$ and $\Delta v = 600\frac{\mathrm{m}}{\mathrm{s}}$

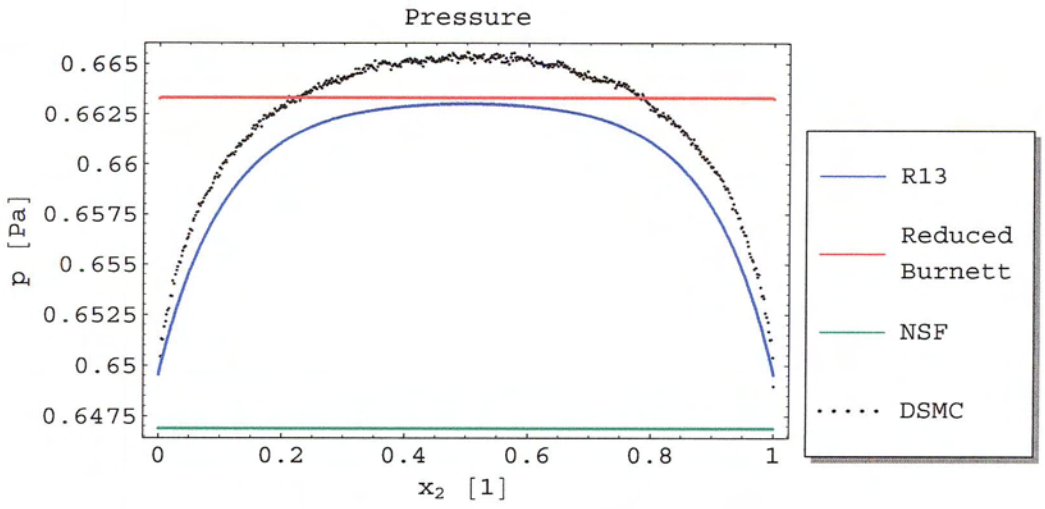

Figure 5-2d: Pressure at $Kn = 0.1$ and $\Delta v = 600\frac{\mathrm{m}}{\mathrm{s}}$

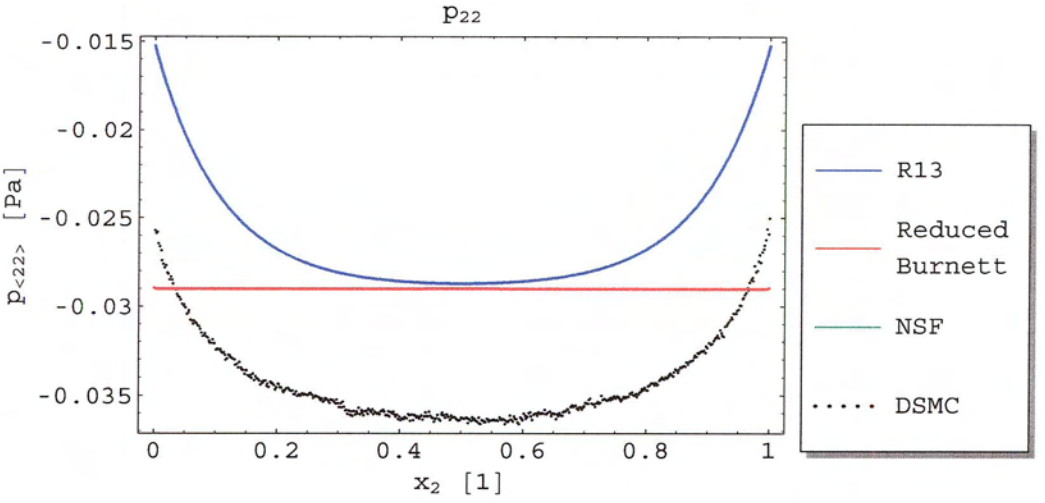

Figure 5-2e: $p_{<22>}$ at $Kn = 0.1$ and $\Delta v = 600\frac{\mathrm{m}}{\mathrm{s}}$

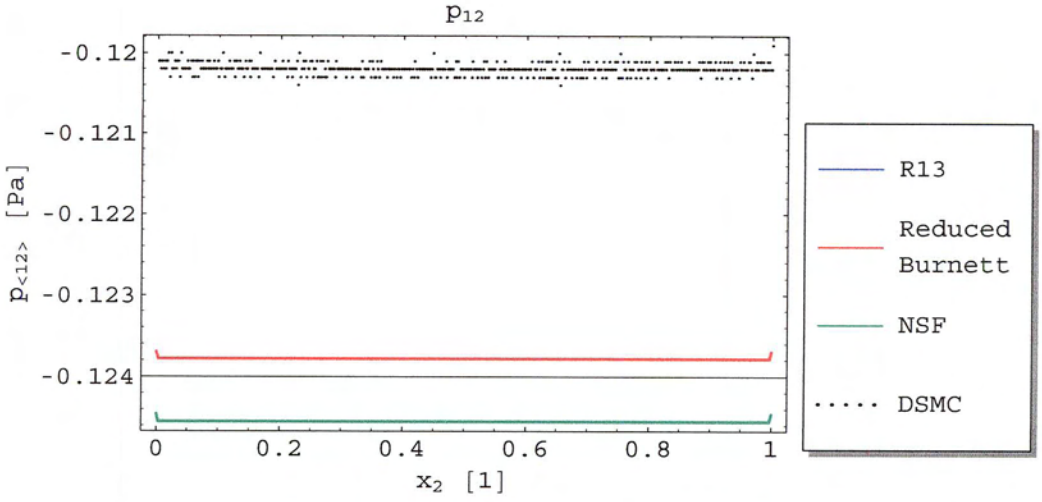

Figure 5-2f: $p_{<12>}$ at $Kn = 0.1$ and $\Delta v = 600\frac{\mathrm{m}}{\mathrm{s}}$

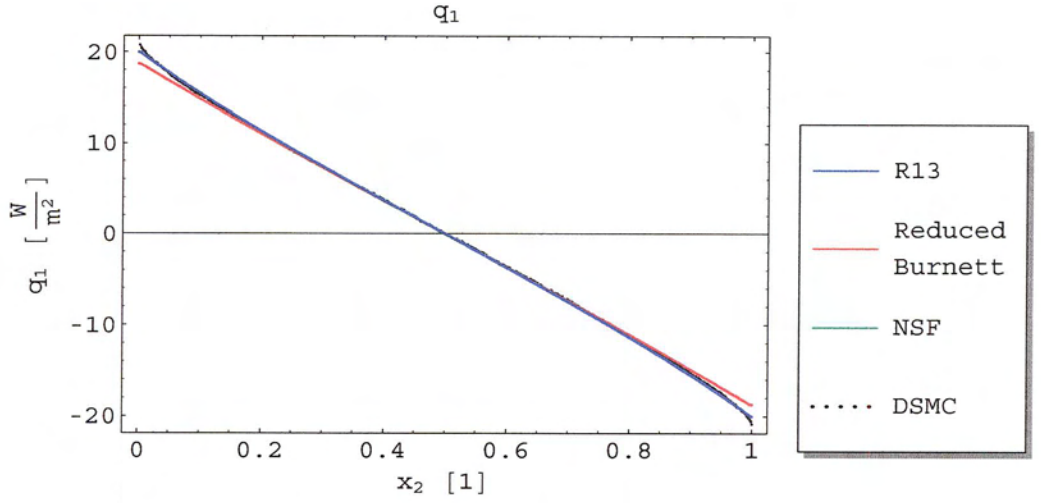

Figure 5-2g: q_1 at $Kn = 0.1$ and $\Delta v = 600\frac{\mathrm{m}}{\mathrm{s}}$

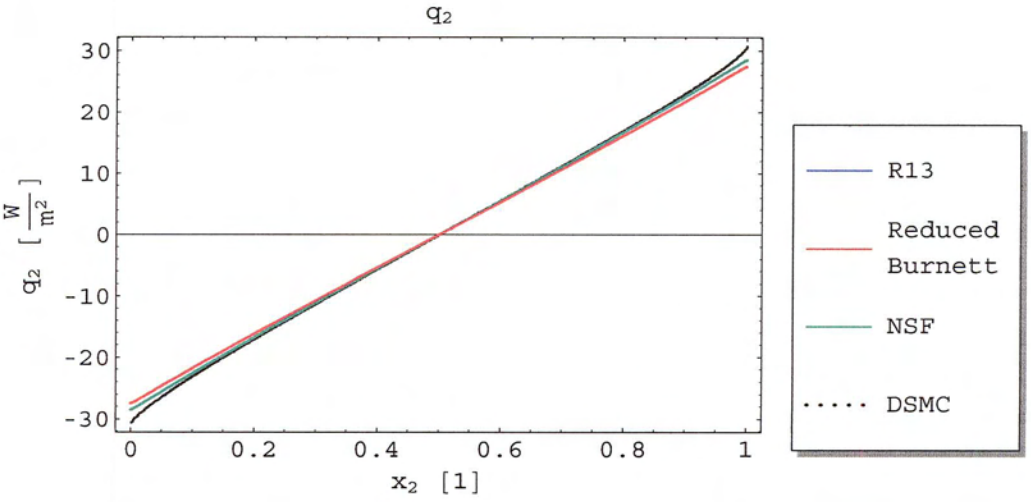

Figure 5-2h: q_2 at $Kn = 0.1$ and $\Delta v = 600\frac{\mathrm{m}}{\mathrm{s}}$

Chapter 6

Conclusions and recommendations

6.1 Conclusions

Using the moment method on the Boltzmann equation, Grad's 13 moment equations can be found. These equations represent a set of continuum equations to model gas flow. The advantage of these equations is that they are of higher order in the Knudsen number and potentially useful for unsteady simulations. Being of high order in the Knudsen number means that they have increased accuracy over Navier-Stokes and Fourier (NSF) equations for microscale or rarefied flows. They also provide information about fluid properties that are not present in the NSF solutions.

In order to create a model for microscale flow with the Grad 13 equations there are some problems that must be overcome. First the Grad 13 equations require additional boundary conditions that are not required for the NSF equations. In addition, the Grad 13 equations are hyperbolic with strong non-linear contributions. This hyperbolicity requires the choice of more complex numerical methods. Both of these problems have proved to be much more difficult than originally expected.

In order to keep the scope of the project within reach, yet still demonstrate the application of the Grad 13 equations, the geometry used in this project is restricted to modeling two dimensional gas Couette flow. This is the flow of a gas between parallel plates moving relative two each other in the parallel plane. In this geometry, there are two fluid properties described by the Grad 13 equations that are not present in the NSF equations. These properties are the perpendicular component of the trace free stress or pressure tensor $p_{<22>}$

and the heat flux parallel to the plates q_1. Unlike the traditional NSF flow properties, $p_{<22>}$ and q_1 are more difficult to conceptualize in the physical system. Addition of these two properties requires that one more boundary condition $p_{<22>}$ at both plates is required. To further complicate this, microscale gas flow requires that the boundary layer be accommodated. The boundary layer is taken into account using temperature jump and velocity slip in the NSF equations. A similar boundary condition was obtained for $p_{<22>}$ using a technique, based fluxes and productions in the boundary layer, that can also be used to find temperature jump and velocity slip boundary conditions. An analog of Cercignani's Knudsen boundary layer coefficients was also found for $p_{<22>}$ boundary condition.

Two numerical methods were found and tested that can be used to approximate the solution of the Grad 13 equations. Both methods were applied to the Couette flow problem and compared to NSF solutions and Direct Simulation Monte Carlo solutions. Both methods provided flow information that is unavailable with NSF solutions and were capable of providing transient response. One was based on MacCormack's method with high order Taylor series damping used to stabilize numerical oscillations in the solution. The other method is a newer total variation diminishing method, first proposed for hyperbolic equations by Nessyahu and Tadmor. The Nessyahu-Tadmor method involves using a min-mod reconstruction to prevent oscillations. Both methods proved to have advantages and disadvantages.

The modified MacCormack's method required adjustment of the amount of numerical damping applied. An objective technique for determining the exact amount of damping to apply was not found. The modified MacCormack's scheme however was very quick and could provide solutions over a large range of Knudsen numbers.

The Nessyahu-Tadmor method proved more difficult to implement and was slower when used to compute a solution. Results at larger Knudsen numbers could not be found due to a numerical symmetry error. The symmetry error was not isolated; leaving potential to improve this method. As damping is not required with this method, the confidence in the solution would be higher if the symmetry problem was solved. It also proved more difficult to implement and was slower when used to compute a solution.

In addition to the two numerical methods, a reduced form of the Burnett equations for Couette flow was found and tested. These equations can be added two the NSF equations to solve for some of the unknown flow properties that appear in micro scale Couette flow such as $p_{<22>}$ and q_1. It turned out for our specific case of plane Couette flow at steady state the reduced Burnett solution is more robust and immediately applicable than the Grad 13 solutions.

The solution of the reduced Burnett equations was extended by adding the linear boundary layer contributions of the regularized Grad 13 equations. This provided an excellent fit to the boundary layer and other characteristics. To be fully useful, however, boundary conditions for the regularized Grad 13 equations are needed.

6.2 Recommendations

A lot of unexpected difficulties were encountered with this project, some of which could be overcome with future work. A large majority of problems were associated with the numerical methods and need to be investigated further. The symmetry problems that occurred in the Nessyahu-Tadmor method in particular needs to be isolated. This could be approached by modeling simpler hyperbolic equations to gain more incite into the method. A Riemann based method could be used to further investigate the numerical behavior of the Grad 13 equations.

Beyond enhancements to the numerical work done in this thesis extending, the boundary conditions and solutions to other types microscale flows and geometries such as Poiseuille flow could prove interesting. The extension of the boundary method or the development of a new method, for higher order equations such as the Regularized grad 13 equations is also an obvious next step.

References

[1] Geppert, L. "The Amazing Vanishing Transistor Act." *IEEE Spectrum* pp. 28–33 (2002).

[2] Gad-el Hak, M. "Flow Physiscs in MEMS." *Mécanique & Industries* **2**, 313–341 (2001).

[3] Beskok, A. and G. E. Karniadakis. *Micro Flows: Fundamentals and Simulation*. Springer-Verlag, New York (2002).

[4] Bird, G. *Molecular Gas Dynamics and the Direct Simulation of Gas Flows*. Clarendon Press, Oxford (1994).

[5] Grad, H. "On the Kinetic Therory of Rarefied Gases." *Communications in Pure Appied Mathematics* **2**, 331 (1949).

[6] Cercignani, C. *Theory and Application of the Boltzmann Equation*. Scottish Academic Press, Edinburgh (1975).

[7] Lockerby, D. A. and J. M. Reese. "High-Resolution Burnett Simulations of Micro Couette Flow and Heat Transfer." *Journal of Computational Physics* **188**(2), 333–347 (2003).

[8] Chapman, S. and T. Cowling. *The Mathematical Theory of Non-Uniform Gases*. Cambridge University Press, Cambridge England (1970).

[9] Shavaliyev, M. S. "Super-Burnett corrections to the stress tensor and the heat flux in a gas of Maxwellian molecules." *Journal of Applied Mathematics and Mechanics* **57**(3), 168171 (1993).

[10] Struchtrup, H. "Grad's Moment Equations for Microscale Flows." In "Symposium on Rarefied Gasdynics 23, AIP Conference Proceedings," vol. 663, pp. 792–799 (2003).

[11] Struchtrup, H. and M. Torrilhon. "Regularization of Grad's 13 Moment Equations: Derivation and Linear Analysis." *Physics of Fluids* **15**(9), 2668–2680 (2004).

[12] Myong, R. "A Computational Method for Eu's Generalized Hydrodynamic Equations of Rarefied and Microscale Gasdynamics." *Journal of Computational Physics* **168**, 47–72 (2001).

[13] Struchtrup, H. "Stable transport equations for rarefied gases at high orders in Knudsen number." *Physics of Fluids* **16**(11), 3921–3934 (2004).

[14] Torrilhon, M. and H. Struchtrup. "Regularized 13-Moment-Equations: Shock Structure Calculations and Comparison to Burnett Models." *Journal of Fluid Mechanics* **513**, 171–198 (2004).

[15] Bird, R. B., W. E. Stewart, and E. N. Lightfoot. *Transport Phenomena.* John Wiley & Sons, Inc., New York, 2nd edn. (2002).

[16] Marques, W. J., G. Kremer, and F. Sharipov. "Couette Flow with Slip and Jump Boundary Conditions." *Continuum Mechanics and Thermodynamics* **12**, 379–386 (2000).

[17] Oran, E. "Direct Simulation Monte Carlo: Recent Advances and Applications." *Annual Reviews Fluid Mechanics* **30**, 403–441 (1998).

[18] Bird, G. "Recent Advances and Current Challenges for DSMC." *Computers & Mathematics with Applications* **35**, 1–14 (1998).

[19] Reitebuch, D. and W. Weiss. "Application of High Moment Theory to the Plane Couette Flow." *Continuum Mechanics and Thermodynamics* **4**, 217–225 (1999).

[20] Struchtrup, H. and W. Weiss. "Temperature Jump and Velocity Slip in the Moment Method." *Continuum Mechanics and Thermodynamics* **12**, 1–18 (2000).

[21] Harris, S. *An Introduction to the Theory of the Bolzmann Equation.* Holt, Rinehart and Winston, Inc., New Yrok (1971).

[22] Müller, I. *Thermodynamics.* Pitman, Boston (1985).

[23] Risso, D. and P. Cordero. "Dilute Gas Couette Flow: Theory and Molecular Dynamics Simulation." *Physical Review E* **56**, 489 (1997). Erratum: *Physical Review E* **57**, (1997) 7365.

[24] Cercignani, C. *Rarefied Gas Dynamics: From Basic Concepts to Actual Calculations.* Cambridge University Press, Cambridge England (2000).

[25] Patankar, S. V. *Numerical Heat Trnasfer and Fluid Flow.* Hemisphere Publishing Corp., New York (1980).

[26] Versteeg, H. and W. Malalaserkera. *An Introduction to Computational Fluid Dynamics, The Finite Volume Method.* Pearson Education Ltd., Harlow England (1995).

[27] Hoffmann, K. A. and S. T. Chiang. *Computational Fluid Dynamics for Engineers*, vol. 1. Engineering Education Systems, Wichita (1993).

[28] Hoffmann, K. A. and S. T. Chiang. *Computational Fluid Dynamics for Engineers*, vol. 2. Engineering Education Systems, Wichita (1993).

[29] Roe, P. L. "Approximate Riemann Solvers, Parameter Vectors, and Difference Schemes." *Journal of Computational Physics* **43**, 357–372 (1981).

[30] Press, W. H., et al. *Numerical Recipes in C++: The Art of Scientific Computing.* Cambridge University Press, Cambridge, 2nd edn. (2002).

[31] Burden, R. L. and J. D. Faires. *Numerical Analysis.* PWS Publishing Company, Boston, 5th edn. (1993).

[32] Shapine, L. F., J. Kierzenka, and M. W. Reichelt. "Solving Boundary Value Problems for Ordinary Differential Equations in MATLAB with Bvp4c." Tech. rep., The MathWorks, Inc. (2000).

[33] Lorimer, S. A. *A Numerical Study of Some Linear and Nonlinear Elastodynamic Problems.* Ph.D. thesis, University of Alberta (1986).

[34] Nessyahu, H. and E. Tadmor. "Non-Oscillatory Central Differencing for Hyperbolic Consevation Laws." *Journal of Computational Physics* **87**, 408–463 (1990).

[35] Liotta, S. F., V. Romano, and G. Russo. "Central Schemes for Balance Laws of Relaxation Type." *SIAM Journal of Numerical Analysis* **38**(4), 1337–1356 (2000).

[36] Struchtrup, H. "Failures of the Burnett and Super-Burnett equations in steady state proceses." *Continuum Mechanics and Thermodynamics* (2005). (In press).

[37] Mackowski, D. W., D. H. Papadopoulos, and D. E. Rosner. "Comparison of Burnett and DSMC predictions of pressure distributions and normal stress in one-dimensional, strongly nonisothermal gases." *Physics of Fluids* **11**(8), 2108–2116 (1999).